LATTICE GAUGE THEORY ON A PARALLEL COMPUTER

Thesis by

Jonathan William Flower

In Partial Fulfillment of the Requirements

for the Degree of

Doctor of Philosophy

California Institute of Technologoy

Pasadena, California

1987

(Submitted February 4th, 1987)

ACKNOWLEDGEMENTS

Of the many people who have helped me during my years at Caltech none have advised me longer than Geoffrey Fox. From the day of my arrival in Los Angeles to the present his suggestions have never been less than helpful and I am deeply grateful.

My technical research advisor has been Steve Otto. His impact on my career here has also been significant since if it were not for his fascinating talk that originally involved me in lattice gauge theory I probably still be trying to find a study topic. It has been a fascinating experience working with so enthusiastic a collaborator and I value immensely his friendship and teaching.

The friends I have made at Caltech, both at work and on numerous auditorium platforms, are too many to mention individually but I value their contributions enormously. My parents also played a significant role for, despite being many thousands of miles away for the majority of my years of study, it was their effort that led to my coming to Caltech. I owe them a great debt.

Finally, I would like to thank my wife, Linda, for the love and care she has shown me in the past two years. I eagerly look forward to spending the next fifty with her and our family rather than a word-processor.

ABSTRACT

The results of several numerical simulations of QCD by Monte Carlo lattice gauge theory are presented. Studying the mesonic potential on a 20^4 lattice, we conclude that asymptotic scaling does not hold over the range $6.1 \leq \beta \leq 6.7$, although we are not able to quantify the discrepencies. The effect of discrete rotational symmetry on physical parameters is examined and seems to modify the string tension by 15 % at $\beta = 6.1$, while at $\beta = 6.3$ the change was less than 1 %. The potential between three charges is studied and yields a string tension of .18 GeV^2, consistent with mesonic calculations and relativised potential models. Contributions to the potential from low-energy string vibrations appear small in the range $x \lesssim .5$ fm. We perform energy density measurements in the colour fields surrounding both mesons and baryons, which provide strong evidence in favour of the dual superconductor picture of confinement. It is also suggested that the confining strings in the baryon meet at a central point rather than joining the quarks pairwise.

Several algorithms are explored in an attempt to develop simulation methods which are able to directly account for the currents generated by colour sources. The extension of the Langevin equation to complex degrees of freedom is derived leading to a Fokker-Planck equation for a complex 'Probability distribution'. Using this technique we are then able to calculate energy densities in U(1) gauge theory at large charge separations. The extension of the method to non-Abelian theories comes up against an unresolved problem in segregation for certain types of observable.

We discuss methods for the simulation of full QCD, including the effects of dynamical fermions. The Langevin approach is analysed in detail, and the systematic error associated with the discretisation of the equations of motion is derived. We propose a mixed Langevin/Metropolis algorithm and explore its properties on a small lattice. Finally, the method is tested on the finite temperature deconfinement transition and applied to the mesonic potential. It is found that shielding effects lead to deconfinement at $\beta = 6.1$ on a lattice of size $12^2 \times 16^2$.

CONTENTS

CHAPTER 1

Introductory Remarks

The world in which we live seems to be dominated by the gauge principle. Each of the four fundamental interactions, strong, weak, electromagnetic and gravitational forces, seems to be well described by a theory with a local gauge symmetry and obviously the study and understanding of such theories is of vital importance. Despite the unifying concept upon which all of these theories are built, however, the extent to which we can be said to have 'solved' their problems varies markedly. For example, the weak coupling of the electron and photon allows perturbative calculations in quantum electrodynamics whose successes are quite spectacular [e.g., 1]. Similarly, the prediction of the existence of the intermediate weak vector bosons from the unified theory of the weak and electromagnetic interactions [2] and their subsequent discovery [3] is well known. In contrast, the properties of the strong interactions are much less well understood theoretically and few quantitative predictions have been made.

Quantum Chromodynamics (QCD) is the theory most often associated with the strong interactions. It describes the interaction of massive spin ½ particles known as quarks and massless vector quanta known as gluons in a manner exactly analogous to that between electrons and photons. However, perturbative calculations in QCD are hampered by the fact that the quark-gluon coupling is not small except at very high energies, a property known as 'asymptotic freedom' [4]. Non-perturbative techniques do exist, such as the large N expansion [5], mean field methods [6] and instanton calculations [7] which have led to qualitative understanding of certain aspects of the theory, but it seems that our best chance of directly extracting quantitative predictions which can be compared with experiment is by numerical simulation.

One approach which has attracted much attention is the method of Wilson [8]. By constructing the theory on a discrete space-time lattice it was hoped to render QCD tractable to calculational methods in which the various approximations could be monitored and controlled, and which would yield results appropriate to both the high- and low-energy regimes. At large distance scales, for example, the latticised theory allows a particularly elegant perturbative expansion in inverse powers of the coupling strength and such calculations predict confinement. At smaller distance scales the major computational tool has been numerical investigation via Monte Carlo. Early results in the field showed that approximate quantitative results could indeed be obtained, albeit with the expenditure of great computational effort, which were not inconsistent with the data to be found in the particle tables.

This work investigates further the features of QCD as revealed in Monte Carlo calculations and develops techniques which may be of use in the next generation of numerical simulations.

In Chapter 2 are discussed, mainly for notational purposes, the conventional concepts upon which numerical lattice calculations are typically based. Chapter 3 then utilises

these methods in an extensive study of the properties of systems containing heavy quarks. Among the questions to be addressed are the degree to which Monte Carlo simulations are able to extract quantitative information and to what extent the lattice itself distorts the calculated parameters. Of more physical interest is the examination of the origin of the short and long range interquark forces, particular attention being paid to the question of the mechanism responsible for confinement. This chapter concludes with a discussion of the contact areas between experimental, phenomenological and numerical work. Chapter 4 presents a new and novel algorithm for determining path integrals. While derived in the context of enhancing signal/noise ratios in the calculation of exponentially small lattice correlation functions it is believed to be applicable to other physical domains. Chapter 5 is devoted to the long standing problems posed by the study of systems including light, dynamical fermions. An approximate algorithm is introduced and some of its systematic errors calculated explicitly. After demonstrating its effectiveness on a problem whose solution is well known we study the interquark potential. Finally, in Chapter 6, are discussed our conclusions and also the next generation of lattice calculations as prompted by this work. Some effort is made to assess the required computational resources.

CHAPTER 2

Fundamentals of Lattice Gauge Theory

2.1 - Yang-Mills Theory on the Lattice

In this section the construction and properties of a gauge theory on the lattice will be considered. Since the aim here is to merely introduce the principles and notation, our discussion will be brief and will centre on the pure Yang-Mills theory [9]. Excellent reviews of the subject are available in the literature [10,11].

The lattice itself is merely a construction which allows us to make sense of the path integral formulation of the theory. We start with a regular four-dimensional hypercubic mesh and associate gauge degrees of freedom with each link by the prescription

$$U_{x,\mu} = e^{igA_\mu^\alpha(x)\,\lambda_\alpha\,dx_\mu} \tag{2.1}$$

where g is the coupling constant, $A_\mu^\alpha(x)$ are the gauge fields and $\{\lambda_\alpha\,;\alpha = 1,\cdots,N^2-1\}$ are the generators of SU(N). The index μ denotes a direction in four-dimensional Euclidean space. From the properties of the exponential map it is trivial to see that the U matrices so defined are elements of SU(N). They represent the colour rotation involved in the transport between adjacent lattice sites denoted by x and $x+\hat{\mu}$ and in order for the return path to leave physical quantities unchanged it is natural to impose the constraint that

$$U_{x+\hat{\mu},\,-\mu} \;=\; U^{-1}_{x,\,\mu} \;=\; U^{\dagger}_{x,\,\mu} \tag{2.2}$$

In order to see the effect of a local gauge transformation, $G(x)$, on the theory defined in this way it is instructive to consider the continuum case where, for compactness, we define $A_\mu \equiv \sum_\alpha g\, A^\alpha_\mu\, \lambda_\alpha$

$$A_\mu(x) \rightarrow A_\mu'(x) \;=\; -i\,\partial_\mu G(x)\, G^{-1}(x) \;+\; G(x)\, A_\mu(x)\, G^{-1}(x) \tag{2.3}$$

To discretise this expression expand the exponential factor in Eq. (2.1) assuming that the lattice spacing is small

$$1 + iA_\mu \mathrm{d}x_\mu \;\rightarrow \tag{2.4}$$

$$1 + \left\{ \Big[G(x+\mathrm{d}x) - G(x) \Big] / \mathrm{d}x_\mu\, G^{-1}(x) + iG(x) A_\mu(x) G^{-1}(x) \right\} \mathrm{d}x_\mu$$

$$\simeq G(x + \mathrm{d}x)\,(1 + iA_\mu \mathrm{d}x_\mu)\, G^{-1}(x)$$

i.e., a link variable transforms bilinearly

$$U_{x,\,\mu} \;\rightarrow\; G(x+\hat{\mu})\, U_{x,\,\mu}\, G^{-1}(x) \tag{2.5}$$

Next consider the transformation properties of a product of consecutive links taken along a path, C, of M lattice sites, $\{x_1, x_2, \cdots, x_M\}$

$$P(C) \;=\; \prod_{x_i \in C} U_{x_i,\,\mu} \;\rightarrow\; G(x_1) \prod_{x_i \in C} U_{x_i,\,\mu}\; G^{-1}(x_M) \tag{2.6}$$

where the gauge transformations at the intermediate points, $\{x_i\ ;\ 1 < i < M\}$, have cancelled in pairs as a consequence of the bilinear nature of the transformation.

We can thus define the quantity

$$W(C) = \text{tr} \prod_{x_i \in C} U_{x_i, \mu} \tag{2.7}$$

which is seen to be invariant under gauge transformations as long as the loop C is closed. This is an extremely important feature of the lattice scheme since the invariance of physical quantities under local gauge transformations is a fundamental property of gauge theories.

Having thus discretised space-time and introduced the link variables $U_{x,\mu}$ we define the lattice gauge theory by a partition function

$$Z = \int \prod_{links\ l} [\mathrm{d}U_l]\ e^{-\beta S(U)} \tag{2.8}$$

where S(U) is the gauge invariant action for the fields $U_{x,\mu}$ and β is the analogue of the inverse temperature. The particular action which we will use almost exclusively in this work is the 'Wilson Action', which takes the form

$$S(U) = \sum_p \left(1 - \frac{1}{2N} \text{tr}(U_p + U_p^\dagger)\right) \tag{2.9}$$

where U_p denotes the ordered product of links around an elementary square (Plaquette) of the lattice (Fig. 1)

$$U_p = U_{x,\mu}\, U_{x+\hat{\mu},\nu}\, U^\dagger_{x+\hat{\nu},\mu}\, U^\dagger_{x,\nu} \tag{2.10}$$

This action has the virtue that if one identifies $\beta \equiv \frac{2N}{g^2}$ and expands in powers of the lattice spacing, denoted hereafter by a, then

$$\int [\mathrm{d}U]\, e^{-\beta S} = \int [\mathrm{d}A]\ e^{-1/4 \int \mathrm{d}^4x\ F^\alpha_{\mu\nu} F^{\mu\nu\alpha}} \tag{2.11}$$

and

$$F^{\alpha}_{\mu\nu} = \partial_\mu A^{\alpha}_{\nu} - \partial_\nu A^{\alpha}_{\mu} + igf_{\alpha\beta\gamma} A^{\beta}_{\mu} A^{\gamma}_{\nu} \tag{2.12}$$

with $f_{\alpha\beta\gamma}$ the structure constants of SU(N). Thus the lattice formalism, in the limit of small lattice spacing, reproduces the continuum path integral of the Yang-Mills theory in Euclidean space. That this is true should, however, come as little surprise since the original derivation of the path integral formalism was based on a discretisation of space-time [12]. The only really new feature is the clever choice of variables which resulted in our being able to exhibit local gauge invariance in such a neat manner.

Having said that the limit $a \rightarrow 0$ reproduces the required path integral, however, raises an important question. How exactly is the continuum limit to be realised and what are the systematic effects of a finite lattice spacing ?

Particularly obvious is the fact that the continuous translational and rotational symmetries of the continuum have been replaced by the discrete symmetries of the lattice. However, one might hope that if $1/a$ is significantly smaller than all momenta involved in a given process, then the distortions due to the lattice will be small. In a section 3.3 we will in fact attempt to quantify one such effect, namely that due to the discrete rotational symmetry.

At the opposite extreme one can ask whether there are effects due to the finite lattice volume. In particular the cost of computer simulations typically increases as some power of the number of degrees of freedom modelled rather than any bulk physical scale and this often imposes an upper limit on the number of lattice sites which can be studied. Thus, by reducing the lattice spacing we are typically forced to consider a smaller physical volume. At some point, for example when the total lattice diameter is only a small fraction of the proton radius, we will lose contact with reality and the physical quantities extracted will become meaningless.

In order to obtain an idea of the lattice sizes required we note that all physical quantities with dimensions of mass must be expressible in units of $1/a$. Furthermore two loop perturbation theory for SU(N) Yang-Mills theories yields the result that a is related to the coupling, g, via [13]

$$a = \frac{1}{\Lambda_L} \left(g^2\gamma_0\right)^{\gamma_1/(2\gamma_0^2)} \exp\left(-1/(2\gamma_0 g^2)\right) \tag{2.13}$$

where

$$\gamma_0 = \frac{11N}{48\pi^2} \qquad \gamma_1 = \frac{34N^2}{768\pi^4} \tag{2.14}$$

In these expressions Λ_L is a constant which can be related to $\Lambda_{\overline{MS}}$ in perturbation theory [14]. To the extent that perturbation theory holds in the regime where lattice calculations are executed we can thus calculate the lattice spacing directly from a knowledge of $\Lambda_{\overline{MS}}$. We shall return to this approach later when we attempt to compare lattice results with experimental data.

In connection with the realisation of the continuum limit it is important to note that Eq. (2.9) is not the only lattice action which has the property, Eq. (2.11), of yielding the Yang-Mills theory in the limit $a \to 0$. A possibility which has provoked considerable research is to add to Eq. (2.9) terms containing higher representations of SU(N) than the fundamental, each with its own coupling, β_r. The Symanzik improvement scheme [15] then consists of selecting these couplings so as to remove high-order dependencies on the lattice spacing. (For example, the mixed fundamental-adjoint action with $\beta_F / \beta_A = -6$ removes the term of order a^8 from the expansion of the expression analogous to Eq. (2.9).) The hope is that by doing so the approach of the continuum limit is accelerated.

An even more advanced scheme, that of the Monte Carlo Renormalisation Group [16], is to attempt to calculate the trajectory in coupling space $\{\beta_r\}$ along which the

continuum limit is approached most quickly. In this approach one chooses an initial set of couplings, $\beta_r^{(0)}$, for a lattice of spacing $l^{(0)}$ and then, by local averaging over the degrees of freedom, constructs a new lattice with spacing $l^{(1)} > l^{(0)}$ on which the same physics can be measured, albeit at new couplings $\beta_r^{(1)}$. Proceeding in this way one hopes to find a limiting set of couplings at which one measures continuum physics on a coarse lattice.

These studies will probably be of crucial importance in developing good numerical approximations to QCD but since neither has yet yielded conclusive results we will let computational simplicity be our guide and henceforth consider only the Wilson form of the action, Eq. (2.9).

2.2 - Computational Lattice Gauge Theory

The lattice version of the partition function, Eq. (2.8), can readily be seen to correspond to a statistical mechanics problem in four dimensions. As such there are simple diagrammatic methods which allow a consistent expansion to be made in the $\beta \to 0$ limit. This has been thoroughly explored to high orders [17] and predicts that quarks are permanently confined into hadrons by a potential which increases linearly with separation. Unfortunately this limit is far from the continuum which, as can be seen from Eq. (2.13) corresponds to the opposite $\beta \to \infty$ limit.

In this large β limit weak coupling perturbation theory may be valid since the coupling strength $\alpha_S \equiv g^2/4\pi$ decreases at high energies. However it is an experimentally observed fact that $\alpha_S = O(1)$ at hadronic energies [18,19] rendering conclusions drawn from perturbation theory somewhat questionable. As a last resort then, we turn to numerical simulations.

Initially the prospects for even this solution do not look bright. Examination of Eq. (2.8) shows that for a lattice with 20^4 sites the partition function involves integration over approximately 5×10^6 coupled degrees of freedom. Obviously such a task is beyond even the fastest of supercomputers. However, alternative Monte Carlo techniques are available which make the problem tractable although the demands made upon computational resources, both memory and raw CPU power, are still large.

In this section we will describe some aspects of the implementation of lattice gauge theory on the concurrent computer designed and built at Caltech. This work has been extensively described elsewhere [20] and so we shall restrict ourselves to a few salient points.

The Caltech/JPL hypercubes are parallel computers of the MIMD type (Multiple Instructions, Multiple Data). This means that they can be thought of as a network of independent processors each executing its own programme and possessing its own data. In order to communicate with other processors messages must be sent along fixed communication paths which are built into the machine such that the processors are connected with the topology of a hypercube in d dimensions. (See Fig. 2).

The decomposition of the lattice gauge theory problem onto such a computer is particularly simple. One takes a lattice with $M\times2^d$ sites and splits it up into sublattices each containing M sites, of which one is placed in each processor. Due to the locality of the action, Eq. (2.9), it is possible to assign the sublattices so that each processor needs only to communicate with others to which it is directly connected in hardware. As a result of this fact the characteristic timescale of the communication, t_{comm}, is minimal and corresponds to roughly the time taken to transfer a single SU(N) matrix from one processor to its neighbour. Conversely we can characterise the calculational part of the algorithm by a timescale, t_{calc}, which is roughly the time taken to multiply together two SU(N) matrices.

Given the nature of the hardware we have

$$t_{comm} \ll t_{calc} \tag{2.15}$$

and hence the gauge theory simulations are extremely 'efficient', where efficiency is defined by the relation

$$\epsilon = \frac{T_1}{N\, T_N} \tag{2.16}$$

and T_k is the time taken for k processors to perform the given calculation. Typically our calculations have efficiencies in the range $\epsilon \gtrsim .90$ which means they are ideally suited to this type of computation since doubling the number of processors approximately halves the total computational time required for solution.

A further important property of the problem is its homogeneity - no sites in the lattice are distinguished from any other. This results in extremely easy coding of the problem - with the insertion of a few well chosen boundary conditions a programme that runs on a conventional sequential machine can be parallelised. In order to understand this claim better, however, we must first discuss the basic computational technique.

The measurement of physical quantities on the lattice is typically a two-part procedure, the generation of lattice configurations and the measurement of lattice operators $O(U)$. Since all physical observables correspond to gauge invariant quantities the operator O must be of the type discussed earlier, Eq. (2.7), i.e., the trace of an ordered product of lattice links forming a closed path in the lattice. The calculation proceeds, therefore, by generating a sequence of field configurations $\{U_1\},\{U_2\},\cdots$ by some method and then measuring the quantity

$$\langle\, O \,\rangle = \frac{1}{N} \sum_{i=1}^{N} O(\{U_i\}) \tag{2.17}$$

which quantity reproduces the required physical measurement in the limit $N \rightarrow \infty$.

In carrying out this procedure we are considerably aided by the homogeneity of the lattice formulation. If the lattice were inhomogeneous the observable O might be calculable only once per generated configuration $\{U_i\}$. However in the homogeneous case there are many equivalent orientations of O which all contain equivalent physics. (For example, there are 960,000 different 1×2 rectangular loops in a 20^4 lattice). Thus we can obtain a huge increase in statistics by measuring all orientations. The exact improvement is obviously somewhat less then the counting factor of 10^6 since the measurements are extremely correlated but remains extremely important. For example, in Chapter 4 we will discuss algorithms which spoil the homogeneity of the lattice and in most cases the associated drop in statistics is crucial in determining their success or failure.

Having thus said that we wish to calculate all possible orientations of observables O on the lattice, one is left with another tricky problem in the organisation of such a task. This would be hard enough in three dimensions but with the fourth dimension making ones intuition somewhat less reliable and with the extra complication of the boundaries between the processors it becomes particularly difficult. However, an elegant and simple solution to this problem is available [21].

Take, for example, the measurement of a rectangular Wilson loop with extents 2 and 3 units in orthogonal lattice directions. This loop is shown in a uniprocessor environment in Fig. 3. Note that we assume periodic boundary conditions so that the loop is allowed to wrap around the edge of the lattice. A particularly simple explanation of the adopted algorithm is to introduce some fictitious creature, 'Fred, the mathematical fly' who will perform the operations leading to the required result. We start off by placing Fred at point A in the lattice, carrying an identity matrix. We then issue simple instructions such as 'Move in the positive x-direction' or 'Move in the negative z-direction'. On each command Fred flies to the appropriate lattice site picking up the matrix over which he flies and

multiplying it into his current product. Obviously we have to build in the boundary conditions by having Fred fly, for example, from B to C upon encountering a boundary, but this is essentially trivial. Finally when Fred reaches point A again, his accumulated product is the required matrix.

The extension of this algorithm to a parallel environment is also easy. As emphasised before, the homogeneity of the lattice allows all processors to carry out the same calculation on their own private data. Thus one simultaneously calculates the equivalent loop in all processors as shown in Fig. 4. In order to achieve this we merely have to modify Fred's behaviour upon reaching a sublattice boundary such as point B. Whereas in the sequential case we would have Fred fly to point C′ and continue, we now have him fly into the communication channel connecting the processors, emerging at point C. The process then carries on as before with Fred in a different processor. Finally, since all paths must be closed, Fred will return to his starting point in his own processor carrying the desired result.

While the above example might seem rather 'silly' it does serve to show how simply one can modify sequential code in order to take advantage of the parallel machine. It also shows how the lattice gauge simulations are more or less ideally suited to these machines. (Indeed, in some sense they may be said to have promoted their development.) However, various technical difficulties remain. As new algorithms are developed care must be taken that they do not conceal features which reduce the 'efficiency' of the computation. It would be disastrous, for example, to build a machine with ten times the number of processors and then find that a speed-up of only two were possible. Also attention must be paid to the locality and homogeneity of the algorithms. As stated above the lattice theory described here is almost ideal for our machines although we shall discuss a minor source of inefficiency in Section 3.1 and Appendix A.

2.3 - Generation of Lattice Configurations

In this section will be discussed the methods used to generate configurations of link variables. This is one of the more complicated questions in lattice gauge theory and in keeping with the introductory nature of this chapter we will merely explain the principle of each of the more popular methods leaving the details for later chapters.

2.3.1 The Monte Carlo Method and Markov Chains

This particular approach to lattice QCD was the first used and is inspired by the observation that physical quantities, measured in terms of a lattice observable, O, require the evaluations of integrals of the form

$$\langle O \rangle = \frac{\int [dU]\ O(U)\ e^{-\beta S(U)}}{\int [dU]\ e^{-\beta S(U)}} \tag{2.18}$$

For the Wilson action, Eq. (2.9), $S(U) \geq 0$ for all possible gauge configurations and hence $e^{-\beta S(U)}$ can be treated as a probability density. Then Eq. (2.18) takes the simple form of the normalised expectation value of $O(U)$ in a set of gauge fields with the Boltzmann distribution $e^{-\beta S(U)}$. It can thus be calculated by constructing a set of appropriately distributed gauge configurations $\{U_1\},\{U_2\},\{U_3\},\cdots$ and evaluating the quantity

$$\langle O \rangle = \lim_{N\to\infty} \frac{1}{N} \sum_{i=1}^{N} O(\{U_i\}) \tag{2.19}$$

which is exactly of the form Eq. (2.17).

The non-trivial task at hand is the construction of the sequence of gauge configurations. To do this we appeal to the Markov chain procedure [22].

Given a configuration $\{U_i\}$ we generate another, $\{U_j\}$ with probability W_{ij}. Following this procedure guarantees that the asymptotic distribution of the configurations will be the

correct Boltzmann as long as the transition probabilities satisfy the condition of 'Detailed Balance'

$$\frac{W_{ij}}{W_{ji}} = \frac{e^{-\beta S(U_j)}}{e^{-\beta S(U_i)}} \tag{2.20}$$

Less formally stated this condition simply requires that in equilibrium the rate of transition from $\{U_j\} \rightarrow \{U_i\}$ is equal to that from $\{U_i\} \rightarrow \{U_j\}$.

Two simple methods of satisfying this constraint are commonly used. In the Metropolis method [23] a 'trial move' is made from the current configuration $\{U\}$ to a new one $\{U'\}$. One then calculates the quantity

$$\Delta S = S(\{U'\}) - S(\{U\}) \tag{2.21}$$

and allows the move to stand if $\Delta S < 0$. If this is not the case the move is rejected with probability

$$P_{rej} = (1 - e^{-\beta \Delta S}) \tag{2.22}$$

It is simple to show that this strategy indeed fulfills the detailed balance condition. Its weakness, however, lies in the fact that if $\{U\}$ and $\{U'\}$ are totally uncorrelated then the probability of rejecting $\{U'\}$ becomes large and as a result the fields evolve slowly. The common way of avoiding this problem is to chose $\{U'\} = \{U + \Delta U\}$ with ΔU small in some appropriate sense. Unfortunately this results in field configurations which are strongly correlated.

The second method of satisfying detailed balance is the heat bath in which one choses the new configuration $\{U'\}$ with probability $e^{-\beta S(U')}$ independent of the old configuration $\{U\}$. Using this method, which trivially satisfies the detailed balance requirement, successive configurations are completely independent and the simulation can explore its

phase space considerably faster than in the Metropolis method. The difficulty with this method is that it is typically very hard to invert the density function $e^{-\beta S(U)}$ and in fact the only genuine heat bath in use in lattice gauge theory is for the gauge group SU(2). We will return to this in more detail when we discuss the 'pseudo' heat bath in Section 3.1.

2.3.2 - The Langevin Algorithm

The Langevin equation was first studied in the context of Brownian motion [24,25] and its range of application is extremely wide, from the abstract study of diffusive processes on arbitrary manifolds to the study of emissions from lasers [26]. Since we will be discussing this algorithm in great detail in Chapter 4 we merely exhibit at this point the relationship between the simple Langevin equation and the condition of detailed balance stated in the last section.

The Langevin equation for a field ϕ described by an action $S(\phi)$ is given by

$$\frac{\partial \phi}{\partial \tau} = -\frac{\partial S}{\partial \phi} + \eta \tag{2.23}$$

where η is a Gaussian fluctuation normalised by the condition

$$\langle\langle \eta(t)\, \eta(t') \rangle\rangle = \delta(t - t') \tag{2.24}$$

in which the angle brackets denote averages over the fluctuations. In order to best show the above mentioned relationship we discretise time τ in Eq. (2.23) leading to

$$\phi(\tau + \delta\tau) = \phi(\tau) - \delta\tau \frac{\partial S}{\partial \phi} + \sqrt{2\delta\tau}\, w \tag{2.25}$$

where w is now a Gaussian random number with zero mean and unit width.

Using the fact that w has the distribution function

$$P(w)\, \mathrm{d}w = e^{-1/2\, w^2}\, \mathrm{d}w \tag{2.26}$$

it is easy to show that the probability of transition $\phi(\tau) \rightarrow \phi(\tau')$, $P_{\tau \rightarrow \tau'}$ satisfies (with $\delta\tau = \tau' - \tau$)

$$\frac{P_{\tau \rightarrow \tau'}}{P_{\tau' \rightarrow \tau}} = \exp\left\{ -\left[\phi(\tau') - \phi(\tau)\right] \frac{\partial S}{\partial \phi} + O(\sqrt{\delta\tau}) \right\} \tag{2.27}$$

Detailed balance is indeed satisfied to first order in $\sqrt{\delta\tau}$ and hence the sequence $\phi(\tau)$, $\phi(\tau+\delta\tau)$,ϕ $(\tau+2\delta\tau)$, $\cdots$ is Markovian and the conclusions of the previous section apply.

We finally note in this respect that the condition of detailed balance is sufficient but not necessary for the asymptotic fields to have the correct Boltzmann distribution. In fact the Langevin equation discussed here describes a process which, in general, does not satisfy this condition but which still generates the correctly weighted ensemble averages in the limit $T \rightarrow \infty$.

2.3.3 - The Micro-Canonical Method.

The above methods are distinguished by the fact that they operate in the classical canonical ensemble of statistical mechanics, i.e., we calculate directly the path integral with Boltzmann factor $e^{-\beta S(U)}$. In considering the microcanonical approach [27] we introduce a fictitious time, τ, as in the Langevin procedure, and a Hamiltonian, H, defined by

$$H = p^2 + S(U) \qquad\qquad p \equiv \frac{\partial U}{\partial \tau} \tag{2.28}$$

If we were to use this definition of H and evaluate the partition function over the phase space $[\mathrm{d}p\,\mathrm{d}U]$ with weighting $e^{-\beta H}$ we would simply recover Eq. (2.8) since the integral over p is quadratic. This is again the conventional canonical ensemble. To pass to the microcanonical formalism one fixes the total energy of the system to be a constant, E, and integrates instead over the phase space $[\mathrm{d}p\,\mathrm{d}U]\,\delta(H-E)$. It is easy to show that long time averages

$$\langle O \rangle = \frac{1}{T} \int_0^T O(t)\, \mathrm{d}t \tag{2.29}$$

evaluated in the canonical and microcanonical ensembles differ only by corrections of order $1/V$, where V is the lattice volume [28].

The advantage of the microcanonical approach is that the system is conservative and hence Hamilton's equations can be solved

$$\dot{p} = -\frac{\partial H}{\partial U} \qquad \dot{U} = \frac{\partial H}{\partial p} \tag{2.30}$$

to study the dynamical behaviour. Being fully deterministic these equations are more easily solved numerically than the equivalent Langevin equations.

Unfortunately, as it stands this scenario has two disadvantages. Firstly the temperature β is only determined empirically by appealing to the equipartition theorem. Recent research has provided a possible resolution to this problem by introducing additional degrees of freedom which act as a heat sink and thus allow the temperature to be externally adjusted [29].

The second problem is as yet unresolved and is rather more serious. The expression for the long-term average given in Eq. (2.29) relies upon the assumption of ergodicity, i.e., that the system in time explores its entire phase space. Unfortunately, given the deterministic nature of the microcanonical equations this can no longer be guaranteed and hence one must be slightly wary of these simulations. A recent development is the 'hybrid' scheme [30] which is a cross between the Langevin and microcanonical approaches and is explicitly ergodic.

Briefly then, these are the approaches most often used in lattice gauge theory simulations. Each has advantages and disadvantages and is most appropriate for a particular kind of problem. All however suffer from a particular weakness of the Monte Carlo method

first noticed by Binder [31]. In the vicinity of phase transitions the dynamics of the Monte Carlo process itself become very slow, independent of the particular method being used, a process known as 'critical slowing down'. Its relevance to QCD can most easily be seen by considering some physical quantity such as the pion mass, m_π. In our simulations such physical quantities are typically extracted from two point functions of some operator, O, as

$$\langle 0 | O(T)\, O(T+\delta T) | 0 \rangle \simeq e^{m_\pi \delta T} \tag{2.31}$$

Given the fact that $T \equiv ta$ in terms of the lattice spacing, it is clear that the dimensionless quantity ma plays a role similar to the inverse correlation length, ξ^{-1}, of the equivalent statistical system. However, we know that the continuum limit is $a \rightarrow 0$ and that the pion mass, $m_\pi = 140$ MeV, is in fact finite. Thus we must conclude that in the continuum limit $\xi \rightarrow \infty$, i.e., we are at a phase transition of the statistical system and the problem of 'critical slowing' is very real. An interesting scheme which has some chance of reducing this problem will be discussed in Section 5.0.

This chapter has attempted to provide a fairly swift introduction to the methodology of lattice gauge theory. As the field is still developing, with new techniques to combat problems of one kind or another, it is quite difficult to present 'best' algorithms or results. In the following chapters, therefore, we concentrate on specific details and results which seem interesting. Some of the work presented here is thus of an exploratory nature rather than being definitive, the exception to this being the next chapter where we present a set of state-of-the-art calculations into the properties of heavy quarks.

CHAPTER 3

Heavy Quarks in the Quenched Approximation

Quantum Chromodynamics (QCD) is the gauge theory that is applied to the study of the strong interactions. Its fundamental constituents, at the most elementary level, are an exact SU(3) colour symmetry and a badly broken SU(6) flavour symmetry from which it is hoped that the properties of the physical world will emerge. Although the theory is, for the most part, analytically intractable it has already met with considerable success in various approximations. At high energies, for example, the property of asymptotic freedom [4] reduces the quark-gluon coupling to a value where perturbation theory should hold and in this case the three colours of quarks neatly explain the rate for the decay $\pi^0 \rightarrow 2\gamma$ [32]. Furthermore, the charges and masses of the quarks in the broken flavour symmetry account for the regular structure seen in the ratio of total cross sections [33]

$$R = \frac{\sigma\,(e^+e^- \rightarrow \textit{hadrons})}{\sigma\,(e^+e^- \rightarrow \mu^+\mu^-)} \tag{3.1}$$

At the opposite extreme, strong coupling expansions in lattice gauge theory [17] predict that quarks are permanently confined into hadrons by a potential which increases linearly with the interquark separation.

In this chapter we attempt to extract some of the properties of QCD at intermediate couplings. Important questions to be addressed involve the existence of a confining interquark potential in mesons and baryons, and the mechanism generating such a potential. Also to be discussed is the origin of the Coulombic force between quarks and the detailed structure of the baryon. From the standpoint of the lattice method itself we examine the question of the continuum limit and the restoration of continuous rotational symmetry at finite lattice spacings.

In order to perform these calculations we make two initial restrictions. Firstly, attention is restricted to heavy quark systems in non-relativistic motion. Since the vast majority of known hadrons are made of light quarks (u, d, s) this might at first sight seem to be a significant error. However, the discovery in 1974, of the J/ψ [34] and later of the Υ [35] provided a perfect setting in which to test the predictions of such lattice gauge theory calculations. These particles are supposedly bound states of very heavy charmed and bottom quarks, systems entirely analogous to positronium and the hydrogen atom. It is thus reasonable to assume that they may be modeled by a simple non-relativistic potential. Typically in such calculations a functional form is assumed for the potential and then parameters are adjusted to fit experimental data. In this chapter, however, we will be able to calculate directly from the Lagrangian some of the properties of such models. The lattice forms a natural environment in which to perform an expansion in inverse powers of m, the heavy quark mass [36], and we concentrate mainly on the leading (spin independent) term. Higher order corrections yielding spin-orbit and spin-spin effects have also been attempted and are discussed in Section 3.6.

The second major departure from the full theory of QCD lies in the adoption of the quenched approximation. In order to more fully understand this simplification we introduce the QCD Lagrangian density

$$L = F_{\mu\nu}F^{\mu\nu} + \sum_{i=1}^{N_f} \bar{\psi}_i (\not{D} + m_i) \psi_i \tag{3.2}$$

where $F_{\mu\nu}$ is the gauge field energy density introduced in the previous chapter and N_f is the number of flavours of quarks, with masses m_i, which are described by four component Dirac spinors ψ_i. $\not{D}$ is the covariant derivative and so depends directly on the gauge fields themselves.

Now consider some physical quantity described by a lattice operator O and thus measured by

$$\langle O \rangle = \frac{\int [dU] [d\psi] [d\bar{\psi}] \, O(U) \, e^{\int -\beta F_{\mu\nu}F^{\mu\nu} + \bar{\psi}(\not{D} + m)\psi}}{\int [dU] [d\psi] [d\bar{\psi}] \, e^{\int -\beta F_{\mu\nu}F^{\mu\nu} + \bar{\psi}(\not{D} + m)\psi}} \tag{3.3}$$

Since the integration over the (Grassman) variables $\psi,\bar{\psi}$ is Gaussian it can be calculated exactly yielding

$$\langle O \rangle = \frac{\int [dU] \ \mathrm{Det}\,(\not{D} + m) \ O(U) \ e^{-\beta \int F_{\mu\nu}F^{\mu\nu}}}{\int [dU] \ \mathrm{Det}\,(\not{D} + m) \ e^{-\beta \int F_{\mu\nu}F^{\mu\nu}}} \tag{3.4}$$

The "quenched" approximation is then to take the determinant in Eq. (3.4) as a constant dividing out of numerator and denominator and leaving the path integral of the pure Yang-Mills theory discussed previously, Eq. (2.8).

The numerical motivation for such a procedure is very strong. The determinant represents an extremely complicated function of the gauge fields and renders simulations at least an order of magnitude more difficult. Its inclusion in a dynamical way is an area of

active research about which we will have more to say in Chapter 5. Attempts to include the effects of the determinant by redefining the operator $O(U)$ are also possible but typically unsuccessful. (See Chapter 4.)

Fortunately, our neglect of the determinant in Eq. (3.4) can also be justified on physical grounds. The particular effect of including this term is to generate vacuum polarisation - i.e., internal light quark loops. Our neglect of these effects can be seen to be adequate by considering the huge success of the static quark picture of hadrons. In this model hadrons are composed of two (mesons) or three (baryons) 'valence' quarks and an undetermined number of pairs of light 'sea' quarks. Nearly all of the properties of the hadrons are then explainable in terms of the interactions of the 'valence' quarks. For example, while it is true that QCD explains very accurately the deviations from scaling in deep inelastic scattering experiments, a phenomenon associated with the 'sea' quarks, it is also true that over a vast energy range (roughly $2\ \text{GeV}^2 < q^2 < 200\ \text{GeV}^2$) the scaling functions behave as though only the 'valence' quarks were present.

A second motivation comes from consideration of the string models of hadrons [37] wherein quarks are bound together by 'flux tubes' of constant tension. This picture leads simply to the prediction of linearly rising Regge trajectories with a universal slope for both mesons and baryons. The effect of vacuum polarisation would be to enhance the string's tendency to break leading to irregularities in the Regge paths. That such effects are not observed is evidence in favour of our approximation.

Finally we consider what effects this assumption might have on the questions that we sought to answer concerning the Coulombic and confining parts of the interquark potential. The former is supposedly dominated by single gluon exchange whilst the latter is probably the result of multiple gluon exchanges (See Fig. 5) both (presumably) qualitatively accounted for by the Yang-Mills theory. We might expect that charge renormalisation due to vacuum polarisation might have a quantitative effect on the single gluon

exchange and we shall discuss this point more in Section 3.7 when we compare the lattice parameters with experimental results.

Having thus introduced the questions we wish to address and having justified our approach we turn to the details of the calculations themselves. The rest of this chapter is then arranged as follows. In Section 1 the specific details of the lattice calculation are presented. Then in Sections 2 and 3 properties of mesonic systems are investigated with an eye on the scaling behaviour of the quark potential and the restoration of rotational symmetry. In Section 4 these calculations are extended to the baryonic sector and a comparison of two common string models is undertaken. In Section 5 the energy density in both mesonic and hadronic systems is investigated with a view to understanding the mechanism which confines the quarks. In Section 6 higher order corrections to the potential are introduced and in Section 7 the relevance of these calculations is discussed in the light of experimental data.

3.1 The Lattice Calculation

Most of the calculations in this chapter are made by measuring different observables on the same set of lattice configurations, so it makes sense at this point to discuss the parameters and methods by which these were generated.

The particular lattice size chosen is 20^4 which is the largest which fits within the physical memory of our computer. As such it may be considered a large lattice in the sense that it contains many lattice sites. The physical size of the space-time volume is, however, dependent on the coupling β according to some renormalisation function. In practice we will assume that the two loop perturbative result holds (c.f. Eq. (2.13))

$$\xi = ca \left[\frac{8\pi^2\beta}{33} \right]^{-51/121} \exp \left(\frac{4\pi^2\beta}{33} \right) = \frac{c}{\Lambda_L} \tag{3.5}$$

$$\Lambda_L = \text{constant.}$$

although one of our goals is to provide a consistency check on the range of validity of this expression.

Given that we wish to model real physical processes on this lattice, the range of couplings at which calculations can be made is restricted. At low coupling the lattice is very coarse and continuum symmetries are badly broken. Conversely at high coupling the lattice models only a small piece of physical space and large finite size effects are encountered. In particular the system undergoes a phase transition at finite β in which quarks become deconfined and a quark-gluon plasma results. Given that one of our goals is to study the confinement mechanism it is obviously important that one stay below this transition. Previous studies have shown that lattice artifacts begin to disappear at couplings $\beta \gtrsim 5.7$. In particular the discrete rotational symmetry of the lattice becomes less noticeable [38] and approximate scaling of the deconfinement transition [39] set in, although this does not satisfy the asymptotic form, Eq. (3.5), until $\beta \gtrsim 6.1$ [40]. This last criteria is, however, somewhat unreliable since it is extremely difficult to locate the first order phase transition especially in the light of earlier comments about the performance of Monte Carlo algorithms near phase transitions. (For a discussion of two major efforts in this direction see [41].)

In order to avoid the worst of these effects we choose to work at couplings significantly higher than $\beta = 5.7$. In order to avoid the deconfinement transition, however, we have to extrapolate the data from smaller lattices to our 20^4 lattice using the perturbative scaling function, Eq. (3.5). This leads us to believe that a 'safe' upper coupling limit is $\beta = 6.7$ and as a result we have chosen to calculate at the four couplings $\beta = 6.1$, 6.3, 6.5 and 6.7.

At each coupling we generated lattice configurations by the 'pseudo' heat bath algorithm. As mentioned in the previous chapter the only genuine heat bath is for gauge group SU(2) but Cabibbo and Marinari [42] devised a scheme by which this algorithm could be applied to arbitrary SU(N), $N \geq 2$. Briefly the method is as follows.

Consider M SU(2) subgroups of SU(N) defined by deleting all but two rows and columns of the SU(N) matrix. Then consider the update move $U \rightarrow U'$ where

$$U' = u_M \, u_{M-1} \, u_{M-2} \cdots u_2 \, u_1 \, U \tag{3.6}$$

and the $\{ u_k \ ; \ k=1, \cdots, M \}$ are matrices, generated by the SU(2) heat bath which act in the relevant subgroup of SU(N) . This algorithm defines a single link 'hit', i.e., the process by which each link in a given configuration is updated. The process in which each link in the lattice is updated once is termed a 'sweep'. Note that this algorithm is not a true heat bath since the new matrix U' does in fact depend on the old value U. It does, however, have a significantly smaller sweep to sweep correlation than the Metropolis method. As a final point in this regard it should be noted that the conventionally applied SU(2) heat bath has a weakness when used on massively parallel computers of the type described in Section 2.2. This yields some inefficiency and is discussed more fully, together with some simple solutions, in Appendix A.

The lattices used in our calculations were generated from approximately 850 full sweeps using the above heat bath with hits in all three SU(2) subgroups. The first 350 sweeps were discarded for thermalisation purposes. (At each value of β we derived the new set of lattices from the previous β-value, except that the lattices with $\beta = 6.3$ were derived from a cold start - i.e., all link matrices equal to the identity). Over the next 500 sweeps each 25^{th} lattice was saved yielding 20 independent configurations at each value of β. In order to check that equilibrium had indeed been reached at each β-value we checked for a systematic trend in Wilson loop values and found none.

In order to reduce statistical errors in the measured observables we also applied the variance reduction technique of Parisi et al. [43]. Basically this method involves averaging the gauge variables over several 'hits' when measuring observables. This has the effect of integrating out certain degrees of freedom. For example if we were calculating the trace of the path ordered product of links

$$O = \mathrm{tr}\, U_1 U_2 U_3 \cdots U_n \tag{3.7}$$

then we would replace some of the links U_i by averages obtained over several heat bath 'hits' at that site with all its neighbouring links held fixed.

$$O = \mathrm{tr}\, \bar{U}_1 \bar{U}_2 \bar{U}_3 \cdots \bar{U}_n \tag{3.8}$$

where

$$\bar{U}_j = \frac{1}{k} \sum_{i=1}^{k} U_j^{(i)} \tag{3.9}$$

with the superscript (i) denoting 'hits'. This process might seem strange since the $\bar{U}$ matrices are not even elements of SU(N) but expansion of the sum, Eq. (3.8), yields a set of terms each of which corresponds to a configuration which could have been reached without violating the detailed balance condition, and thus the algorithm is actually exact. Naively one might imagine that the reduction in statistical errors be by a factor of $\sqrt{k^n}$ due to the number of terms in the expanded sum. Unfortunately there are significant correlations among the terms but typically one is still able to achieve an improvement by an order of magnitude using this technique.

Note that above we said that only some of the links would be replaced by their averages. In implementing this technique one has to be careful not to 'bar' links which are coupled directly by the action, S, since to do so would generate terms in the expansion, Eq. (3.8) which could not be reached without violating detailed balance. For the Wilson

action this means that all the links along the sides of a rectangular loop can be barred *except* those at the corners. If we had chosen to include larger loops than simple plaquettes in our action then the application of the Parisi trick would be more complicated.

3.2 The Mesonic Potential

As a first calculation on these lattices we looked at the mesonic $q\bar{q}$ potential. This quantity has been extensively studied in the literature, both in strong coupling [17,44] and Monte Carlo calculations [45], and as such it provides a useful benchmark and testing ground. A further possibility is that we might be able to examine the scaling behaviour of the theory on a large lattice [46]. This is especially important since it has been suggested that the scaling limits discussed in the previous chapter might be too low and that asymptotic scaling is not realised until $\beta = 7.2$ [47].

In order to understand the potential observable consider the following process. At $T = 0$ two quarks are created and instantaneously separated to a distance of R lattice spacings. They are then allowed to evolve for a time T, without moving, and then come together and annihilate. The world lines of the two quarks are shown in Fig. 6. Note that we have to arrange that the quarks are created and destroyed in a gauge invariant manner consistent with being colour singlet states. The simplest way to do this is to form the Wilson loop operator

$$W(R,T) = \mathrm{Re}\ \delta_{ij}\delta_{pq}\ U^{q}_{ip}\ U^{\bar{q}}_{jq} \tag{3.10}$$

In this expression the real part is taken because the two quarks can be interchanged leading to a term the complex conjugate of the original.

We can connect this object with the static quark potential by appealing to the Hamiltonian form of the theory in which the transition matrix evolving the system from time T to $T + \delta T$ is just

$$\hat{T} = e^{H \delta T} \tag{3.11}$$

Noting that $H = p^2/2m + V$ is the non-relativistic Hamiltonian relevant to heavy quarks yields the simple result that

$$W(R,T) = e^{-V(R)\,T} \tag{3.12}$$

in the limit $m \to \infty$.

We thus see that the potential is measured by calculating the expectation values of many Wilson loops and fitting to the functional form, Eq. (3.12). This is to be contrasted with the alternative approach in which the world lines of the quarks are taken to be Polyakov lines closed by means of the periodic boundary conditions. In this approach one obtains only one data value for each value of the temporal lattice size T which leads to greater difficulty in assessing statistical errors than the above approach in which these can be estimated by assessing the degree to which the data fits Eq. (3.12).

The restrictions on the loops which can be used in these measurements can be deduced by considering the quantity

$$\begin{aligned} \langle 0 \,|\, W(R,T) \,|\, 0 \rangle &= \langle 0 \,|\, e^{-V(R)T} \,|\, 0 \rangle \\ &= \sum_n \langle 0 \,|\, e^{-V(R)T} \,|\, n \rangle\langle n \,|\, 0 \rangle \\ &= \sum_n |\langle 0 \,|\, n \rangle|^2 \; e^{-V_n(R)T} \end{aligned} \tag{3.13}$$

where $\{\,|\,n\rangle\,\}$ is a complete set of energy eigenstates.

Thus we can see that excited states also enter into the measured quantity but are suppressed by at least $e^{-\delta VT}$ where δV is the energy gap between the ground state and first excited state. We thus expect that in the $T \to \infty$ limit the Wilson loop measures the static potential between a $q\bar{q}$ pair in their ground state. It is typically observed, however, that in lattice calculations the above condition on T can be relaxed to $T \geq R$ and this is indeed true in our case.

The adopted procedure then, is to measure expectation values of Wilson loops and then extract lattice potentials $V_l(R)$ according to Eq. (3.12). The subscript l here is to denote that these potentials are still specific to a certain lattice spacing a. Results of this process at each of the four couplings considered are shown in Table 1.

The next stage is to combine the data from individual β-values by rescaling. A convenient method of performing this calculation is to introduce a lattice correlation length, ξ, defined by Eq. (3.5). In this expression we chose the value $c = .011$ which has the virtue that it leads to a correlation length that takes reasonable values when expressed in terms of the string tension K. Now introduce dimensionless potentials $\tilde{V}(x)$ defined by

$$\xi V(R) = \tilde{V}(x) / x \qquad \text{where} \quad x = R/\xi \tag{3.14}$$

This is the point at which we can test the perturbative scaling relation. If this were correct the rescaled data would now lie on a smooth curve when plotted against the scaling variable x. Our data yields the curves shown in Fig. 7. The point that has been overlooked is the quark self-energy contribution to the potential. Each lattice potential V_l contains a lattice spacing dependent additive self-energy contribution which should be subtracted out.

One way of performing such a subtraction is to note that since this effect is constant for each lattice spacing it has no effect on the interquark force $\partial V/\partial x$. We could thus calculate the forces at each β-value and integrate back to obtain the potential. This approach

was successfully used in a previous calculation [48]. A simpler method, however, is to merely manipulate the vertical offsets of the various data-sets until a smooth curve is obtained. In order to quantify this 'smoothness', however, we must turn to a phenomenological model of the potential.

At large distances it is supposed that quarks are confined into hadrons by a linearly rising potential. Conversely at short distances the leading contribution is expected to be from single gluon exchange. As a result one expects the potential to follow the form

$$\tilde{V}(x) = \alpha/x + V_0 + Kx \tag{3.15}$$

We can thus quantify 'smoothness' by adjusting the subtractions until our potential is best fit to this form. This procedure results in the curve shown as Fig. 8.

At first glance this data looks quite reasonable. The points do in fact lie upon a relatively smooth curve. This is not surprising and merely confirms once again the conclusions of earlier studies. However closer inspection of the data reveals some interesting points. In Table 2 are shown the χ^2 values for the fits of various combinations of data sets to Eq. (3.15). Along the diagonal are the values for individual fits to this form and as can be seen the agreement is excellent. However, in the off-diagonal elements are shown the results of pairwise fits. These values are rather large considering the numbers of degrees of freedom involved and the situation deteriorates dramatically when further β values are included. The final χ^2 for all four sets is over 50 - a totally unreasonable value.

The resolution of this disaster is hinted at by Fig. 9. There we take the data sets and show their individual best fits to Eq. (3.15). As can be clearly seen each data set shows slightly more curvature than would be required to form a smooth curve, the effect becoming more pronounced as β increases. This, however, is just the effect which might be expected as the deconfining transition approaches. The string tension is decreasing, finally becoming zero at the transition itself, making the curves roll over faster at large distances.

This is indicative that the asymptotic scaling assumption, Eq. (3.5) is breaking down at these β values - we are not entirely within the continuum limit.

The implications of this fact for lattice gauge theories are quite significant. In particular it means that we are not able to reliably extract quantitative results from our calculations on such small lattices at these intermediate couplings. However, it does point the way to future detailed calculations. If one could generate extremely accurate data for the potential then there would be the possibility of deriving the real scaling behaviour of the lattice at these couplings. Specifically one could define a correction factor $\gamma(\beta)$ such that

$$x' = \gamma(\beta)\ x \tag{3.16}$$

and then try to fit the function $\tilde{V}(x')$. In this way the factor $\gamma(\beta)$ should be calculable and hence real quantitative results extracted. This calculation was in fact attempted on the data presented here but without success - the β values at which we have measurements are too widely spaced and the statistical errors too large to allow reliable calculations.

Having made the point that quantitative predictions from lattice QCD seem to elude us, it must be stressed that valuable lessons can still be learned from these calculations. Since the deviations from scaling behaviour seem to be small it is certainly true that approximate physical quantities can be measured albeit with rather uncertain errors. We can also obtain important qualitative results. For example, the fact that the string tension is measurably non-zero lends support to the idea that quenched QCD confines quarks. One can also make useful comparisons between different lattice systems, such as the meson and baryon, and we shall make extensive use of this in future sections.

One particularly intersting parameter is α, the coefficient of the Coulombic force in Eq. (3.15). The origin of this term is somewhat controversial. While at high energies it is expected that the dominant contribution will be from single gluon exchange yielding a contribution (α_S is the running coupling constant)

$$V \sim -\frac{4\alpha_S}{3R} \tag{3.17}$$

at lower energies the theory is supposedly described by a simple vibrating string model [49] in which transverse oscillations generate a potential [50]

$$V \sim -\frac{\pi}{12R} \tag{3.18}$$

independent of the gauge group. Since α is a dimensionless number it is modified from our lattice calculations only by the correction factor $\gamma(\beta)$ and so we might hope to address this question with some degree of confidence. The best fits to the data yield the value

$$\alpha = -.29 \pm .04 \tag{3.19}$$

remarkably close to the value $-\pi/12 = -.26$. The exact status of this parameter and the applicability of the string models is, however, in some question [51] and we shall return to this point after looking at the baryonic potential.

As a final point in this discussion we examine the form of the chosen fit. Given the ansatz, Eq. (3.15), for the overall form of the potential the exponent of Eq. (3.12) is seen to be

$$V(R)T = \alpha T/R + V_0 T + K\,RT \tag{3.20}$$

which is asymmetric in R and T despite the fact that the lattice is completely invariant under the interchange $T \leftrightarrow R$ and thus distinguishes no particular directions. It has been suggested therefore [52] that one should fit instead to the symmetrised form

$$\alpha(T/R + R/T) + V_0\,(R+T) + K\,RT \tag{3.21}$$

leading to the Wilson loop value

$$W(R,T) = e^{-V(R)T + f(R)/T} \tag{3.22}$$

with f an arbitrary function of R only.

We examined this procedure and found that in all cases it yielded worse fits to our data than the simpler alternative, Eq. (3.12). This approach is also somewhat questionable theoretically since it involves an assumption about the exact form of the potential while the earlier method is based merely on the analogy with the Hamiltonian system. For such reasons we will not consider it further.

3.3 Restoration of Rotational Symmetry.

One of the primary goals of this chapter is to compare the properties of mesons and baryons as determined in lattice gauge theory. However in doing so one comes across one of the fundamental problems of the lattice regulator - namely that of discrete symmetries. The mesonic potential discussed in the previous section seemed to pose no problems since the Wilson loop observable corresponding to the potential lay nicely in a lattice plane and the only requirement was that the latticised theory be insensitive to details at the scale of the lattice spacing, a. In treating baryons, however, another problem arises since the observable used to measure the three quark potential is no longer planar and hence the discrete rotational symmetry of the lattice must be considered. Previous calculations have shown [38,52] that continuous rotational symmetry is approximately restored at $\beta \gtrsim 5.7$ and indeed this was one of our criteria for choosing the couplings at which to carry out these calculations. However, since we wish to carry out a quantitative comparison between the latticised mesonic and baryonic systems we need to calculate the systematic

errors associated with the discrete symmetry at our higher couplings, verifying that such effects are indeed small [53].

In order to achieve this we return to the mesonic calculation of the last section but consider the so called 'off-axis' Wilson loops $W(R1,R2;T)$ such as the one shown in Fig. 10. In principle the potential should be insensitive to the details of the loops at the scale of the lattice spacing and one should be able to extract quantities whose dependence on the quark separation is determined solely by the distance between temporal world lines rather than the path length used to join them.

Note that care must be taken in applying the Parisi trick to configurations such as these. Specifically, links can be barred in only one of the two spatial directions. There are thus more unbarred links in these observables than in the planar observable of corresponding size and statistical errors are larger.

The results of calculating various 'off-axis' lattice potentials are shown in Table 3. These have been extracted using Eq. (3.12) and scaled according to Eqs. (3.5) and (3.14) with $c = .011$ as before, but no self-energy subtractions have been done. This is because we are predominantly interested in seeing how the distortions due to discrete symmetry behave as β increases and the lattice spacing, a, decreases. Furthermore attention has been restricted to the two lower β-values, $\beta = 6.1,6.3$, which suffered from less severe finite volume effects in the previous section.

In order to quantify the systematic errors the calculated potentials are fitted to two differing functional forms. If the lattice calculation is indeed insensitive to the lattice spacing then we expect that the potential will be given by Eq. (3.15) with x the actual quark separation neglecting the lattice.

$$x \equiv x_{pyth} = \frac{1}{\xi}\sqrt{R1^2 + R2^2} \tag{3.23}$$

Effects due to the discrete symmetry are expected to contribute a term to the potential derivable in strong coupling as

$$\delta\tilde{V} = K' x' \tag{3.24}$$

where

$$x' \equiv x_{taxi} = \frac{1}{\xi}(R1 + R2) \tag{3.25}$$

is the 'taxi-cab' metric corresponding to the strong coupling force where the confining flux tubes are constrained to lie along lattice links. By fitting the data to forms both with and without the strong coupling piece, Eq. (3.24), one can then assess the quantitative effect of the lattice's discrete symmetry on the physical string tension, K.

The results of such a comparison are shown in Table 4. As can be seen the string tension suffers modifications of around 15 % at $\beta = 6.1$ but is apparently insensitive at the higher coupling $\beta = 6.3$. The overall conclusions to be drawn from this study, therefore, are quite encouraging. As expected, the deviations in physical parameters due to discrete rotational symmetry are quite small and in particular the systematic error in the string tension is less than 1% at $\beta = 6.3$. This fact will enable us to directly compare mesonic and baryonic properties in the next section.

3.4 The Baryonic Potential

The calculation of the heavy baryonic potential [54] might at first seem to be a wasted effort since heavy baryons analogous to charmonium have not been detected experimentally. However the calculation is important for several other reasons. Firstly, it is crucial to know if the lattice theory is consistent in predicting similar properties for both types of hadron. In particular one expects the string tensions to be the same in both

systems, given a sensible picture of the internal string configuration in the baryon. This question leads directly to the second point - namely that potential models of baryons, both non-relativistic [55,56] and more recently relativised [57,58], are extremely successful in predicting the spectrum of known states, even in mass ranges where it might be expected that such models are inappropriate. It is thus important to see if the physical parameters extracted from the lattice calculation bare any resemblance to those used in these models. Obviously such a calculation can at best be approximate given that the scaling behaviour of the lattice theory is unclear but reasonable agreement can hopefully be reached. We consider this last question in more detail in a later section, restricting attention here to a comparison of mesonic and baryonic parameters as deduced from the lattice.

To construct the lattice operator, analogous to the Wilson loop, from which we may extract the baryonic potential an obvious generalisation is made. Consider the products

$$U^{(i)} = \prod_{l \in C_i} U_l \tag{3.26}$$

where the matrices U_l lie along the world lines C_i of the i^{th} quark ($i = 1,2,3$). As before, the leading term in the $1/m$ expansion requires these world lines to be straight. Finally the ends have to be closed off in a manner consistent with the colour singlet constraint yielding the observable

$$Q = \epsilon_{ijk}\, \epsilon_{pqr}\, U^{(1)}_{ip}\, U^{(2)}_{jq}\, U^{(3)}_{kr} \tag{3.27}$$

The particular directions in which the world lines are chosen to come together is obviously irrelevant in the continuum limit but the discreteness of the lattice could play a role here. However, in the last section we saw that the systematic errors associated with the lattice's discrete rotational symmetry are fairly small at the couplings which were used and so we adopt the simplest policy in this regard, shown in Fig. 11. Two of the quarks are chosen to lie in a particular lattice plane with the third displaced perpendicularly. For

further simplicity attention was restricted to the case where all three quarks lay in a single space-like plane (e.g., the $x-z$ plane, y=constant).

The calculation then proceeds in a manner analogous to that used in the mesonic case. The observable Q is measured for several sets of parameters ($R1, R2, R3, T$) and lattice potentials are extracted from the exponential behaviour, Eq. (3.12). As in the previous section (and for the same reasons) we concentrated on the two lower β values, $\beta = 6.1, 6.3$. The results of this procedure are shown in Table 5 where the values have been rescaled by the perturbative prescription, Eqs. (3.5) and (3.14).

As in the mesonic case, further progress is made by examining models. In judging which models to consider we will again be guided by the predicted high- and low-energy behaviour which led to the mesonic form

$$V(x) = \alpha^{q\bar{q}}/x + V_0 + K^{q\bar{q}}\, x \tag{3.28}$$

where the superscripts denote that these parameters are specific to the mesonic model.

As previously remarked the exact source of the Coulombic term is somewhat unclear. Single gluon exchange in the baryonic sector between pairs of quarks would lead to a term of the form

$$V^{Coul} = \sum_{i<j} \alpha^{qqq}/r_{ij} \tag{3.29}$$

where r_{ij} is the separation of the i^{th} and j^{th} quarks. In supplement of this term however, there is presumably a contribution from the zero point fluctuations of the effective low energy string model. Since no (full) quantised solution to the problem of three strings yet exists (although for progress see [59]) we will neglect this effect and let the quality of the associated fits attest the degree to which this assumption is justified †.

† Physically one might expect that since the quarks are infinitely heavy in this approximation the low energy modes might decouple in the 'Δ' model yielding an expression of exactly the form Eq. (3.29) with coefficient $-\pi/12$ just as in the mesonic sector.

The form of the confining term is also model dependent and relies on the assumptions made about the configuration of the confining strings [60]. Phenomenological models typically make the assumption that the strings form between pairs of quarks, often for no better reason than this makes the harmonic oscillator potential exactly soluble for three charges. This assumption does have some justification, however, in that the quark-diquark picture of the baryon is quite reasonable in the limit where one charge is displaced far from its partners. We will denote this model by the subscript 'Δ' since the strings typically form in the configuration shown in Fig. 12a). The contribution to the potential from this type of model is expected to be

$$V_{\Delta}^{conf} = \tfrac{1}{2} K_{\Delta}^{qqq} \sum_{i<j} r_{ij} \tag{3.30}$$

Note that the factor of ½ inserted here normalises the string tension to be equal to that of the mesonic strings in the case where one quark is pulled far from the other pair [61].

The second popular model is that of [62] which minimises the total length of the string. It can easily be shown that this leads to configurations in which the strings meet mutually at 120°, the so called 'Toricelli' point [56,63]. This configuration, denoted by the subscript 'Y', is shown in Fig. 12b) and its contribution to the potential is given by

$$V_{Y}^{conf} = K_{Y}^{qqq} \sum_{i} r_{iT} \tag{3.31}$$

where r_{iT} is the distance of the i^{th} quark from the central point.

Thus the two baryonic models which we wish to examine are characterised by the potentials

$$V_{\Delta} = \alpha^{qqq} \sum_{i<j} 1/r_{ij} + V_0 + \tfrac{1}{2} K_{\Delta}^{qqq} \sum_{i<j} r_{ij} \tag{3.32}$$

and

$$V_Y = \alpha^{qqq} \sum_{i<j} 1/r_{ij} + V_0 + K_Y^{qqq} \sum_{i=1}^{3} r_{iT} \tag{3.33}$$

The results of these fits, together with the corresponding data from the mesonic calculation of Section 3.2 are shown in Table 6. It should be noted that the errors shown here are purely statistical in nature and as was shown in the previous section there is an approximately 15 % systematic error in the parameters at $\beta = 6.1$ due to the deviations from continuous rotational symmetry.

Since this data represents a function of three independent variables it is quite difficult to plot in any meaningful way so in Table 7 are shown the fitted points obtained from the parameters of Table 6 for the data obtained at $\beta = 6.3$. As can be seen the agreement is quite excellent with values of χ^2 around $1.0 \sim 1.5$ per degree of freedom. From this fact we deduce that the low energy string vibrations neglected earlier either contribute little to the static potential or else yield a potential of exactly the same functional form as the regular Coulombic contribution, Eq. (3.29).

It is interesting to note that the string tensions obtained in both 'Y' and 'Δ' models are roughly the same. Also the quality of fit shown in Table 7 is roughly model independent. This is a simple consequence of the geometric fact that [64]

$$\frac{1}{2} \leq \frac{L_Y}{L_\Delta} \leq \frac{1}{\sqrt{3}} \tag{3.34}$$

where $L_{Y,\Delta}$ is the length of the string in the two models. As a result this calculation is unable to differentiate conclusively between the two string configurations. It is, however, interesting to note that the string tension obtained from the 'Y' configuration is closer to that obtained from the mesonic sector. We shall return to the question of which string model is most appropriate in the next section.

Finally as regards the comparison between bare lattice parameters we turn to the coefficient of the Coulombic term, α. If this interaction were purely gluonic with no contribution from string vibrations we would expect the trivial result that

$$\alpha^{q\bar{q}} = 2\,\alpha^{qqq} \tag{3.35}$$

which follows simply from the algebra of the SU(3) generators in the qq and $q\bar{q}$ channels. Examination of Table 6 shows that this relation holds to a fair accuracy and may thus be indicative of the fact the string vibrations play little part in the potential at the length scales accessible to this calculation, $\lesssim .5$ fm.

In conclusion this calculation has answered several questions. Firstly, the lattice calculations are consistent in that the physical parameters associated with mesonic and baryonic systems are similar. Secondly it has suggested a resolution of the puzzling '$\pi/12$' factor in the Coulombic term. Unfortunately geometry and statistics prevent us from making a definitive statement about the detailed structure of the confining strings in the baryon, but more will be said about this when we have calculated the energy density in the colour fields in the next section.

3.5 Energy Density Distributions

In studying the hadronic energy density distributions our main goal is to examine the mechanism which leads to confinement. Quantitatively this is understood to be due to the linearly increasing potential between the charges, but qualitatively it is not known how this potential arises. Two popular theories concerning this are the 'colour dielectric' and 'dual superconductor' models and we shall discuss each in turn.

Consider, for simplicity, classical electromagnetism. In a medium with dielectric constant $\kappa > 1$ a small positive charge distribution is screened by negative charges (Fig. 13a)). Conversely, if $\kappa < 1$ the medium is antiscreening meaning that the introduction of a small charge distribution into the vacuum leads to the formation of a 'hole' on the inside of which are charges of similar sign (Fig. 13b)). Since these charges repel the test charge it requires work to reduce the size of the hole and it can easily be shown [65] that the system has energy proportional to $\kappa^{-3/4}$ so that $E \to \infty$ as $\kappa \to 0$. Next consider a dipole distribution. Again it is easy to show that a 'hole' forms around the charges but in this case the electric field lines are tangential to the inner surface. As a result the energy contained within the system, and hence its mass, stays finite as one takes the limit $\kappa \to 0$.

Converting this model to the environment of QCD is simple. One assumes that the physical vacuum is a colour dielectric with $\kappa \simeq 0$ in which hadrons are formed from coloured quarks. By analogy with the electrodynamic case one sees that coloured states are forbidden since they have infinite mass while colour singelts such as mesons and baryons have finite mass. Furthermore it is easy to show that since the energy density of the 'hole' grows as $1/r^2$ [66], the system is confining. This model is very similar to the 'bag' model of QCD in which the hadrons are constrained to regions typically characterised as the soliton solutions of the equations of motion [67]. The chief characteristic of this model, for our purposes, is that it is essentially Abelian in nature and there are no chromomagnetic fields in the rest frame of the quarks [68].

An alternative picture of the confining mechanism is the 'dual-superconductor' model [69] where again an Abelian analogy is most convenient. We consider the Nielson-Olesen string model [70] in two dimensions in which a charged scalar field ϕ is coupled to the gauge field with Lagrangian density

$$\mathrm{L} = F_{\mu\nu} F^{\mu\nu} + |D_\mu \phi|^2 - \lambda(a^2 - |\phi|^2)^2 \tag{3.36}$$

and

$$D_\mu \equiv \partial_\mu - ieA_\mu \tag{3.37}$$

is the (Abelian) gauge covariant derivative.

If we allow the scalar field to acquire a non-zero vacuum expectation value such that $\langle 0|\phi|0\rangle = \Phi_0 \neq 0$ then it is easy to show that magnetic vortices of radius r_c form which contain most of the energy density and in which the ϕ field has values reduced from its vacuum value (Fig. 14). These vortices are stabilised by the competing effects of the magnetic field trying to spread out and the scalar ('Higgs') field trying to eliminate the vortex entirely. In three dimensions it is easy to see that the simple vortices become strings which can end on monopoles and the model becomes a simple example of a type II superconductor. The Meissner effect squeezes the magnetic flux into thin regions driven by the condensation of the Cooper pairs which endow the non-zero vacuum expectation value to the scalar field.

The dual superconductor model is obtained by exchanging the roles of the magnetic and electric fields [71]. One thus expects the formation of chromoelectric flux tubes which terminate on the charges and give rise to a linearly increasing potential due to the constant string tension. The role of the Cooper pairs in this scenario will be seen to be played by the chromomagnetic field which circulates around the tube squeezing the electric flux distribution. This model is thus characterised by a non-zero transverse magnetic field which is excluded from the region containing the electric string.

In lattice gauge theory these phenomena can be explored by use of the correlation function [72,73]

$$P_{\mu\nu} = \frac{\langle \mathrm{tr}W \ \mathrm{tr}S_{\mu\nu}\rangle}{\langle \mathrm{tr}W\rangle} - \langle \mathrm{tr}S_{\mu\nu}\rangle \tag{3.38}$$

where W is a rectangular Wilson lop and $S_{\mu\nu}$ is a single plaquette with orientation $\mu\nu$ relative to the axes defined by W. Expansion of this operator in weak coupling shows that

$$P_{\mu\nu} = a^4 \left(\langle \mathrm{tr} F^2_{\mu\nu} \rangle_{q\bar{q}} - \langle \mathrm{tr} F^2_{\mu\nu} \rangle_{vac} \right) + O(a^6) \tag{3.39}$$

i.e., $P_{\mu\nu}$ measures the squared energy density generated by the $q\bar{q}$ pair relative to the vacuum. This expression also explains how the various field components are to be extracted. If the large loop, W, is taken to define the $z-t$ plane then timelike plaquettes measure chromoelectric densities while spacelike ones measure magnetic contributions (See Fig. 15).

The numerical technique adopted might be described as 'brute force' in that we measure directly the correlation function $P_{\mu\nu}$. This method is, however, fairly inadequate when applied to correlation functions of this type since the signals fall very rapidly as loop and test probe are separated leading to extremely noisy data. Furthermore, the effect being sought is an extremely delicate property of a mesonic system whilst the Monte Carlo configurations generated are typical of the vacuum. As a result of these problems it proved impossible to measure correlations with loops larger than 4×5.

A further difficulty with quantitative measurements is due to the contributions from higher energy states. In the case of the static potential we required only the constraint $T \gtrsim R$ in order to suppress the higher energy levels. However, the effect of dividing the correlation function by the bare loop value in Eq. (3.38) has the effect of reducing the factor by which the contributions from higher energy states are suppressed [74] and thus one expects to see signals which depend strongly on T. This is not really too surprising physically since the confinement mechanism is a low energy phenomenon and might thus be expected to be similar in all states.

The combined effect of the problems discussed in the previous two paragraphs is to make quantitative results impossible. Consider, for example, the data in Table 8 where we

show the peak and midpoint contributions to the squared electric field parallel to the $q\bar{q}$ axis. As can be seen the results depend strongly on the temporal extent of the Wilson loop. However, also shown are the ratios of the two quantities which characterise the shape of the flux distribution and as can be seen this ratio is fairly insensitive to T. For this reason we are confident that qualitative results can still be extracted.

With this in mind we consider in detail the energy density distributions extracted from correlations with a 4×4 Wilson loop. The contributions $\langle E_{\parallel}^2 \rangle$, $\langle E_{\perp}^2 \rangle$ and $\langle -B_{\perp}^2 \rangle$ are shown in Figs. 16a)-c) (The negative sign in the magnetic case is due to the Wick rotation to Euclidean space †). The measured values of $\langle -B_{\parallel}^2 \rangle$ were consistent with zero and so are not presented. The characteristic statistical error associated with these measurements is around 10%.

These results are quite exciting. $\langle E_{\parallel}^2 \rangle$ clearly shows that an electric flux tube has formed between the charges with a width of approximately one lattice spacing. Furthermore both $\langle E_{\perp}^2 \rangle$ and $\langle B_{\perp}^2 \rangle$ are measurably non-zero and of similar magnitude. This latter point provides a useful check on the correctness of the measurements since it is a simple consequence of the choice Eq. (3.38). Consider, for example, the correlation with a 3×3 Wilson loop which measures $\langle E_{\perp}^2 \rangle$, shown in Fig. 17. Making use of the discrete rotational symmetry ($z \rightarrow t$, $t \rightarrow -z$) of the lattice we can transform this observable into one which measures $\langle B_{\perp}^2 \rangle$. Thus we expect that $\langle E_{\perp}^2 \rangle \simeq \langle B_{\perp}^2 \rangle$ in the vicinity of the centre of the flux tube. That this is so is a heartening feature of our results.

The most interesting feature of our data is the contribution of $\langle B_{\perp}^2 \rangle$. This shows *exactly* the features predicted by the Nielsen-Olesen string model, viz., the exclusion of the magnetic field from the region between the quarks containing the flux tube. This is strong evidence in favour of the 'dual-superconductor' picture.

† This point was neglected in Ref. [73] and led to an erroneous interpretation of the results.

The existence of $\langle E_\perp^2 \rangle$ is also quite interesting. If we consider the effective low-energy string model then at strong coupling we expect the string to be rigid and to lie along lattice links. As the coupling decreases kinks develop (See Fig. 18) that eventually, at the so-called 'roughening' point, delocalise the string entirely [75]. It is not unreasonable, therefore, to see non zero transverse components in the electric field. An interesting quantity to measure in connection with this model is the transverse width of the flux distribution which is expected to increase logarithmically as the quark separation is increased. Such a study, however, would require much better data than we have available and is probably beyond the capabilities of the 'brute force' technique.

This calculation has also been extended to the baryonic sector [76]. Our motivations for doing so are twofold. Firstly, it is important to see whether the evidence supporting the 'dual-superconductor' model is again apparent in this different context. Secondly, by examining the field distributions it may be possible to distinguish between the two baryonic string models discussed in the previous section.

The baryonic operator analogous to Eq. (3.38) is shown in Fig. 19. As before it is the correlation between the operator used to measure the potential and a single test plaquette. The relative orientations of Q and the test probe again determine the measured field component. As in the mesonic sector it proved impossible to measure correlations with large Q observables and so our detailed results are only presented for the case $Q(2,2,3\ ;\ 4)$. At these separations the statistical errors are in the range 20-40%, but we have checked that the qualitative features of the distributions at these scales are consistent with those obtained with better statistical accuracy at smaller distances.

In Figs. 20a),b) are presented the electric and magnetic energy distributions derived from our data. From these plots it is clear that the support for the Nielsen-Olesen picture is also present in the baryonic sector. Furthermore the magnetic field distributions lend considerable support to the 'Y' picture of the confining strings (Fig. 12b)). The area of

maximum exclusion of the magnetic field is clearly seen to be towards the centroid of the three quarks where the Toricelli point lies rather than along the lines joining the charges as would be the case in the 'Δ' model.

In conclusion, the energy densities have proved very informative. While quantitative data are impossible to extract with the simplistic 'brute force' methods the qualitative results support strongly the idea that the linearly confining potential is due to the formation of narrow electric 'flux tubes' which are themselves a consequence of the dual Meissner effect. The 'flux tubes' are stabilised by the circulating chromomagnetic fields which play the role of the Cooper pair condensate in the 'dual superconductor'. The internal structure of the flux tube is not inconsistent with the 'roughening' behaviour of the effective string model but detailed analysis of this effect will require much better data than is currently available. In the baryonic sector the calculated energy densities strongly support the model in which the confining strings meet at the Toricelli point leading to a potential which is essentially three body, rather than the superposition of two body pieces as is often assumed.

3.6 Beyond First Order - Spin Dependent Potentials

So far all the calculations we have performed have been to first order in powers of $1/m$ (or equivalently v^2/c^2, where v is the relative quark velocity). While this has painted an interesting picture of static quark systems it is not the whole story. For example, in this first-order approximation the nucleon and Δ are degenerate since their mass splitting is a spin-spin effect which would only appear in second order.

Corrections to this first-order approximation come from two sources. Firstly one has to treat the quark spins, which requires solving the Dirac equation, and secondly there are finite velocity effects due to the relative motion of quark and anti-quark. As mentioned earlier the lattice provides a natural setting in which to systematically account for these various effects and as an example we consider the finite velocity effect.

One would naively imagine that the effect of finite velocities on the lattice is to necessitate the inclusion of quark world lines which are not entirely straight. In order to see this consider the outlined argument shown in Fig. 21. The derivative acting on the zero velocity quark world line is represented by a sum of terms each corresponding to a line with a single kink at some temporal value. However, to first order in the lattice spacing the gauge field can be treated as Abelian so that path ordering makes no difference. It is then easy to see that the relations shown in the second line of the figure hold and that the effect of finite quark velocity is incorporated by the inclusion of 'electric' plaquette insertions at all points on the quark line. ('Electric', in the sense of the previous section, means timelike).

Detailed calculations of the remaining spin-dependent corrections have been made [77,78] although early attempts mistakenly assumed that the electric confinement mechanism at long range implied that there was no long range magnetic field. (This assumption is reasonable in the static limit but the motion of the quarks must generate a magnetic field [78]). The expression for the interquark potential correct to second order in $1/m$ is then

$$V = V_{static} + V_{spin-orbit} + V_{spin-spin} + V_{tensor} \tag{3.40}$$

where the various components are given by

$$V_{spin-orbit} = \left(\frac{\mathbf{L}_1 \cdot \mathbf{S}_1}{2m_1^2} - \frac{\mathbf{L}_2 \cdot \mathbf{S}_2}{2m_2^2} \right) \left(\frac{V_{static}'}{r} + \frac{2V_1'}{r} \right) \tag{3.41}$$

$$+ \left(\frac{L_1 \cdot S_2}{m_1 m_2} - \frac{L_2 \cdot S_1}{m_1 m_2} \right) \frac{V_2'}{r}$$

$$V_{spin-spin} = \frac{S_1 \cdot S_2}{3 m_1 m_2} V_4 \tag{3.42}$$

$$V_{tensor} = \frac{1}{m_1 m_2} \left(\frac{r \cdot S_1 r \cdot S_2}{r^2} - \frac{S_1 \cdot S_2}{3} \right) V_3 \tag{3.43}$$

and primes denote derivatives with respect to r.

On the lattice these potentials are given by

$$\frac{r^k}{r} V_1' = \lim_{T \to \infty} \frac{g^2 \epsilon_{ijk}}{2T} \int dt \int dt' \, (t - t') \, \langle B^i(r_1, t) \, E^j(r_1, t') \rangle_C \; / \; \langle 1 \rangle_C \tag{3.44}$$

$$\frac{r^k}{r} V_2' = \lim_{T \to \infty} - \frac{g^2 \epsilon_{ijk}}{2T} \int dt \int dt' \, t' \, \langle B^i(r_2, t) E^j(r_1, t') \rangle_C \; / \; \langle 1 \rangle_C \tag{3.45}$$

$$\left(\frac{r^i r^j}{r^2} - \frac{\delta^{ij}}{3} \right) V_3 + \frac{\delta^{ij}}{3} V_4 = \tag{3.46}$$

$$\lim_{T \to \infty} \frac{g^2}{T} \int dt \int dt' \, \langle B^i(r_1, t) B^j(r_2, t') \rangle_C \; / \; \langle 1 \rangle_C$$

Note that in these expressions the subscripts 1 and 2 refer to the quark and anti-quark lines, and the subscript C denotes that the expectation values are to be calculated as insertions into regular Wilson loops, the trace of which, with no insertions, is denoted by $\langle 1 \rangle_C$.

It is immediately obvious from these expressions that this lattice calculation will be extraordinarily difficult. In the previous section it was found to be difficult to measure the correlation between a loop and a single plaquette - these expressions are essentially the correlation between a loop and two plaquettes. Not only that but the resulting integrals over relative times involve cancellation among terms of similar magnitudes.

These predictions are rather sadly borne out by the data shown in Fig. 22. This represents the off diagonal contribution to the tensor term, V_4, at separations of $R = 1, 2, 3$ lattice spacings. These trial measurements were made on a small lattice ($10^2 \times 12^2$) at $\beta = 6.0$. As can be seen the statistical errors for $R > 1$ are extremely large and furthermore no clear limit is seen as T increases, even at $R = 1$. This latter point is not so surprising since the division by the bare loop value in Eqs. (3.44)-(3.46) heralds the same problems as were seen in the energy density calculation due to excited states. Recently [79] mammoth computational effort has been devoted to this problem with mediocre success. Results have been extracted for the range $1 \leq R \leq 4$ which are approximately consistent with expectations. In particular the relation deduced in [78] solely on the basis of Lorentz invariance, that

$$V_{static} + V_1 - V_2 = 0 \tag{3.47}$$

seems to be satisfied. This result is extremely important phenomenologically since it implies the existence of a long range spin-orbit interaction which will be discussed further in the next section.

3.7 Comparison with Experiment

Before the picture developed in this chapter can sensibly be compared to experimental data a fundamental question must be answered, namely that of the physical lattice size. The fact that the lattice spacing, a, is an undetermined parameter is both a strength and a weakness of the Monte Carlo method. On the one hand it allows direct simulation of the theory at all length scales with no modifications. On the other one has to pin down the exact numerical value of this parameter at some coupling in order to make contact with

experiment.

There are several ways in which this might be achieved of which the simplest is just to assume that the relation between Λ_L and $\Lambda_{\overline{MS}}$ derived in perturbation theory holds [14] allowing us to use experimentally determined values of $\Lambda_{\overline{MS}}$ to set scales. Alternatively one could take a physical quantity such as the string tension calculated in Sections 3.2 and 3.4 and fit it to some phenomenological model. The former method suffers from an excessive reliance on perturbation theory and scaling behaviour while the latter requires assumptions which one of our goals was to test. A third method exists, however, in that we can use parameters extracted from other lattice gauge calculations. Since we are far from having solved all the problems associated with full QCD simulations on the lattice it might seem that such an approach is unjustified. It does, however, have some virtue in that whatever approximations are contained in our calculations are presumably also present in other lattice calculations and so the value obtained is, in some sense, consistent.

As our scale setting calculation then, we choose quenched mass spectrum calculations which incorporate the same assumptions as were made in earlier sections. These calculations are typically hampered by fairly large statistical errors but should serve to set our scales in an internally consistent manner. From these calculations [80] can be derived the result that

$$1/a \simeq 2.1 \text{ GeV} \qquad \text{at } \beta = 6.0 \tag{3.48}$$

i.e., the lattice spacing is approximately .1 fm.

Initially this result seems very disappointing since it implies that we have been able to study objects whose size is considerably smaller than the proton radius ($\simeq$ .8 fm). The question then arises as to exactly how much real physics can have been observed. In order to answer this question we appeal to the known fact that lattice QCD has no phase transition going from strong to weak coupling. Furthermore, we already see phenomena in our

potentials associated with both high- and low-energy regimes and so have good reason to believe that our results are correct. Indeed, in the absence of any externally imposed length scale, it is reasonable to suppose that our quantitative results (modulo, of course, the scaling behaviour seen in Section 3.2) are also representative of the true physical situation.

Having thus justified the extraction of quantitative information from our observables we turn to more careful examination of heavy quark spectroscopy [81]. As previously noted, the discovery of charmonium generated an enormous interest in potential models [82,83], many of which accounted quite reasonably for many features of the experimental data. The functional forms of these potentials also varied quite substantially from the form assumed in Eq. (3.15). Two reasonable alternatives, for example, are logarithmic [84] and (small) power law [85] behaviour, both of which are also consistent with our data. However the form which we have used was derived in a way that was deliberately chosen to be consistent with expected strong and weak coupling behaviour and so we shall henceforth concentrate on this model.

Given that the mesonic potential is, in our approximation, entirely non-relativistic the most comparable model is that contained in the classic work of Eichten et al. [82] whose model potential took the form (with a rather unfortunate clash of notation)

$$V(r) = -\frac{\kappa}{r} + \frac{r}{a^2} \tag{3.49}$$

which is exactly that assumed throughout the previous sections. To proceed from this potential to predictions it is necessary to fit the parameters κ and a. The choice of physical quantities to use in performing this fit is very wide and often the choice is to fit the $2S - 1S$ mass difference and the leptonic widths $\Gamma(2S \rightarrow e^+e^-)$, $\Gamma(1S \rightarrow e^+e^-)$. However, As shown in [82], this procedure is flawed if one assumes the usual Van Royen Weisskopf formula for the leptonic width [86]

$$\Gamma(e^+e^-) = \frac{16\pi e_Q^2 \alpha^2}{M^2} |\psi(0)|^2 \tag{3.50}$$

since it leads to relativistic motion for the quarks, explicitly violating one of the assumptions of the model. Instead the parameters in [82] were extracted by fitting to the $\psi - \psi'$ mass difference and the centre of mass of the triplet P states. This process yields values which, cast into the notation applicable to our calculation, are

$$\begin{aligned} m_c &= 1.84 \text{ GeV} \\ \alpha &= -.52 \\ K &= 0.18 \text{ GeV}^2 \end{aligned} \tag{3.51}$$

with quark velocities $v^2/c^2 \simeq .2$, a quite acceptable non-relativistic value.

The successes of this model are well known. It accurately predicts the masses of the excited charmonium states even above $D\bar{D}$ threshold and also accounts for the leptonic widths once QCD corrections to Eq. (3.50) are made [87]. Given the experimental mass differences between the triplet and singlet S states it reproduces the $M1$ transition rates and branching ratios. Further, given a mass for the bottom quark, $m_b = 5.17$ GeV, it also accounts for the large scale structure of the bottomonium potential.

Given these facts the crucial question is how well do our parameters agree with those quoted above. As indicated before the scaling behaviour of the lattice spacing is taken from mass spectrum calculations and the potential of Section 3.2 then yields the values

$$\alpha = -.31 \pm .04 \tag{3.52}$$

$$K = .18 \pm .04 \ \text{Gev}^2$$

While the string tension is in remarkable agreement we see that the Coulomb strength is appreciably too small. This leads, for example, to significant overestimation of quantities which are sensitive to the wavefunction near the origin such as the leptonic width and $2S - 1S$ mass difference [88]. The resolution of this difficulty seems to lie in the neglect of vacuum polarisation effects - i.e., in the quenched approximation itself. It can be shown [89] that in the case where the confining potential transforms as a Lorentz scalar the effect of internal quark loops is to modify the form Eq. (3.15) to

$$V'(r) = \frac{\alpha + \alpha'}{r} + K r \tag{3.53}$$

where $\alpha' \simeq -.16$. With this correction it is obvious that the lattice potential is in excellent agreement with the work of Eichten.

In passing here it should be noted that the resolution of the different types of potential models will be greatly facilitated by the discovery of the top quark. With a mass of around 80 GeV it is expected that the toponium spectrum should be sensitive to the potential at length scales of around .05 fm in which region the different models are easily distinguishable [90].

It is important to note that the correction to the Coulombic term used above to account for the discrepancy between the lattice and phenomenological models required the long range confining potential to transform as a Lorentz scalar. The validity of this assumption is, in itself, an interesting question about which lattice gauge theory may be able to make a statement. The question of the Lorentz nature of the confining potential is best addressed by examining the level splittings in the triplet P states, χ, which are due to

spin-orbit interactions. Early models which fit only to the charmonium spectrum [91] found that the relevant spin-orbit term could be generated if the potential was almost exclusively scalar, although a large anomalous moment for the quarks was also required. Recent data from ARGUS [92] and Crystal Ball [93] has accurately located the equivalent states, χ_b, in the considerably less relativistic environment of bottomonium and these confirm the scalar nature of the confining potential. It should be noted, however, that the spin-dependent corrections used in these calculations are exactly those which we attempted to study in the previous section. As mentioned there, the most recent lattice calculations on this topic are consistent with the existence of a long range spin-orbit coupling and hence also lend credence to the idea of scalar confinement.

Given that the model Eq. (3.49) with spin-dependent corrections can so ably predict the properties of heavy quarkonia, it is natural to inquire as to whether a treatment of light mesons is possible. A recent calculation [94] by Godfrey and Isgur seems to indicate that this is so. Starting solely from this model they incorporate spin-dependent effects in a way consistent with scalar confinement and finally make relativistic corrections to the wavefunctions by applying smearing operators and in this way they are able to fit the masses, couplings and decays of the meson spectrum over the entire range from .1 to 10 GeV in terms of a handful of parameters. This seems to be substantial evidence indeed that the linear + Coulomb form of the potential observed in lattice gauge theory is correct.

Having thus disposed of the mesonic spectrum *in toto* we turn to baryons. In this case we have no immediately obvious starting place since 'heavy' baryons have not been detected. Indeed this situation is likely to prevail for some time for two reasons. Firstly, the production rate of baryons such as Ω_{ccc}^{++} and Ω_{bbb}^{-} in e^+e^- experiments is extremely small. Secondly, even if such species were to be created their detection is an horrendous problem. Consider, for example, the decay mode

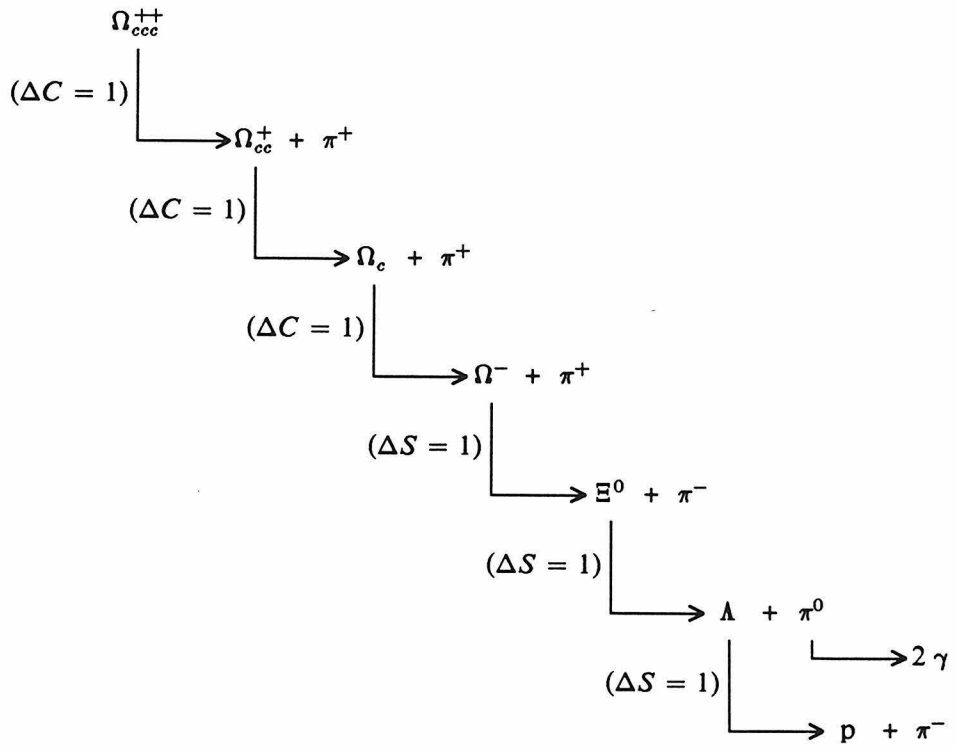

The final state contains eight assorted particles and would thus render reconstruction extremely difficult.

We must, therefore, immediately go on to the question of whether or not potential models can explain the properties of lighter baryons. Extensive work analogous to that performed in the mesonic case [57] shows that this is indeed possible. Working with a potential which is essentially a superposition of two body potentials of the type Eq. (3.15) and treating the three body effects such as those mentioned in Section 3.4 in perturbation theory, most of the features of the known baryonic spectrum have been reproduced. An interesting difference, however, is found in the spin-orbit couplings. In the mesonic sector the scalar confinement mechanism was responsible for a long range spin-orbit force which explained the splitting of the triplet P states. In contrast, baryonic models seem to show that the equivalent long range term is almost exactly cancelled by the Breit-Fermi contribution arising from the single gluon exchange. Thus the mass splittings in baryons seem to

be predominantly spin-spin effects.

It would be extremely interesting to see if such cancellation is a feature of the lattice model. The formulation of this problem is in principle a straightforward extension of that shown in Section 3.6 and requires the correlation of two plaquettes and the three quark observable, Q. In the light of our difficulty with the baryonic energy density, however, it seems that such calculations are likely to be beyond the capability of the 'brute force' algorithm even on the most powerful of supercomputers. For this reason, among others, we turn in the next chapter to the development of alternative Monte Carlo algorithms.

CHAPTER 4

The Complex Langevin Equation

In order to perform detailed lattice gauge calculations deep into the scaling region it is necessary, as we have seen in the previous chapter, to work at weak couplings, g. Unfortunately this means that larger lattices will also be required, since increasing β decreases the physical lattice spacing exponentially. This in turn means that lattice observables will have to extend over more lattice spacings to be probing physics at the same length scale.

Current constraints on lattice sizes come predominantly from the available computer architectures. Supercomputers tend to gain speed at the expense of physical memory, which results in our ability to calculate with small statistical errors on lattices with somewhere on the order of twenty lattice spacings in each direction. However, future generations of computers will probably see this restriction lifted and lattices with forty sites per direction will not be impossible.

It is not clear, however, that this will solve all of the problems. As we saw in the last chapter, quantitative results are difficult to obtain. Even in the relatively simple static potential calculation we saw that perturbative scaling behaviour was not obeyed, and in the more complicated correlation function measurements of the energy density and spin dependence quantitative results were unobtainable at even quite modest lattice separations. Thus, while larger lattices will allow calculation at higher β where convergence tends to be enhanced, one is still faced with the problem of measuring small correlations over many lattice spacings, a formidable problem for the 'brute force' algorithms previously described.

The main reason for our failure to accurately measure these observables is easily traced to their correlative nature. In the static potential calculations, the aim is to calculate a property of the first excited $q\bar{q}$ state relative to the vacuum whereas in the energy density and spin-dependent calculations one is examining the properties of the $q\bar{q}$ system in the presence of certain 'test' probes relative to the bare $q\bar{q}$ system. However, our field configurations are all generated from the pure gauge action

$$F_{\mu\nu} F^{\mu\nu} \tag{4.1}$$

and hence contain no explicit knowledge about the charges themselves. Our ability to measure a static potential is evidence that some of the configurations generated from Eq. (4.1) do have overlap with the $q\bar{q}$ states, but it is an entirely different matter to expect to take these few states and then extract a subtle expectation value such as the loop-plaquette correlation. It is thus no real surprise that the measurements of such correlation functions are fraught with large statistical errors and deteriorate rapidly with increasing quark separation.

The particularly simple idea that will be explored in this chapter, is to include the effects of the static quark pair in the action used to generate field configurations. Then we

would, hopefully, be in the same position as in the static potential calculation in that loop-plaquette correlations would be measured against a background which explicitly contained the effects of the loop. In the first section will be discussed the most naive attempts to fulfill this aim and in subsequent sections we will go on to discuss the application of the Langevin equation in this context.

4.1 - Simple-Minded Algorithms

Typically our problem requires the measurement of the correlation between a Wilson loop, W, and some other observable, P. For the purposes of this and further sections we will consider only the problem of measuring

$$\langle O \rangle = \frac{\int [dU]\, W \cdot P\, e^{\beta S}}{\int [dU]\, W\, e^{\beta S}} \tag{4.2}$$

which is of the same form as that used in both the energy density and spin-dependent calculations. (Note that the path integral including the fermionic determinant, Eq. (3.4), can be cast into this form by the identification $W \rightarrow \mathrm{Det}(\not{D}+m)$.) Our attempts to include directly the effects of the $q\bar{q}$ pair stem from the replacement (in somewhat schematic notation)

$$S^* = S + \frac{1}{\beta} \log W \tag{4.3}$$

in which case $\langle O \rangle = \langle P \rangle^*$, where the star denotes that the operator P is to be averaged in the ensemble generated from action S^*.

For definiteness, consider a simple model integral

$$\frac{\int_0^{2\pi} d\theta\, \cos\theta\, e^{i\theta}\, e^{\beta\cos\theta}}{\int_0^{2\pi} d\theta\, e^{i\theta}\, e^{\beta\cos\theta}} \tag{4.4}$$

which is of exactly the form encountered in Abelian lattice gauge theory. (To be discussed in more detail in the next section.) In the notation of Eq. (4.2) we then have $P \sim \cos\theta$, $W \sim e^{i\theta}$ and

$$S^* = \cos\theta + \frac{i\theta}{\beta} \tag{4.5}$$

The problem with this action is immediately apparent - S^* is not real so $e^{\beta S^*}$ is not positive definite which means that standard probabilistic algorithms such as the Metropolis and heat bath techniques are not applicable.

A straightforward method which avoids this problem is the 'phases' method. One defines two real functions by

$$W \equiv r_W e^{i\theta_W} \qquad r_W, \theta_W \quad \text{real} \tag{4.6}$$

and writes $\langle O \rangle$ in the form

$$\langle O \rangle = \frac{\int [dU]\, P\, e^{i\theta_W} r_W e^{\beta S}}{\int [dU]\, r_W e^{\beta S}} \quad \frac{\int [dU]\, r_W e^{\beta S}}{\int [dU]\, W\, e^{\beta S}} \tag{4.7}$$

$$= \frac{\langle P\, e^{i\theta_W} \rangle' \langle r_W \rangle}{\langle W \rangle}$$

where the prime denotes the average in the ensemble with weighting $r_W e^{\beta S}$. Since this is positive by construction, the standard Monte Carlo algorithms can be applied and the problem is reduced to the calculation of separate expectation values in ensembles characterised by different actions.

Unfortunately, problems with this method are not hard to find. Firstly, the factor $e^{i\theta_W}$ which multiplies P leads to large cancellations amongst the measured values of P and as a result it is extremely hard to obtain reasonable statistical accuracy. This problem

is directly analogous to the well known difficulty encountered when numerically adding two numbers which are very similar in magnitude but with opposing signs - large loss of significant figures can result. A second problem with this technique is due to the fact that in the primed ensemble an inhomogeneity has been introduced into the lattice by virtue of selecting specific links to lie in the Wilson loop, W. These links are then updated differently from the others and hence translational invariance has been lost. We can no longer average over all plaquettes in calculating P since each individual plaquette now has a specific position and orientation relative to the large loop and the large counting factor discussed in section 2.2 is of no account.

These problems might not be so serious if we had indeed managed to incorporate the effect of the charges into the effective action, S', but it is obvious that this is not the case since the phase information $e^{i\theta W}$ is missing. Indeed, in the simplest case of the energy density in U(1) lattice gauge theory $r_W \equiv 1$ and this algorithm reduces to the 'brute force' method !

A second possible approach to the problem lies in the construction of 'biased' algorithms. Using this technique one attempts to increase the overlap between states generated by the action S' and the test probes by applying physical intuition in modifying the lattice action.

As a specific example consider the measurement of the squared electric field distribution parallel to the $q\bar{q}$ axis given by (see Fig. 23)

$$\langle E_{\parallel}^2 \rangle = \frac{\int [dU]\, W \cdot P_{\parallel}\, e^{\beta S}}{\int [dU]\, W\, e^{\beta S}} \tag{4.8}$$

where $P_{\parallel}$ is a plaquette lying in the plane of the rectangular Wilson loop, W. The physical insight we attempt to use is the fact that an electric flux tube is expected to form between the charges leading to enhanced expectation values of the operator $W \cdot P$. In order to bias

configurations towards this effect we therefore define an action

$$S' = \frac{1}{\beta} \sum_p \beta(p) \, \mathrm{tr} \, (U_p + U_p^\dagger) \tag{4.9}$$

where the sum is over all plaquettes U_p. Note that this form differs from the Wilson action, Eq. (2.9), only in that the coupling β is now a function of position. Furthermore, we consider the simple form

$$\beta(p) = \beta + \delta_{p \in R} \, \Delta\beta \tag{4.10}$$

where the delta function selects only plaquettes contained in a set R. The required operator is then measured by

$$\langle E_{\parallel}^2 \rangle = \frac{\int [dU] \, W \cdot P \; e^{\beta S'}}{\int [dU] \, W \; e^{\beta S'}} \quad \frac{\int [dU] \, W \; e^{\Delta\beta \sum_{p \in R} S} \; e^{\beta S}}{\int [dU] \, W \; e^{\beta S}} \tag{4.11}$$

$$= \frac{\langle W \cdot P \rangle' \langle W \; e^{\Delta\beta \sum_{p \in R} S} \rangle}{\langle W \rangle' \quad \langle W \rangle}$$

where $\langle \cdots \rangle'$ denotes an average in the ensemble S' and $\sum_{p \in R}$ is the plaquette sum restricted to the set R.

Note that in this form all positional information about the flux tube lies in the $\langle W \cdot P \rangle'$ factor while the other terms serve only to normalise the values. Unfortunately this method again spoils the homogeneity of the lattice and means that the 'biasing' procedure must be extremely efficient if it is to overcome the loss of translational invariance. We attempted to calculate the position dependent factor in SU(3) lattice gauge theory by choosing the set R to be those plaquettes lying inside the Wilson loop. Choosing $\Delta\beta > 0$ on these plaquettes was hoped to stimulate the growth of the flux tube leading to larger and more consistent

signals but we were unable to observe any significant enhancements for several values of $\Delta\beta$ and were thus forced to conclude that this method cannot, in fact, overcome the loss of the homogeneous lattice counting factor.

4.2 - Langevin and Fokker-Planck Equations

In the previous section algorithms were discussed which attempted to directly include the effects of current loops in generating lattice configurations. This led to the introduction of modified actions which were in general complex. In this section we will discuss an algorithm which is capable of simulating such actions and hence generating a 'complex probability distribution'. Before discussing the exact meaning of this last phrase we must first examine the connection between the Langevin (stochastic differential) equation which describes the motion of an individual degree of freedom and the associated Fokker-Planck equation for the probability density of sample paths.

In order to introduce this connection it is instructive to consider a treatment of Brownian motion in one dimension first proposed by Langevin [25]. We consider a single particle with velocity v. There are two basic forces acting on this particle: a viscous force γ due to the medium in which it travels and a fluctuating force due to impacts with other particles. On average this fluctuating force is equally likely to be positive or negative and if the particle density is not too high then successive impacts can be considered to be statistically independent events.

A simple model of the dynamics of such a system is, therefore, given by the stochastic differential equation

$$\dot{v} + \gamma v = \eta(t) \tag{4.12}$$

where $\eta(t)$ represents the fluctuating force, which we take to be a Gaussian normalised by

$$\langle \eta(t)\, \eta(t') \rangle = q\, \delta(t-t') \tag{4.13}$$

If we assume the boundary condition that $v = v_0$ at $t = 0$ then this equation can be immediately integrated to give

$$v(t) = v_0 e^{-\gamma t} + \int_0^t dt'\, e^{-\gamma(t-t')} \eta(t') \tag{4.14}$$

whence the velocity correlation function is obtained from the normalisation condition, Eq. (4.13)

$$\langle v(t_1)\, v(t_2) \rangle = v_0^2\, e^{-\gamma(t_1+t_2)} + \int_0^{t_1} dt_1' \int_0^{t_2} dt_2'\, q\, \delta(t_1'-t_2')\, e^{-\gamma(t_1+t_2-t_1'-t_2')} \tag{4.15}$$

$$= v_0^2\, e^{-\gamma(t_1+t_2)} + \frac{q}{2\gamma} \left[e^{-\gamma|t_1-t_2|} - e^{-\gamma(t_1+t_2)} \right]$$

If we now take the limit $t_1, t_2 \to \infty$, then we can evaluate the average particle kinetic energy

$$\mathrm{E} = \tfrac{1}{2} m \langle v^2 \rangle = \tfrac{1}{2} m \frac{q}{2\gamma} \tag{4.16}$$

and by appealing to the equipartition theorem one obtains the normalisation

$$\mathrm{E} = \tfrac{1}{2} k\,\mathrm{T} = \tfrac{1}{2} m \frac{q}{2\gamma} \Rightarrow q = 2\gamma k\,\mathrm{T}/m \tag{4.17}$$

We can do more than this by calculating all of the moments of the velocity. In order to accomplish this note that the Gaussian distribution has the property that

$$\langle \eta(t_1)\,\eta(t_2)\,\cdots\,\eta(t_{2n-1})\rangle = 0 \tag{4.18}$$

$$\langle \eta(t_1)\,\eta(t_2)\,\cdots\,\eta(t_{2n})\rangle = \sum_{perms} \delta(t_{i_1}-t_{i_2})\,\delta(t_{i_3}-t_{i_4})\,\cdots\,\delta(t_{i_{2n-1}}-t_{i_{2n}})$$

which leads to the fact that

$$\langle v^{2n-1}\rangle = 0 \tag{4.19}$$

$$\langle v^{2n}\rangle = \frac{(2n)!}{2^n n!}\langle v^2\rangle^n = \frac{(2n)!}{2^n n!}\left(\frac{q}{2\gamma}\right)^n$$

In the stationary limit, $t \to \infty$, we can thus define a moment generating function for v

$$C(u) = 1 + \sum_{n=1}^{\infty} (iu)^n \langle v^n\rangle / n! \tag{4.20}$$

$$= 1 + \sum_{n=0}^{\infty} (iu)^{2n} \langle v^{2n}\rangle / 2n!$$

$$= \exp -\left(\frac{u^2 q}{4\gamma}\right)$$

This in turn leads to a stationary probability distribution for the velocity v

$$F(v) = \langle \delta(v(t)-v)\rangle = \frac{1}{2\pi}\int_{-\infty}^{\infty} du\; C(u)\, e^{-iuv} \tag{4.21}$$

$$= \left(\frac{\gamma}{\pi q}\right)^{1/2} \exp -\frac{\gamma v^2}{q}$$

$$= \left(\frac{m}{2\pi k\,\mathrm{T}}\right)^{1/2} \exp -\frac{mv^2}{2k\,\mathrm{T}}$$

This last expression is immediately familiar as the solution of the diffusion equation

$$\frac{\partial F}{\partial \mathrm{T}} = \frac{k}{2m} \frac{\partial^2 F}{\partial v^2} \tag{4.22}$$

and we have linked the distribution function for velocities, given by solutions of the above equation, to the Langevin equation describing the time evolution of a single particle's trajectory, Eq. (4.12). An extremely important point is that the initial particle velocity v_0 which appeared in the Langevin solution has vanished from the stationary probability distribution. This is the property of ergodicity whereby the final velocity distribution assumes the Maxwellian form, Eq. (4.21), independent of initial conditions.

The crucial question, however, is whether or not this apparent link between diffusion equation and Langevin equation can be made rigorous. In Appendix B we show that to the Langevin equation

$$\dot{x} = -\beta \frac{\partial S}{\partial x} + \eta \tag{4.23}$$

where $\langle \eta(t)\eta(t') \rangle = 2\delta(t-t')$ there corresponds a Fokker-Planck equation

$$\frac{\partial F}{\partial t} = \frac{\partial}{\partial x} \left[F \beta \frac{\partial S}{\partial x} \right] + \frac{\partial^2 F}{\partial x^2} \tag{4.24}$$

and an eigenvalue expansion yields

$$F(x,t) = e^{-\beta S} + \sum_{n=1}^{\infty} f_n(x)\, e^{-\lambda_n t} \tag{4.25}$$

If S is positive definite it can be shown that $\lambda_n > 0$ for all $n \geq 1$ and thus $F(x,t)$ converges exponentially to the Boltzmann distribution [95]. The vital point for our calculations is that Eqs. (4.23)-(4.25) still hold for complex S [96,97], albeit that the condition on the eigenvalues, λ_n is unknown [98]. This means that we may indeed be able to generate configurations with 'complex probability density' $e^{-\beta S}$ from the associated Langevin

equation.

This brings to light an interesting question. In our example, Eq. (4.5), we find a Langevin equation

$$\frac{\partial\theta}{\partial t} = -\beta\sin\theta + i + \eta \tag{4.26}$$

which evolves real values of θ into complex ones. However, Eq. (4.4) involves integrals over real values of θ only. How is the integral evaluated over complex values of θ by the procedure, Eq. (2.19), related to that from which we began ? This problem is not restricted to our simple model. In SU(N) gauge theories, for example, the Wilson loop operator takes values in the range [-1,1] and hence its logarithm is not real. Further, the gauge integration measure, $[dU]$, is not over the N^2 complex components of the matrix but the N^2-1 real parameters, the gauge field components which become complex under the action of the complex Langevin procedure. We shall have more to say about this in Section 4.4. In order to reconcile the real and complex integrals consider the following simple contour integral argument [99].

Let $g(z)$ be an entire function with the property that

$$g(z + 2\pi) = g(z) \qquad \text{for all } z \in \mathbb{C} \tag{4.27}$$

Define $I(y)$ to be the integral taken along a contour parallel to the real axis

$$I(y) = \int_{x+iy}^{x+2\pi+iy} dz\ g(z) \tag{4.28}$$

Then consider the contour Γ shown in Fig. 24. By the assumed periodicity of $g(z)$

$$\int_{B}^{C} dz\ g(z) = \int_{A}^{D} dz\ g(z) \tag{4.29}$$

and hence by Cauchy's theorem

$$\int_{x}^{x+2\pi} \mathrm{d}x \;\; g(x+iy) \;=\; \int_{x+iy}^{x+2\pi+iy} \mathrm{d}x \;\; g(x+iy) \tag{4.30}$$

We have thus shown that $I(y)$ is independent of y.

Now take two functions $f(z)$ and $P(z)$ which satisfy the analyticity and periodicity requirements. Then for any Y

$$\frac{\int_{0}^{2\pi} \mathrm{d}x \;\; f(x)\,P(x)}{\int_{0}^{2\pi} \mathrm{d}x \;\; P(x)} = \frac{\int_{-Y}^{Y} \mathrm{d}y \int_{0}^{2\pi} \mathrm{d}x \;\; f(x)\,P(x)}{\int_{-Y}^{Y} \mathrm{d}y \int_{0}^{2\pi} \mathrm{d}x \;\; P(x)} \tag{4.31}$$

and hence taking the limit $Y \to \infty$ we have that

$$\frac{\int_{0}^{2\pi} \mathrm{d}x \;\; f(x)\,P(x)}{\int_{0}^{2\pi} \mathrm{d}x \;\; P(x)} = \frac{\int_{S} \mathrm{d}z \;\; f(z)\,P(z)}{\int_{S} \mathrm{d}z \;\; P(z)} \tag{4.32}$$

where S is any strip of width 2π extending to $\pm\infty$ in the imaginary direction. Now cover the complex plane with such strips and it follows that

$$\frac{\int_{0}^{2\pi} \mathrm{d}x \;\; f(x)\,P(x)}{\int_{0}^{2\pi} \mathrm{d}x \;\; P(x)} = \frac{\int_{\mathbb{C}} \mathrm{d}z \;\; f(z)\,P(z)}{\int_{\mathbb{C}} \mathrm{d}z \;\; P(z)} \tag{4.33}$$

and the mysterious question of how the real and complex integrals are related is solved for periodic functions - both give the same value.

In conclusion, we have seen in this section how it may be possible to calculate moments of complex 'probability distributions' by use of the associated (complex)

Langevin equation. Further, for periodic functions it has been shown that correlations can be measured in the complex plane by direct analytic continuation. The only open question is whether the exponential convergence of the real Langevin equation still holds. This question should be easily resolved by numerical simulation since the alternative is exponential divergence.

4.3 - Abelian Lattice Gauge Theory

As a first step in understanding and implementing these techniques we will study U(1) lattice gauge theory in two and three dimensions [99]. Although extremely powerful techniques already exist for Abelian models [100], we begin our investigation here since the exact solubility of the U(1) theory in two dimensions is extremely helpful allowing direct comparison of Monte Carlo results with those obtained analytically.

The particular correlation function to be measured is that introduced earlier, namely the correlation between a Wilson loop, W, and a test plaquette, P. As discussed in Section 3.5 this corresponds to the squared electric field. The relevant path integral is

$$\langle W \cdot P \rangle = \frac{\int [d\theta\,]\; e^{i\theta_l \delta_{l\in P}}\; e^{i\theta_m \delta_{m\in W}}\; e^{\beta S}}{\int [d\theta\,]\; e^{i\theta_m \delta_{m\in W}}\; e^{\beta S}} \tag{4.34}$$

where $\delta_{m\in W}$ and $\delta_{l\in P}$ are used to pick out the links occurring in the loop and plaquette respectively. The action S is the conventional Wilson action

$$S = \sum_{plaquettes,n} \cos\theta_{\mu\nu}(n) \tag{4.35}$$

and $\theta_{\mu\nu}$ is the path ordered plaquette angle

$$\theta_{\mu\nu} = \theta_{\mu}(n) + \theta_{\nu}(n+\hat{\mu}) - \theta_{\mu}(n+\hat{\nu}) - \theta_{\nu}(n) \tag{4.36}$$

Thus the Langevin equation that must be solved is for the 'probability distribution'

$$P(\theta_m)\, \mathrm{d}\theta_m = e^{\beta \sum_{j=1}^{2(d-1)} \cos(\theta_m + \mathrm{E}_j) \; + \; i\delta_{m\in W}\theta_m} \mathrm{d}\theta_m \tag{4.37}$$

(in d dimensions) where E_j is the *jth* 'environment' † associated with link m.

which leads to the Langevin equation

$$\frac{\partial \theta_m}{\partial t} = \left(-\beta \frac{\sum_{j=1}^{2(d-1)} \cos(\theta_m + \mathrm{E}_j)}{\sum_{j=1}^{2(d-1)} \sin(\theta_m + \mathrm{E}_j)} + i\delta_{m\in W} \right) + \sqrt{2}\,\eta(t) \tag{4.38}$$

As has been observed elsewhere [101] there are numerical problems with this sort of equation. In particular the trigonometric functions grow exponentially as distance from the real axis increases causing numerical overflows. Previous authors [96,102] have just truncated paths which wandered too far from the real axis but this approach is unsuitable in lattice gauge calculations where considerable computation is required to generate lattice configurations - discarding an entire system when the imaginary part of one of the links becomes too large would be unworkable.

Consider, however, a generalised Langevin equation

$$\dot{\xi} = h(\xi,t) + g(\xi,t)\,\eta(t) \tag{4.39}$$

with the first-order discretisation

† The 'environments' of link m are defined to be the plaquette angles of the $2(d-1)$ plaquettes containing that link with θ_m subtracted out.

$$\xi(t+\delta t) = \xi(t) + h(\xi)\,\delta t + g(\xi)\sqrt{2\delta t}\;\eta \tag{4.40}$$

The criterion for accurate numerical simulation of this equation is that the time step δt must be chosen to satisfy

$$|g(\xi)| \gg |h(\xi)|\,(\delta t)^{1/2} \tag{4.41}$$

i.e., the deterministic 'drift' force must be smaller than the stochastic force.

In our numerical simulations, therefore, the time step is dynamically chosen to satisfy this constraint. Paths still exist which travel far into the complex plane, since the system is ergodic, but they are now evolved in a controlled manner and remain within a bounded area rather than heading off to infinity.

The dynamical time-stepping algorithm is as follows. Say that we wish to evolve the system from Langevin time T to $T + \delta T$. Denote by $T_i \in [T, T + \delta T]$ the Langevin time to which variable i has evolved. Then a lattice update is a series of sweeps through all the sites updating by δt_i chosen according to

$$\delta t_i = \min(\, T+\delta T - T_i \,,\, t_\Delta) \tag{4.42}$$

where t_Δ is defined by (Δ is some predefined value, let us say 0.1)

$$(t_\Delta)^2 = \frac{|g(\xi(t))|^2}{|h(\xi(t))|^2}\;\Delta^2 \tag{4.43}$$

This constrains the individual links to evolve according to the constraint, Eq. (4.41). The procedure is repeated until all variables have been evolved to $T + \delta T$.

This raises an interesting issue for the execution of this algorithm on parallel computers. A concurrent implementation could have load balancing difficulties since some of the links require more updating 'hits' than others. Our experience, however, shows that the

areas where this is the case are few in number and small in size. Thus the extra calculation required is small by comparison with the total amount of work on any update. It is also possible, by suitable choice of the input parameters δT and Δ, to make small the number of extra 'hits' required. Furthermore, the areas where extra cycles must be spent tend to move fairly slowly through the lattice and so we expect that 'dynamic load-balancing' algorithms [103] should be reasonably effective.

The results of simulations in two dimensions are shown in Fig. 25a) and b). They represent the correlation of a plaquette with a 5×5 Wilson loop. The theory is analytically soluble in two dimensions, yielding the following values depending on whether or not the test plaquette is inside or outside the current loop.

$$\langle W.P \rangle_{inside} = \frac{I_0(\beta)}{I_1(\beta)} - \frac{1}{\beta} \tag{4.44}$$

$$\langle W.P \rangle_{outside} = \frac{I_1(\beta)}{I_0(\beta)} \tag{4.45}$$

A periodic 10×10 lattice was used, with $\delta T = .01$, $\Delta = .1$. At each value of β about 3000 sweeps were carried out for a total evolved Langevin time of 30. This calculation was previously carried out (by a similar method) [104] for large values of β and our agreement with those results is good. At these larger values it is observed that the configurations depart only slightly from the real axis (i.e., the links values θ_i have only small imaginary parts) but as β decreases these excursions become larger and larger, thus necessitating the use of the algorithm described above.

In Figs. 26a) and b) are shown the results of simulations in three dimensions. This theory is confining for all values of β [105] and we chose to calculate at $\beta = 2.0$, where the string tension has a significant value [106] and one might expect to find a non-trivial flux tube. The values shown are for the squared parallel electric field density - i.e., for

plaquettes lying in the plane of the current loop and we do indeed see an electric flux tube. Again we work with $\delta T = 0.01$ and $\Delta = 0.1$. The data for the 5×5 loop corresponds to about 5000 sweeps through the system or a total elapsed Langevin time $T = 50$ while the data for the 7×7 loop has slightly fewer sweeps, around $T = 40$. In both cases the relative errors are around 1-2 % and it is encouraging that the Langevin time required for equilibration is fairly insensitive to the size of the current loop involved since this means that with only modest computer resources one might hope to study the behaviour of the theory at quite large distances.

4.4 - Non Abelian Lattice Gauge Theory

Having discussed in the previous section the application of the complex Langevin equation to Abelian theories, we turn in this section to the more interesting non-Abelian cases. Obviously it is crucial to discover whether or not the success of the technique in the U(1) theory extends to other cases.

As a guide to understanding the problems involved we study SU(2) and the integral

$$L(\beta) = \frac{\int [dU]\ (\mathrm{tr}\ U)^2\ e^{\frac{\beta}{4}\mathrm{tr}(U+U^{-1})}}{\int [dU]\ \mathrm{tr}\ U\ e^{\frac{\beta}{4}\mathrm{tr}(U+U^{-1})}} \qquad U \in SU(2) \tag{4.46}$$

which leads to the probability distribution

$$P(U)\,[dU] = \mathrm{tr}\ U\ e^{\frac{\beta}{4}\mathrm{tr}(U+U^{-1})}\ [dU] \tag{4.47}$$

This is of similar form to the loop-plaquette correlation discussed in Sections 3.5 and 4.1, but restricted to the case where the lattice has been replaced by a single link. (Analogous

to our model problem, Eq. (4.4).)

Using the identity

$$\chi_F^2(U) = \chi_A(U) + 1 \tag{4.48}$$

for the traces of group elements in the fundamental (F) and adjoint (A) representations one can calculate

$$L(\beta) = \frac{3\, I_3(\beta) + I_1(\beta)}{4\, I_2(\beta)} \tag{4.49}$$

To address the problem of the distribution function (4.2) one first constructs the Fokker-Planck equation restricted to the SU(2) group manifold. To do this introduce covariant derivatives, ∇_α, which satisfy the same commutation relations as the group generators

$$[\nabla_\alpha, \nabla_\beta] = i\, \epsilon_{\alpha\beta\gamma} \nabla_\gamma \tag{4.50}$$

and which can be defined in terms of Pauli matrices, σ_α, by

$$\nabla_\alpha U = \tfrac{1}{2}\, i\sigma_\alpha \cdot U \qquad\qquad U \in SU(2) \tag{4.51}$$

$$\nabla_\alpha U^{-1} = -\tfrac{1}{2}\, iU^{-1} \cdot \sigma_\alpha$$

In terms of these derivatives the Fokker-Planck equation corresponding to the distribution $P(U) = e^{-\beta S(U)}$ is

$$\frac{\partial p(U,t)}{\partial t} = \nabla_\alpha \nabla_\alpha\, p(U,t) - \nabla_\alpha \left\{ - p(U,t)\, \beta\, \nabla_\alpha\, S(U) \right\} \tag{4.52}$$

and following [107], this equation is solved by introducing a discretised Langevin equation for the group elements

$$U(t+\delta t) \;=\; U(t)\,\exp(\,\delta t\;\boldsymbol{\mu}\;+\;\sqrt{2\delta t}\;\boldsymbol{\epsilon}) \tag{4.53}$$

where, to first order in δt,

$$\boldsymbol{\mu} \;=\; -\,(\,\beta\nabla_\alpha S(U))\;\sigma_\alpha \tag{4.54}$$

$$\boldsymbol{\epsilon} \;=\; \tfrac{1}{2}\,i\sigma_\alpha\,\eta_\alpha$$

and η_α is a vector of independent normal random numbers with mean zero and unit variance.

In the case where $S(U)$ is real, both $\boldsymbol{\mu}$ and $\boldsymbol{\epsilon}$ are traceless and anti-hermitian which is sufficient to guarantee that elements evolving according to Eq. (4.53) remain on the SU(2) manifold. However, when $S(U)$ is complex, the matrices $\boldsymbol{\mu}$ and $\boldsymbol{\epsilon}$ remain traceless, but are no longer anti-hermitian. This results in the extension of the SU(2) manifold to SL(2,$\mathbb{C}$). The inverse of a matrix is still a well defined quantity since all have unit determinant and the first two relations of Eq. (2.2) still make sense, but it is no longer possible to identify U^{-1} with $U^\dagger$. (This is the reason for specifying the inverse explicitly in Eq. (4.46).)

Taking these factors into account we can write the discretised Langevin equation corresponding to the distribution Eq. (4.47)

$$U(t+\delta t) \;=\; U(t)\,\exp\left\{-\tfrac{1}{2}\,i\,\delta t\;\boldsymbol{\chi}(\beta)\cdot\sigma\;+\;\sqrt{\delta t/2}\;i\,\eta\cdot\sigma\right\} \tag{4.55}$$

where

$$\chi_\alpha(\beta) \;=\; \left\{\frac{\beta}{4}+\frac{1}{\mathrm{tr}(U+U^{-1})}\right\}\;\mathrm{tr}\left[(U-U^{-1})\,\sigma_\alpha\right] \tag{4.56}$$

In Fig. 27 are shown the results of simulations of this equation. Obviously the dynamics are faulty at low values of β. Comparing the distributions Eqs. (4.37) and (4.47)

the most obvious difference is that the latter has a zero corresponding to a non-analyticity in the complex action, $S(U)$. To study the effect of this zero consider a much simpler integral which again admits a simple analytic value.

$$K(\beta) = \frac{\int_0^\pi d\theta \ \cos^2\theta \ e^{\beta\cos\theta}}{\int_0^\pi d\theta \ \cos\theta \ e^{\beta\cos\theta}} = \frac{I_0(\beta)}{I_1(\beta)} - \frac{1}{\beta} \tag{4.57}$$

We thus attempt to model the distribution function

$$P(\theta)\, d\theta = \cos\theta \ e^{\beta\cos\theta} \ d\theta \qquad 0 < \theta < \pi \tag{4.58}$$

Since θ is at this point a purely real variable the conditions of the segregation theorem apply [108, appendix C] which means that the interval $[0,\pi]$ is divided up into two non-communicating regions $[0,\frac{1}{2}\pi)$ and $(\frac{1}{2}\pi,\pi]$. This in turn means that solutions of the associated Langevin equation

$$\frac{\partial\theta}{\partial t} = -(\beta\sin\theta + \tan\theta) + \sqrt{2}\,\eta(t) \tag{4.59}$$

move on trajectories which are confined to whichever of the pieces contains the starting value. On these regions the motion is still ergodic and so time averages of $\theta(t)$ generate results which correspond to the restriction of the integrals to the appropriate interval.

However, we can try to defeat the segregation theorem by making an analytic continuation of the variable θ to the complex plane as previously. This is trivial since the range of integrals in Eq. (4.57) can be extended to $[0,2\pi]$ and then the construction of Eqs. (4.31)-(4.33) holds. Having done this one finds the complex Langevin equation to be solved is

$$\frac{\partial z}{\partial t} = -(\beta\sin z + \tan z) + \sqrt{2}\,\eta(t) \tag{4.60}$$

which has the same form as Eq. (4.59) but for complex z. The conditions of the segregation theorem do not now strictly apply but another problem exists. In Fig. 28 are shown the trajectories of the deterministic part of Eq. (4.60) obtained by setting $\eta(t)$ to zero. As can be seen the paths are strongly attracted to the real axis and it is simple to show that once there they never leave. Numerically this means that our trajectories are drawn towards the real axis and eventually when the resolution of the floating point numbers is exceeded the paths collapse to the real axis, never to leave. The conditions of the segregation theorem then take effect and the situation discussed in connection with Eq. (4.60) holds.

To see this in practice we have plotted, in Fig. 29, the results of our simulations with Eq. (4.60) together with the analytic result, Eq. (4.57), and a numerical estimate of the integral

$$\frac{\int_0^{\pi/2} d\theta \;\; \cos^2\theta \;\; e^{\beta\cos\theta}}{\int_0^{\pi/2} d\theta \;\; \cos\theta \;\; e^{\beta\cos\theta}} \tag{4.61}$$

which is the predicted outcome according to the segregation theorem.

As can be seen our results are in agreement with the segregation theorem and examination of the complex parts of the variable z show that it rapidly becomes zero as the simulation proceeds.

4.5 - Conclusions and Prospects

In the previous section we tested Complex Langevin methods on several non-trivial theories, meeting with great success in the U(1) problems but less in the non-Abelian models. Before discarding the method as "Just another technique which only works in the Abelian case" we should examine carefully the reason for the failure.

In the Abelian case the Langevin force due to the Wilson loop was of constant magnitude independent of the actual link value, and so had some effect at every update. In the non-Abelian case, however, the Langevin force due to the loop was zero along a certain path which we shall call the "critical trajectory", and to which the links were strongly attracted. Furthermore, along this critical trajectory the 'probability density' $W e^{-\beta S}$, had zeros.

If we consider the simple case where the links are constrained to evolve only along the critical trajectory then the segregation theorem holds rigorously and predicts the partitioning of the space into non-communicating disjoint sectors upon which, individually, the motion is ergodic.

If we were to consider the continuum time evolution of the Langevin paths, with the initial position chosen to lie off the critical trajectory then all would be well. In particular it is possible to prove that the links reach the critical trajectory with probability zero. This is reasonable since the path is attractive for less than its entire length and the strength of the attraction becomes arbitrarily weak as one approaches thus allowing the fluctuating force to kick the link into a region where the critical trajectory is (strongly) repulsive. Thus the segregation theorem can be defeated and the Complex Langevin sample paths are ergodic, over the entire complex plane.

Unfortunately our numerical studies cannot be performed in the continuum and as a result our paths are indeed attracted arbitrarily close to the critical trajectory. When there, the limited resolution of the standard representation of floating point numbers limits the

length of time within which the fluctuating force can 'kick' the path away since the imaginary parts of the variables become zero after a fairly short while. As a result we 'fall' into a situation where the segregation theorem effectively holds and our simulations are spoilt.

However, there still remain encouraging features of our calculations. While it is true that the correlation we set out to measure suffers from the above described malaise, this is not necessarily true for all lattice observables. In particular, 'probability densities' without zeros will be immune from segregation, as will those whose stable paths do not correspond to the restriction to the real Langevin manifold. As examples of problems which have actually been solved with the Complex Langevin technique we can cite the chiral SU(2) model in an external field [109] and the extremely interesting finite baryon number simulations [110] both of which have yielded interesting results. It is also true, of course, that the Abelian models do not seem to suffer from segregation at all, and so are amenable to this treatment.

As a final comment we consider a possible way of defeating segregation for our flux tube observables. As stated, in the continuum, paths collapse to the critical trajectory with zero probability, so it has been suggested [111] that one might perform extremely accurate simulations of paths which approach this trajectory in the hope that it may be possible to find examples which do evade the segregation problem by tunneling into another sector. These paths could then be 'tacked' onto more realistic simulations whenever a variable came too close to the critical trajectory hopefully restoring the ergodicity property.

In conclusion the complex Langevin equation is a potentially very powerful tool which may allow observables to be measured at considerable lattice separations. Its viability in several circumstances has already been demonstrated, and while there appear to be numerical difficulties in some cases, it may ultimately prove possible to circumvent even these.

CHAPTER 5

Heavy Quarks and Dynamical Fermions

In previous chapters the quenched approximation to full QCD has been discussed, in which the effects of light quark pairs are neglected. In this chapter we presented a preliminary case study of an algorithm which includes such effects.

The first question to be answered is why bother with the full theory when the quenched approximation apparently works so well ? In particular, a powerful argument was outlined at the beginning of Chapter 3 supporting the use of this approximation. Furthermore our heavy quark potential and energy densities provided excellent qualitative understanding of heavy quark systems and several calculations of the quenched mass spectrum [80,112] have yielded quite good agreement with experimental data. Obviously the relevant question is whether or not the full theory can make up for the small discrepencies between the quenched approximation and experiment. For example, it was suggested in Section 3.7 that vacuum polarisation effects might account for the apparent discrepency between the Coulombic strength of our heavy quark potential and that required

phenomenologically. A second effect we might expect to see is the weakening of the string tension at large separations due to string breaking and meson pair creation.

A further motivation for the study of dynamical fermions comes from other areas of QCD beyond the interquark potential. For example the quenched theory has a first-order deconfinement transition at finite temperature due to the breaking of the Z_3 symmetry on the timelike links of the lattice [113]. The inclusion of dynamical fermions breaks this symmetry explicitly and the transition becomes that from the hadronic confined phase to a high temperature quark-gluon plasma [114]. The study of the order and temperature of this transition are of central importance in the evolution of the early universe and accurate calculations of the deconfining temperature are becoming especially important since preliminary simulations suggest that the critical temperature might be attainable in heavy ion collisions.

Having discussed the importance of these calculations the next question is how they are to be realised. The problems encountered in simulating the fermionic action are well known. In particular the derivative appearing in the Dirac equation leads to species doubling such that the naive action for a single flavour becomes, on the lattice, 2^d flavours (in d dimensions). The two common solutions to this problem both have weaknesses. The Wilson prescription [8,115] adds to the action a term which breaks the degeneracy of the doubled flavours, with all but one becoming infinitely massive when the continuum limit is taken. Unfortunately the extra term breaks all continuum chiral symmetries. The Kogut-Susskind scenario [116] thins out the flavours by putting different spinor components at different lattice sites. This approach maintains a continuum chiral symmetry, but only reduces the number of flavours by a factor of $2^{d/2}$.

The deficiencies of the two methods exhibit the Nielsen-Ninomiya [117] 'no-go' theorem which effectively prohibits both a single flavour and continuous chiral symmetries in a local lattice theory. Methods by which this theorem can be circumvented are

currently under active study since it is expected that unified theories will be chiral. Two possible solutions are the non-local SLAC derivative [118] and the more recent suggestion [119] which involves a long range sum over string configurations in the Hamiltonian. At this point the former solution seems to be intractable numerically and little investigation of the second has been performed. We view this field as one currently developing and shall have no more to say about it.

A second difficulty with dynamical fermion simulations is best seen by examining the full QCD partition function after integration over the fermionic degrees of freedom and application of the result [120]

$$\text{Det } M \;=\; \int [\mathrm{d}\phi][\mathrm{d}\bar{\phi}]\, e^{-\bar{\phi}M^{-1}\phi} \tag{5.1}$$

to replace the Grassman fermionic fields by bosonic 'pseudo-fermions', ϕ.

$$Z \;=\; \int [d\phi]\,[d\bar{\phi}]\,[dU]\;\exp\left(\beta F_{\mu\nu}F^{\mu\nu} \;+\; \bar{\phi}Q^{-1}\phi\right) \tag{5.2}$$

(Q is some lattice representation of the Dirac operator $\not{D} + m$.) The problem lies in the fact that the matrix Q is not positive definite and so a simple probabilistic treatment is not possible. This situation is exactly analogous to that examined in Chapter 4 and suggests the use of the Complex Langevin equation. However, rather than fence again with the segregation theorem, we can make use of a simple property of the Q matrix to replace Eq. (5.2) with

$$Z \;=\; \int [d\phi]\,[d\bar{\phi}]\,[dU]\;\exp\left(\beta F_{\mu\nu}F^{\mu\nu} \;+\; \bar{\phi}(Q^{\dagger}Q)^{-1}\phi\right) \tag{5.3}$$

in which we have made the action positive definite at the expense of a further doubling of the number of fermionic species. This turns out to be evanescent, however, since Q is a local operator coupling only nearest neighbour lattice sites which means that $Q^{\dagger}Q$ couples only second nearest neighbour sites. We make the particular choice [121]

$$Q_{xy}^{AB} = im\,\delta_{xy}\delta^{AB} - \tfrac{1}{2}\sum_{\mu=0}^{d-1}\alpha_\mu(x)\left[\delta_{x+\mu,y}\,(U_{x,\mu}^{\dagger})^{AB} + \delta_{x,y+\mu}\,(U_{x-\hat{\mu},\mu})^{AB}\right] \qquad (5.4)$$

where x,y denote sites in the lattice, A,B are colour indices and the factors $\alpha_\mu(x)$ are the spin diagonalised gamma matrices defined by

$$\alpha_0(x) = (-1)^{x_0} \qquad (5.5)$$

$$\alpha_1(x) = (-1)^{x_0+x_1}$$

$$\alpha_2(x) = (-1)^{x_0+x_1+x_2}$$

$$\alpha_3(x) = (-1)^{x_0+x_1+x_2+x_3}$$

For this particular representation it can be shown [122] that no nearest neighbour couplings remain and the number of flavours can be halved by setting $\phi \equiv 0$ on the odd parity sites, defined by the sign of $(-1)^{x_1+x_2+x_3+x_4}$.

Having thus decided on a fermionic representation with requisite symmetries and species, it remains to decide upon an algorithm by which field configurations will be generated. Several 'exact' algorithms exist [123,124] in the sense that they involve no systematic error in the limit of infinite CPU power, but the time taken to perform calculations with these methods typically grows as some large power of the lattice volume. This renders them effectively useless on the large lattices required to reproduce continuum physics.

There do exist, however, several 'approximate' algorithms which are computationally more attractive but involve systematic errors even in the infinite CPU limit. A question of crucial importance, therefore, is the quantification of these errors. Zwanziger has theoretically derived the systematic error of a particular algorithm [125] and numerical evidence [126] suggests that plausible arguments regarding the error of the pseudofermion algorithm

may be correct. A careful study of some of these questions has been performed by Weingarten [127]. In the first section of this chapter we discuss in detail the systematic errors associated with the discretisation of the Langevin equation which is then used in Sections 2 and 3 to simulate the full theory, QCD with dynamical fermions.

5.1 Systematic Errors

The question of which fermionic algorithm to use is by no means clear-cut and in choosing the Langevin method one has passed over two common alternatives. The pseudo-fermion method [128] has been widely applied to all aspects of QCD [129,130] with reasonable quantitative success. Basically the method is a Metropolis update with matrix elements of the inverse Q^{-1} calculated by means of a second Monte Carlo. It is this which makes the method unappealing for while the systematic errors associated with the Metropolis algorithm are calculable, the errors due to the finite execution of the second Monte Carlo are uncalculable and quite hard to estimate. The microcanonical method, discussed briefly in 2.3 is currently quite popular but its lack of explicit ergodicity represents a worrying question. The 'hybrid' algorithms, which are explicitly ergodic variants, have been shown by Duane [30] to be closely related to the Langevin process and so we expect that lessons learned from the latter will be of relevance in their study.

As further motivation for studying the Langevin equation, recent work [131] suggests that additional computational acceleration can be achieved by solving the equations of motion in momentum space where separate time steps can be assigned to the high and low frequency components. The exact status of these results is unclear since the gauge degree of freedom typically mixes high and low frequencies but preliminary experiments in which the gauge is fixed are quite interesting [132].

In order to assess the systematic error of the Langevin equations [133] we first consider the simplest case of a quadratic action among real scalar fields ϕ_i.

$$S(\phi) = \tfrac{1}{2} \sum_{i,j} \phi_i M_{ij} \phi_j \tag{5.6}$$

to which there corresponds the Langevin equation

$$\frac{\partial \phi_i}{\partial t} = -\frac{\partial S}{\partial \phi_i} + \eta_i \tag{5.7}$$

in which the $\eta_i(t)$ are independent Gaussian random variables. This equation can be solved exactly, yielding

$$\phi(\tau) = e^{-\tau M} \phi(0) + \int_0^\tau ds\ e^{-(\tau - s)M} \eta(s) \tag{5.8}$$

in an obvious vector notation. Since we are interested only in the long time equilibrium distribution we can take the origin of τ time to $-\infty$, giving

$$\phi(\tau) = \int_{-\infty}^\tau ds\ e^{-(\tau - s)M} \eta(s) \tag{5.9}$$

Any equilibrium correlation function can now be computed. For instance

$$\langle \phi_i \phi_j \rangle = \overline{\phi_i(\tau)\phi_j(\tau)} \tag{5.10}$$

$$= \sum_{k,l} \int_{-\infty}^\tau ds_1 \int_{-\infty}^\tau ds_2 \, [e^{-(\tau - s_1)M}]_{il} \, [e^{-(\tau - s_2)M}]_{jk} \, \overline{\eta_l(s_1)\eta_k(s_2)}$$

$$= 2 \sum_k \int_{-\infty}^\tau ds \, [e^{-(\tau - s)M}]_{ik} \, [e^{-(\tau - s)M}]_{jk}$$

$$= 2 \int_{-\infty}^\tau ds \, [e^{-(\tau - s)2M}]_{ij}$$

$$= [M^{-1}]_{ij}$$

where the bar denotes averages over realisations of the noise η. It is not difficult to show that all correlation functions are reproduced exactly. A proof for general (i.e., non-quadratic) actions is given to all orders of perturbation theory in [134].

To implement the Langevin equation numerically, one discretises τ, and this introduces a systematic error which we now determine. The simplest discretisation of Eq. (5.7) is

$$\phi_i(n+1) = \phi_i(n) - \delta\tau \frac{\partial S}{\partial \phi_i} + \sqrt{2\delta\tau}\, r_i(n) \tag{5.11}$$

$$\overline{r_i(n)\, r_j(m)} = \delta_{ij}\, \delta_{nm} \tag{5.12}$$

where n labels the step number. By direct analogy to Eq. (5.9) the solution of this equation is

$$\phi(n) = \sum_{s=-\infty}^{n-1} (1 - \delta\tau M)^{n-1-s} \sqrt{2\delta\tau}\, r(s) \tag{5.13}$$

and hence the discrete two-point function is

$$\langle \phi_i \phi_j \rangle = \overline{\phi_i(\tau)\, \phi_j(\tau)} \tag{5.14}$$

$$= \sum_{s_1=-\infty}^{n-1} \sum_{s_2=-\infty}^{n-1} (1-\delta\tau M)_{il}^{n-1-s_1} (1-\delta\tau M)_{jk}^{n-1-s_2}\, 2\, \delta\tau\, \overline{r_l(s_1)\, r_k(s_2)}$$

$$= 2\,\delta\tau \left[(1-\delta\tau M)^{2(n-1)} \sum_{s=-\infty}^{n-1} (1-\delta\tau M)^{-2s} \right]_{ij}$$

$$= \left[\frac{1}{M} \frac{1}{1-\frac{1}{2}\delta\tau M} \right]_{ij}$$

Thus the relative error of the two-point function for finite time step $\delta\tau$ goes at worst as $\frac{1}{2}\delta\tau\lambda_{max}$ where λ_{max} is the maximum eigenvalue of M. This same result holds for all the n-point functions. In addition this holds for arbitrary matrices M, e.g., for long or infinite ranged interactions. The particular example of a quadratic interaction which interests us is, of course, the fermionic interaction discussed previously

$$M = [\,(\not{D}+m)\,(\not{D}+m)^{\dagger}\,]^{-1} \tag{5.15}$$

whose eigenvalues are of the form

$$\rho = m^2 a^2 + \kappa^2 \tag{5.16}$$

where the lattice spacing a appears explicitly so that the bare quark mass is measured in fixed physical units. κ^2 is a positive quantity which depends upon the particular gauge fields since $\not{D}$ is a covariant derivative. As we approach the continuum limit, taking $a \to 0$, the relation between a and the correlation length, measured in lattice units is

$$\xi_{\pi} \sim \frac{1}{a} \tag{5.17}$$

where the subscript refers to the lightest particle in the theory - for QCD this is the pion.

Thus the minimum eigenvalue of $(\not{D}+m)(\not{D}+m)^{\dagger}$ varies with the lattice correlation length as

$$\rho_{\min} \sim \frac{1}{\xi_{\pi}^2} \tag{5.18}$$

up to logarithms (The bare mass in Eq. (5.16) moves logarithmically as $a \to 0$). Our bound for the relative error of discretising the Langevin equation is then

$$\epsilon \sim \tfrac{1}{2}\,\delta\tau\,\lambda_{max} = \tfrac{1}{2}\,\delta\tau\,\xi_{\pi}^2 \tag{5.19}$$

and so, as the continuum limit is taken, $\delta\tau$ must also approach zero as ξ_π^{-2} or $V^{-1/2}$ where V is the total lattice volume. This means that the overall speed of the algorithm scales as $V^{-3/2}$ since there is a trivial linear dependence on the volume arising from the necessity of updating each degree of freedom once per update. It is also important to note that higher order discretisations of the Langevin equation lead to higher order errors, i.e., an n^{th} order discretisation leads to errors of order ϵ^n.

At this point we should note that all the measures calculated so far have been for quadratic actions and that while the fermionic contribution to the QCD path integral is of this form, the pure gauge action is not. In order to study this we must therefore examine the behaviour of ϵ in perturbation theory about the quadratic case. Since the algorithm which we will eventually adopt does not require this, however, we will relegate its discussion to the appendix.

5.2 A Mixed Algorithm and Finite Temperature QCD

Having, in the previous section, discussed the systematic errors introduced by the discretisation of the Langevin equation we proceed in this section to test its performance on a much studied problem, that of the deconfining temperature of QCD in the presence of four flavours of light fermions. In studying this problem our goal is not a super accurate determination of the transition point, nor is it a comprehensive analysis of the order of the transition both of which have been discussed elsewhere [135,136]. Rather we aim to study the feasibility of studying the full theory with our algorithm.

The conventional Langevin approach to this problem would be to take the action

$$S = \beta F_{\mu\nu} F^{\mu\nu} + \bar{\phi}(Q^\dagger Q)^{-1} \phi \tag{5.20}$$

and simulate to first order in the timestep $\delta\tau$ the Langevin equations for the gauge fields, U, and the pseudo fermion field ϕ. This is the approach taken successfully in [136] and which the analysis of the preceding section tells us has a systematic error proportional to $\delta\tau$.

We prefer to work to second order in $\delta\tau$ using the algorithm of [137] which yields the discretised equation of motion for the ϕ fields

$$\phi(t+\delta t) = \phi(t) + \tfrac{1}{2}\,\delta t\,(\phi^1 + \phi^2) + \sqrt{2\delta t}\;\eta \tag{5.21}$$

where η is a vector of Gaussian random numbers with zero mean and unit variance and $\phi^{1,2}$ are defined by

$$\phi^1 = 2\,\mathrm{Re}\,(Q\,Q^\dagger)^{-1}\,\phi(t) \tag{5.22a}$$

$$\phi^2 = 2\,\mathrm{Re}\,(Q\,Q^\dagger)^{-1}\,(\phi(t) + \delta t\,\phi^1 + \sqrt{2\delta t}\;\eta) \tag{5.22b}$$

Since this requires the inversion of $Q^\dagger Q$ twice per iteration the method runs approximately twice as slowly as the first-order method. (The matrix inversion is the dominant part of the calculation.) For consistency we should also work to second order for the gauge field evolution but do not take this approach for two reasons. Firstly there is little agreement in the literature as to the exact form of the second order equations for the gauge fields. For example the analysis of Drummond et al. [107] differs in detail from that used in [131] and also the author's derivation. Secondly the algorithm is rather slow - requiring the exponentiation of 3×3 complex matrices. As a result of these problems we make the novel step of replacing the Langevin evolution of the gauge fields with a Metropolis update.

At first sight this might seem a strange approach but it has been shown that for small hitsizes, δU, the Markov process of the Metropolis algorithm converges to that of the Langevin process with stepsize $\delta\tau$ via the identification [138]

$$6\,\delta\tau \sim (\delta U)^2 \tag{5.23}$$

Thus the important question becomes the tuning of the relative evolution rates of the gauge and fermionic fields so that approximate equilibrium is maintained. We will return to this point later in this section.

So far all the approximations made have, in principle, calculable systematic errors. For computational simplicity, however, we make one further approximation most easily envisioned by considering the linearised change in the gauge action due to a gauge field trial move $U \rightarrow U + \delta U$

$$\delta S = -\bar{\phi}\,(Q\,Q^\dagger)^{-1}\left[\frac{\delta Q}{\delta U}Q^\dagger + Q\,\frac{\delta Q^\dagger}{\delta U}\right](Q\,Q^\dagger)^{-1}\,\phi \tag{5.24}$$

This quantity involves the fermionic propagator $(Q^\dagger Q)^{-1}\phi(t)$. Since $Q \equiv Q(U)$ this quantity varies as the gauge fields themselves evolve during the sweep. However, we chose to evaluate it once at the beginning of each sweep and to treat it as a constant for the entire update cycle. This unfortunately leads to a violation of the detailed balance constraint and will lead to a systematic error in the Monte Carlo of which we have little *a priori* quantitative understanding. We know, however, that the error introduced is of order (δU) and could thus repair some of the damage by updating the propagator to this order at each gauge update, a procedure analogous to that employed in [123]. Instead we chose to merely monitor the size of the error by calculating the quantity

$$K = \sum_{sites\ n} \phi(n)^*\phi(n) \tag{5.25}$$

for which we can trivially obtain the identity (For thinned Kogut-Susskind fermions)

$$K \equiv \mathrm{tr}\,(Q^{\dagger}Q) = 3(2 + m^2) \tag{5.26}$$

where m is the bare fermion mass and the factor of 3 arises from the colour trace. The deviations of this parameter thus allow us to monitor the approximate magnitude of the errors incurred due to detailed balance violations in the gauge field update.

Our first priority is to find a suitable range of parameters for our 'mixed' algorithm. In order to facilitate this we studied the theory on a small, 4^4, lattice at a bare mass of $m = .1$ which is the value at which we are predominantly interested in working. Furthermore we fix $\delta\tau$ to be .01 which value was successfully used in the previous (first-order) approach [136] and concentrate on the value $\beta = 6.1$ chosen for comparison with the quenched calculations of Chapter 2. The remaining free parameters, therefore, are the gauge field hitsize and the accuracy to which we invert the matrix $Q^{\dagger}Q$ (and hence calculate the propagator) which is controlled by the number of iterations of the conjugate gradient solver employed [139]. The hitsize is quantified by making gauge hits of the form

$$U \rightarrow U' = g\,U \tag{5.27}$$

where g is an SU(2) group element chosen to lie in one of the SU(2) subgroups of SU(3) (Compare section 3.1) and which are weighted towards the identity by the factor

$$e^{1/2\,\alpha\,\mathrm{tr}\,g} \tag{5.28}$$

Large values of α thus favour matrices close to the identity and slow down the evolution process according to Eq. (5.27). Our measure of the success of each choice is taken to be the parameter K introduced above.

The results of these simulations are shown in Figs. 30a) and b) where each parameter in turn is held fixed and the other varied. Also shown is the value $K = 6.03$ which is the

correct value for this mass. The lattice for which we performed 50 conjugate gradient iterations at $\alpha = 150$ was thermalised for a total Langevin time of $\tau = 10$, i.e., 1000 sweeps and then each subsequent lattice was derived from this one. In each case 200 sweeps were performed for thermalisation and then measurements were made on every sweep for another 100 cycles. From this experiment we see that $\alpha = 150$ together with 50 conjugate gradient sweeps seems to give reasonably good agreement with the required result. We must note, however, that the lattice volume is obviously going to play a role in scaling these parameters as predicted in the previous section.

As stated previously, our first goal is to study the performance of this algorithm in calculating the deconfinement transition with light fermions. To this end we worked on an asymmetric $8^3 \times 4$ lattice using the thermal Wilson line as the order parameter for the transition. The results are shown in Fig. 31. The system was thermalised at $\beta = 5.2$ by performing 1000 sweeps with parameters chosen as above. 500 sweeps were then performed at each of the measured β values with 200 discarded for thermalisation and subsequently measurements made every tenth sweep.

As can clearly be seen there is a swift crossover from the low temperature confined phase to the higher temperature quark-gluon plasma. This picture is consistent with that obtained by several other calculations and validates the correctness of our algorithm. Note that the errors shown are purely statistical in nature and no estimate has been made of the systematic errors introduced by our calculation. These are actually quite significant - for example the values of $\langle \bar{\phi}\phi \rangle$ measured are typically around 5.0 - 5.5 rather than the expected 6.03 for fermions of mass 0.1. In order to examine the origin of this effect we increased to 120 the number of conjugate gradient cycles used to form the propagator and repeated the calculation at $\beta = 5.15$. The observed change was negligible and leads us to suspect that the major source of inaccuracy is caused by the detailed balance violations associated with the assumption that the fermionic propagator is constant throughout a

single lattice update.

In this section we have introduced a new type of mixed Langevin/Metropolis algorithm for the study of the properties of dynamical fermions on the lattice. The major sources of error have been discussed and some of these effects have been quantified by trial simulations on small lattices. Finally we have verified our method by repeating a standard calculation - that of the deconfinement temperature. With these facts in hand we turn in the next section to a more interesting calculation of the interquark potential in the presence of light fermions.

5.3 The Mesonic Potential Revisited

In this section we would like to conclude our preliminary investigation of our algorithm by reexamining the static quark potential. In doing this we are initially interested in observing qualitative effects such as the tendency for the flux tube to break. This reduces the value of β at which deconfinement occurs although it does not necessarily imply that the physical temperature also decreases since there is no reason to expect that the Λ_L parameters both with and without dynamical fermions should be the same. In fact mass spectrum calculations seem to indicate that these values differ by as much as a factor of two [130]. An alternative encouraging sign would be to find the changes discussed in section 3.7, viz., the modification in the Coulomb interaction strength towards the value predicted from Charmonium experiments, the string tension remaining approximately constant. Unfortunately these two indicators that our method correctly accounts for the fermion pairs are mutually exclusive - either the string tension remains constant at around .18 GeV^2 or one finds that deconfinement has occurred and the string tension vanishes.

The calculation we have attempted can not be said to be definitive. Due to the extensive computational requirements of these calculations we have made no attempt to

extrapolate to zero quark mass but have taken the value $m = .1$ commonly used in fermionic calculations. (On the basis of the quenched approximation this yields quarks with masses around 200 MeV at $\beta = 6.0$). The second constraint, that of computer memory, restricted us to a medium size lattice, $12^2 \times 16^2$ †. As a result we cannot consider our results conclusive, but rather indicative of the response of the $q\bar{q}$ system to the dynamical fermions. We do expect, however, that a new generation of supercomputers will be able to perform accurate numerical simulations. This point is considered again in the next chapter.

As for the calculation that was carried out, we worked at $\beta = 6.1$, the lowest value for which we have data in the quenched approximation. The choice of this value, rather than $\beta = 6.3$ which was preferred in the baryonic calculations due to less contamination by discrete rotational symmetry, was motivated by our smaller lattice volume. If one takes the deconfinement temperature from the $8^3 \times 4$ lattice used in the previous section and scales it according to the two loop perturbation theory result for four flavours of quarks

$$\Lambda_L = a \left[\frac{8\pi^2\beta}{25} \right]^{231/625} \exp \left[-\frac{4\pi^2\beta}{25} \right] \tag{5.29}$$

it is found that the critical temperature on our $12^2 \times 16^2$ lattice should be $\beta \simeq 6.2$. Obviously there is some question as to the validity of this asymptotic formula over the large range of β involved, but the best we can do (and still hope to compare to our previous data) is to chose the lowest value.

As mentioned above the quark mass was taken to be $m = .1$ and the Langevin stepsize $\delta\tau = .01$. On the basis of the previous calculations the Metropolis hitsize parameter was taken to be $\alpha = 150$ and 80 conjugate gradient iterations were performed in the

† These rather unusual dimensions result from a combination of two factors. Our machine has 128 processors and the thinning algorithm requires that each processors sublattice have 'even' size in each dimension.

calculation of the fermionic propagator. This value of α is obviously too small for accurate quantitative results given the larger lattice volume used in this calculation but in the spirit of the exploratory nature of this study we prefer to monitor systematic errors by looking at the parameter K, Eq. (5.25).

With the above set of parameters the lattice was thermalised from a cold start for 500 cycles with $\delta\tau = .02$, and a further 500 sweeps with $\delta\tau = .01$, for a total elapsed Langevin time of 15. We then carried out a further 700 sweeps measuring Wilson loops of sizes 1×1 to 6×12 after every tenth. Since the fermion propagator couples, in principle, all degrees of freedom the variance reducing trick employed in the quenched calculations (Section 3.1 and Ref. [43]) cannot be applied and as a result we were unable to extract any significance from the data at $R = 6$. The lattice potentials extracted at the remaining R values are shown in Fig. 32 together with the equivalent values for the quenched approximation. The errors shown here are purely statistical in nature and make no account of the detailed balance violations. The typical values of the parameter K are of order 5.8 rather than the exact value 6.03 and so we estimate a further 5 % systematic error from this source.

The expected 'rolling over' of the potential at large R due to screening is clearly observed. Fitting to the conventional linear + Coulomb form, Eq. (3.15) one finds that

$$\begin{aligned} \alpha^{(4)} &= -.26 \pm .02 \\ V_0^{(4)} &= .64 \pm .02 \\ K^{(4)} &= -.002 \pm .005 \end{aligned} \tag{5.30}$$

where the superscript denotes the number of flavours. Since the scaling properties of these quantities is less well known than in the quenched case we have not cast them into dimensionless form but merely extracted them from the bare lattice potentials. That we have crossed over into the deconfined phase is clear from the value of the string tension. Given

our earlier comments this is not entirely unexpected and obviously renders interpretation of the Coulomb strength somewhat unclear.

In conclusion, we can claim that this algorithm has proven quite successful in simulating the properties of dynamical quarks. Obviously much work remains to be done both in assessing the systematic errors associated with the violations of detailed balance and in extending the range of problems examined. The former is an interesting project in its own right and is certainly within the scope of current machines. As for the latter, a useful task would be to pin down the exact deconfinement transition on a lattice of our size and it is interesting to note in this context the clarity of the deconfinement signal given by our string tension measurement. Conventionally, as in the previous section, one searches for this transition using the thermal Wilson line as order parameter but given the fact that the fermionic action automatically breaks the associated symmetry it might indeed be sensible to use the string tension in this search. As for detailed quantitative results from calculations with really light ($\sim$ 10 MeV) fermions in the continuum scaling regime, it seems that larger computers than our current models must be brought to bear.

CHAPTER 6

Concluding Remarks

Over the past decade the lattice regularisation scheme has shown itself to be the most powerful technique available in our efforts to understand QCD. The work in this thesis has been concerned with a detailed examination of heavy quark systems using old and established techniques and the development of new methods for attacking some of the outstanding problems.

In studying the heavy quark systems we have results of both a positive and negative nature. The rather unhappy conclusion to be drawn from the quenched potential calculation is that extremely accurate quantitative predictions remain elusive. Early suggestions that continuum physics could be extracted from small lattices at modest couplings must be tempered by our discovery that asymptotic scaling behaviour is not observed even on our rather large lattice. Conversely, we have seen that interesting qualitative physical results can be obtained on the lattice. Our energy density calculations provide compelling evidence in favour of the dual superconductor model of confinement and the comparison

between mesonic and baryonic systems points towards a resolution of the questions surrounding the origin of the Coulombic interaction as well as the interior string configurations of the hadrons.

In the second major part of this thesis two new algorithms have been suggested, the complex Langevin and mixed Metropolis/Langevin methods. The study of spin-dependent corrections to the static quark potential is extremely interesting and again qualitative lattice results might be of great value. In this regard we have high hopes for the complex Langevin algorithm assuming that the segregation problem can be overcome. Other interesting calculations such as the finite baryon density simulations are already under study by this method.

Probably the most significant questions still remaining in the field are concerned with the simulation of full QCD with dynamical fermions. Even after several years of effort it remains unclear whether one can, starting from the bare Lagrangian, derive all the observed features of QCD through lattice simulations. Furthermore, given current limitations on available computing power it is unlikely that any of the 'exact' fermionic algorithms will become feasible on the large lattices required to reproduce continuum physics, especially in the near term. For this reason the 'approximate' algorithms with their systematic errors will presumably be our best means of attack on the full theory. It is thus of crucial importance that the methods in use are fully understood and their approximations made in a controlled manner. To this end we have introduced a 'mixed' Langevin/Metropolis algorithm and analysed some of its systematic sources of error. Having tested its behaviour on moderately simple problems it remains to be seen whether the larger picture will be within its grasp.

Concerning the future it is natural to examine which calculations seem to be indicated on the basis of those studied in this work.

It is obviously of vital importance that the lattice be able to produce quantitative as well as qualitative results. Two avenues suggest themselves. The first would be to push higher the values of β used. At some value one would presumably have reduced the lattice spacing to a point where perturbative scaling holds and physical quantities could be extracted directly. Unfortunately, finite size effects dictate that the lattice volume must grow exponentially as β increases which makes this approach extremely expensive. The second approach would be to take a fixed size lattice and to calculate the appropriate β-function by performing an extremely accurate calculation of the quenched quark potential at many values of the coupling. This is the scheme which was discussed briefly in Chapter 3 and proved impossible to implement given the size of our statistical errors and the large spacing between values of β at which we had data.

In order to estimate the computational requirements of such a programme we first consider the calculation previously carried out. If one rates each node of the mark II hypercube at $1/20\text{Mflops}s^{-1}$ then one has a total distributed CPU power of around 6 $\text{Mflops}s^{-1}$. At each value of β we computed for roughly 2000 hours and hence our total CPU usage (Per β value) is around 4.3×10^7 Mflop. Assuming, therefore, a lattice of size 20^4 and a wish to reduce by a factor of ten the statistical errors indicates a computing requirement of around 5×10^9 Mflop per β value. As for memory, our machine has 256 Kbytes per node for a distributed total of 32 Mbytes giving an upper limit of around 150 bytes per lattice site after subtracting space for the code itself. The four 3x3 complex matrices at a given site require, however, nearly 300 bytes if maintained as 32 bit floating point numbers which is why CPU cycles had to be wasted in our calculation to store the matrices in two column form as fixed precision 16 bit numbers. Obviously this time could be saved given sufficient memory per node and further use of the variance reduction method could be considered given the space to store intermediate values. Overall a memory size of 500 bytes per site would probably be adequate to speed up the calculation

by a factor between 2 and 10.

In summary, therefore, the proposed calculation, carried out at 20 β values would require $\sim \times 10^{10}$ Mflop and 80 Mbytes of distributed memory. On a machine such as the proposed Mark III hypercube with floating point accelerator, capable of perhaps 10 Mflops^{-1} per node, a 128 processor system would require less than six months, the memory requirement being easily satisfied.

Moving on to the newer algorithms the requirements are more difficult to assess since less is known about their performance. The crucial question to be addressed concerning the complex Langevin method and segregation is whether or not there exist trajectories that can tunnel between sectors of the complex plane. Our failure to find such a path using the standard 64 bit representation of floating point numbers is obviously inconclusive and further careful work needs to be done. In connection with this algorithm, however, we can make a useful point concerning machine architecture. The conventional heat bath/Metropolis Monte Carlo procedures are extremely synchronous in nature. This was the feature discussed in Chapter 2 which made the parallelisation of the sequential code so straightforward. Another consequence is that the simulations are more or less equally suited to MIMD machines, such as the hypercubes, and SIMD machines such as the Crays and Connection Machine. This is not true, however, for the dynamical timestepping algorithm developed for use with the Complex Langevin equation.

In order to clarify this claim consider an extreme example in which each processor has only one degree of freedom left to update. In the conventional algorithms this is guaranteed to occupy the same relative position in each processors sublattice and there are no problems since the lockstep processing of the SIMD machine enables all processors to simultaneously update the variable. Conversely, in the dynamical timestepping scenario this is usually not true and one can imagine the worst case where each processor's variable is in a *different* relative position. The SIMD machine now suffers a huge penalty since

each processor has to either process or ignore a given instruction. Given the most obvious decomposition of the data this means that while each processor updates its remaining variable all the others must be in the idle state ignoring the instructions to update their equivalent variable. In this case all parallelism would be lost.

Obviously this example represents an extreme case, and considers only a naive programming technique. However, it is easy to see that more realistic dispositions of work do not significantly improve matters and given the data dependent origin of the imbalance it is hard to construct more effective programming methods. For this reason, therefore, we believe that MIMD machines will be of significantly higher performance in implementing this algorithm.

In considering the future of the fermionic algorithms, one is on much less secure ground, since the full systematic errors are unknown. In this regard, therefore, it is imperative that one discover the exact errors associated with the detailed balance violations in the algorithm discussed in Chapter 5. In order to accomplish this one needs to simulate the theory on several different though not necessarily large lattice volumes, using the results of our work to keep the error due to the discretisation of the equations of motion fixed. In this way one can hope to isolate the contributions due solely to the loss of detailed balance. This calculation is certainly within the scope of the 128 node Mark III hypercube discussed earlier in this chapter.

In more hypothetical vein, it is interesting to consider the possibilities of the next generations of supercomputers. In the next few years it is almost certain that machines with performances in the range of Gflops^{-1} will become available and it is not too unreasonable to expect that machines capable of Tflops^{-1} will be built around current ideas in the next couple of decades.

To see the impact of these machines we must consider the requirements which one might make of an 'ultimate' fermionic calculation. Two significant criteria suggest

themselves. Firstly one would wish to calculate on a larger physical volume - at least a couple of proton diameters across. For definiteness we will take 5 fm as a suitable dimension. Given the success of potential models such as those discussed in this thesis; however, it seems unlikely that one need be concerned with very short distance scales. Again for definiteness we assume that a lattice spacing of .1 fm will be sufficiently small to extract most physical quantities. The second simulation parameter which needs attention is the light quark mass. Current simulations work with masses of order 200 MeV and extrapolate to smaller values. Obviously it would be nice if one could directly simulate the theory with light quark masses of order 10 MeV.

Given these requirements, what are the consequences for the Monte Carlo procedures ? The major impact of the increased lattice volume is to necessitate the use of smaller timesteps/hitsizes. This is the area where one needs to know and quantify the sources of systematic error. If we make the assumption that the detailed balance violations require a volume dependence no worse than the $V^{3/2}$ derived for the discretisation of the Langevin equation then a change in lattice volume from $\sim 16^4$ to $\sim 50^4$ requires an increase in computational power of approximately 1000.

The variation in the bare quark mass has its largest effect in inverting the Dirac operator and calculating the fermion propagator. The eigenvalues of this operator decrease with quark mass as m^2 and so the convergence speed of the inversion method, say the conjugate gradient technique, decreases as m^2 [140]. For the more physical quark masses, therefore, this involves increased computational speed by a factor of approximately 500.

From these sketchy calculations it thus seems that to incorporate either of these improvements individually would require power on the order of Gflops^{-1} but both together will have to wait for machines whose computing speed is measured in Tflops^{-1}. Given the developments in parallel computing made over the past decade we confidently expect that realistic numerical simulations of QCD will become possible in the next twenty

to thirty years.

APPENDICES

Appendix A - Heat Baths and Parallel Computers

One avenue along which computing power can be vastly enhanced is in the realm of parallel computers, which is the particular direction that has been explored at Caltech/JPL [20], and as explained in Section 2.2, the machine on which most of these calculations were performed is of this type with 128 identical processors. Already commercially available is a machine with 1024 processors and further developments of the genre are expected. It is entirely likely, then, that such machines will, in the near future, become competitive with computers of more standard architecture and it is thus vital that algorithms for the efficient usage of such a computer be developed. By efficiency here one means that doubling the number of processors should approximately halve the time taken to perform a given calculation.

In this appendix, however, we will show that the conventional heat bath algorithm for generating quenched gauge field configurations contains a significant inefficiency for massively parallel architectures.

The essential ingredient of the algorithm is the generation of the SU(2) matrices by the explicit SU(2) heat bath. This step requires the generation of random numbers distributed according to

$$P(x)\,\mathrm{d}x \;=\; \frac{1}{N}\;(1-x^2)^{1/2}\;e^{kx}\;\mathrm{d}x \qquad (A.1)$$

$$-1 \;\leq\; x \;\leq\; 1 \qquad\qquad k \;>\; 0$$

where N is the normalisation constant expressed in terms of the modified Bessel function

$$N \;=\; \int_{-1}^{1} dx\;\;(1-x^2)^{1/2}\,e^{kx} \;\;=\;\; \frac{\pi}{k}\;\mathrm{I}_1(k) \qquad (A.2)$$

The conventional method of solving this problem [141] is to generate a random number y with distribution

$$P(y)\;\mathrm{d}y \;\;=\;\; e^{ky}\;\mathrm{d}y \qquad (A.3)$$

and then to fix up the square root factor by an accept/reject procedure. In these expressions k is a variable representing the effect of neighbouring gauge links on the one which we are updating and varies, in an average sense, with the coupling β. In Table 9 are shown average values of k at various couplings, β, in typical use in lattice gauge calculations. Also shown are extrapolations to values of β which might be accessible to future generations of supercomputers. Also shown in this table is the average acceptance probability of the accept/reject step discussed above.

For a conventional sequential computer these figures are harmless enough and indicate that the accept/reject cycle is typically performed $\bar{n}_{seq} = 1/p_{acc} \simeq 3$–$5$ times. On a parallel computer, however, this can lead to enormous loss of efficiency as is shown by considering a simple model [142].

Assume that the acceptance probability for any given accept/reject cycle takes a constant value, p, dependent only on the coupling, β. The accept/reject process is then a simple binomial trial. Consider further that N processors execute this process independently. The probability that a single processor rejects every one of n times is q^n, where $q \equiv 1-p$. Thus the probability that a single processor accepts at least once in the first n attempts is $1 - q^n$ and the probability that every processor has accepted at least once in the first n trials is $(1 - q^n)^N$. From this it it simple to see that the expected number of trials needed by the *slowest* processor is given by

$$\bar{n}_{par} = \sum_{i=0}^{\infty} i \left\{ (1 - q^i)^N - (1 - q^{i-1})^N \right\} \tag{A.4}$$

That this is a disaster for massively parallel machines ($N \to \infty$) is shown in Fig. 33 where the value of the 'wastage', $\bar{n}_{par} - \bar{n}_{seq}$ is plotted for several values of p_{acc} against the variable $doc = \log_2 N$. Note that the source of inefficiency discussed here is of an entirely different nature to that described by Eq. (2.16), which is due to the communication between processors.

For the machine used in these calculations $doc = 7$ and so the expected wastage factor is around 12 cycles. While this is not optimal it is tolerable since the updating algorithm involves more than just the generation of x according to Eq. (A.1). In fact the other operations, which are essentially 3×3 matrix multiplications typically take an order of magnitude longer than a single accept/reject cycle so the overall inefficiency is small. However future machines will suffer more since these matrix operations are exactly the ones which can be optimally pipelined or vectorised. Conversely the accept/reject cycle requires the evaluation of exponentials and logarithms and while the former can be effectively tabulated the latter is a quite significant problem. Indeed it is not at all inconceivable that in a fully vectorised conventional heat bath algorithm a single accept/reject cycle

could take as long, if not longer, than the matrix manipulations in which case the inefficiency would become enormous.

The reason for this problem is, however, easy to identify, and thus to at least partially correct. For large k the distribution Eq. (A.1) is sharply peaked near $x = 1$, which is the region in which the square root factor is small, and hence the rejection probability large. A simple solution to the problem is, therefore, to arrange that the analytically inverted part of the distribution generates values further away from this point. For example, we can write Eq. (A.1) as

$$P(x)\,dx = \frac{1}{N}\, e^{\alpha k x}\, (1 - x^2)^{1/2}\, e^{(1-\alpha)kx}\, dx \qquad \text{(A.5)}$$

generating the distribution $e^{\alpha k x}$ analytically and using the second factor to accept/reject. For $k = 15$, the value $\alpha = .90$ increases the acceptance rate from .32 to .90. However this method has the disadvantage that at high values of k, typical near $\beta \simeq 8.0$, the acceptance rate is extremely sensitive to changes in α which makes the method quite unstable.

An alternative solution [143] is to make the change of variable $y = (1 - x^2)^{1/2}$ which leads to the expression

$$P'(y)\,dy = \frac{1}{N}\,(1 - y^2)^{1/2}\, y^2\, e^{-ky^2}\, dy \qquad 0 \le y \le \sqrt{2} \qquad \text{(A.6)}$$

The subexpression $y^2\, e^{-ky^2}$ is strongly peaked towards $y = 0$ for large k which is where the compensating factor $(1 - y^2)^{1/2}$ is large giving hope that this method will succeed. The generation of random numbers according to the distribution $y^2\, e^{-ky^2}$ is surprisingly simple requiring only the evaluation of a logarithm and a couple of trigonometric functions so the method is quite fast. A further beneficial feature of this new algorithm is its acceptance of $p_{acc} = .98$ at $k = 16$ and the extremely desirable feature that this *increases* as k increases. While the algorithm is yet to be tested in any significant

lattice gauge calculation it thus seems that a viable alternative exists for use in massively parallel architectures.

Appendix B - The Kramers-Moyal Expansion

In this appendix the connection between the Fokker-Planck and Langevin equations is shown by deriving the Kramers-Moyal expansion [144].

Consider a two-time (Markovian) transition probability ,P, which relates the probability density, F, at two times via

$$F(x,t+\tau) = \int dx' \, P(x,t+\tau|x',t) \, F(x',t) \tag{B.1}$$

Furthermore define moments of the distribution P by

$$M_n(x',t,\tau) = \langle [\xi(t+\tau)-\xi(t)]^n \rangle|_{\xi(t)=x'} = \int dx \, (x-x')^n P(x,t+\tau|x',t) \tag{B.2}$$

where ξ is a stochastic process constrained such that $\xi(t)=x'$. Now consider the moment generating function, defined by

$$C(u,x',t,\tau) = \int_{-\infty}^{\infty} dx \, e^{iu(x-x')} P(x,t+\tau|x',t) \tag{B.3}$$

$$= 1 + \sum_{n=1}^{\infty} (iu)^n \, M_n(x',t,\tau)/n!$$

By definition, C is the Fourier transform of P, and so we can invert to find

$$P(x,t+\tau|x',t) = \frac{1}{2\pi}\int_{-\infty}^{\infty} du\; e^{-iu(x-x')}\left[1+\sum_{n=1}^{\infty}(iu)^n\, M_n(x',t,\tau)/n!\right] \tag{B.4}$$

Taking the delta function representation

$$\delta(x-x') = \frac{1}{2\pi}\int_{-\infty}^{\infty} du\; e^{-iu(x-x')} \tag{B.5}$$

it can be seen that

$$P(x,t+\tau|x',t) = \left[1+\sum_{n=1}^{\infty}\frac{1}{n!}\left(-\frac{\partial}{\partial x}\right)^n M_n(x,t,\tau)\right]\delta(x-x') \tag{B.6}$$

Finally assume that, for small τ, M_n can be expanded in a Taylor series such that

$$M_n(x,t,\tau)/n! = \tau\, D^n(x,t) + O(\tau^2) \tag{B.7}$$

(The constant term vanishes since $P(x,t\,|x',t) = \delta(x-x')$). Thus, to first order in τ, insert Eqs. (B.6) and (B.7) in Eq. (B.1) to obtain

$$\frac{\partial F}{\partial t} = \sum_{n=1}^{\infty}\left(-\frac{\partial}{\partial x}\right)^n D^n(x,t)\, F(x,t) \tag{B.8}$$

which is known as the Kramers-Moyal expansion.

In order to calculate the expansion coefficients, D^n, consider the general Langevin equation

$$\dot{\xi} = h(\xi,t) + g(\xi,t)\,\eta(t) \tag{B.9}$$

where the stochastic term has the specific normalisation

$$\langle \eta(t)\,\eta(t')\rangle = 2\delta(t-t') \tag{B.10}$$

First write Eq. (B.9) as an integral equation

$$\xi(t+\tau) - x \;=\; \int_t^{t+\tau} dt' \left[h(\xi(t'),t') + g(\xi(t'),t')\eta(t') \right] \tag{B.11}$$

where we have used the boundary condition that $\xi(t) = x$. Next expand h and g in Taylor series

$$h(\xi(t'),t') \;=\; h(x,t') + h'(x,t')(\xi(t')-x) \;+\; \cdots \tag{B.12}$$

$$g(\xi(t'),t') \;=\; g(x,t') + g'(x,t')(\xi(t')-x) \;+\; \cdots$$

where primes denote derivatives with respect to the first argument, x. Substitution in Eq. (B.11) yields

$$\xi(t+\tau) - x \;=\; \int_t^{t+\tau} dt'\, h(x,t') \;+\; \int_t^{t+\tau} dt'\, h'(x,t')(\xi(t')-x) \;+\; \cdots \tag{B.13}$$

$$+ \int_t^{t+\tau} dt'\, g(x,t')\,\eta(t') \;+ \int_t^{t+\tau} dt'\, g'(x,t')\,((\xi(t')-x)\,\eta(t') \;+\; \cdots$$

Proceeding by iteration, one inserts this expression for the $\xi(t')-x$ factors in the second and fourth terms. Finally, taking averages over the stochastic variable η leads to the expression

$$\langle\, \eta(t+\tau)-x \,\rangle \;=\; \int_t^{t+\tau} dt'\, h(x,t') \;+\; \int_t^{t+\tau} dt' \int_t^{t'} dt''\, h'(x,t')\, h(x,t'') \tag{B.14}$$

$$+ \int_t^{t+\tau} dt'\, g'(x,t')\, g(x,t') \;+\; \cdots$$

In the limit $\tau \to 0$ therefore one finds that

$$D^1(x,t) \;=\; h(x,t) + g'(x,t)\,g(x,t) \tag{B.15}$$

and proceeding in a similar manner yields

$$D^2(x,t) = g^2(x,t) \tag{B.16}$$

$$D^n(x,t) \equiv 0 \qquad \text{for all } n \geq 3$$

The remarkable fact that coefficients with $n \geq 3$ vanish identically leads to a significant simplification in the Kramers-Moyal expansion, Eq. (B.8). In fact this expression reduces to the Fokker-Planck equation

$$\frac{\partial F}{\partial t} = -\frac{\partial}{\partial x}\left[h + g'g\right]F + \frac{\partial^2}{\partial x^2}(g^2 F) \tag{B.17}$$

and in order to make contact with lattice gauge theory calculations, make the ansatz

$$g \equiv 1 \qquad\qquad h \equiv -\beta \frac{\partial S}{\partial x} \tag{B.18}$$

in which case the associated Langevin and Fokker-Planck equations become

$$\dot{x} = -\beta \frac{\partial S}{\partial x} + \eta \tag{B.19}$$

$$\frac{\partial F}{\partial t} = \frac{\partial}{\partial x}\left(F\beta \frac{\partial S}{\partial x}\right) + \frac{\partial^2 F}{\partial x^2} \tag{B.20}$$

Appendix C - The Segregation Theorem

For the sake of completeness we present here a formal definition of the segregation theorem as it is used in Chapter 4. The notation used is copied from the original proof of Nagasawa [108].

Let D be a connected domain in $\boldsymbol{R}^d$ with a piecewise smooth boundary ∂D defined by

$$\partial D = \{ \boldsymbol{x} \in \boldsymbol{R}^d ; P(\boldsymbol{x}) = 0 \} \tag{C.1}$$

Also define X_t, the diffusion process on $D \cap \partial D$, and T, the first exit time for the process from D. Then the segregation theorem states that given a time, t_0, and a neighbourhood, U, of the boundary

$$P[\, T<\infty \,, \text{ or } X_t \in U \text{ for all } t > t_0 \,] = 0 \tag{C.2}$$

In other words, the probability that the process exits D in a finite time, or that it stays permanently 'near' the boundary of the domain are both zero.

Appendix D - Systematic Errors for Non-Quadratic Actions

In this appendix we consider systematic errors introduced by the discretisation of the Langevin equation in cases where the action, S, is not quadratic. We shall achieve this by studying perturbation theory around the quadratic case and for simplicity of presentation will restrict ourselves to the simple case of a ϕ^3 scalar field theory defined by the

action

$$S = \tfrac{1}{2}\sum_{x,\mu}(\phi_{x+\mu}-\phi_x)^2 + \sum_x \tfrac{1}{2}m^2\phi_x^2 + g\,\phi_x^3 \qquad (D.1)$$

$$= \tfrac{1}{2}\phi_x M_{xy}\phi_y + g\sum_x \phi_x^3$$

The Langevin dynamics are described by

$$\frac{\partial\phi_x}{\partial\tau} = -M_{xy}\phi_y(\tau) - g\,\phi_x^2 + \eta_x(\tau) \qquad (D.2)$$

which expression can be rewritten as an integral equation

$$\phi(\tau) = \int_{-\infty}^{\tau} ds\; e^{-(\tau-s)M}[\eta(s) - g\,\phi^2(s)] \qquad (D.3)$$

By treating the $g\,\phi^2$ as a perturbation, a series expansion for $\phi(\tau)$ can easily be obtained [145]. The graphical rules in momentum space are summarised in Fig. 34 - each graph for $\phi(\tau)$ contains

a) Propagators G_k with weight $e^{-(s_1-s_2)M_k}\theta\,(s_1-s_2)$.

b) Crosses with weight $\eta(s)$.

c) Vertices with weight $-g$

Furthermore, the total momentum flowing into any vertex is zero.

From these relations one easily obtains the equilibrium correlation functions. For example, the two-point function is given by the diagrams shown in Fig. 35 (Neglecting tadpoles). Note that the crosses always have two propagators due to the normalisation of the noise. As an example the second graph of the set is given by

$$g^2\int\frac{d^dk}{(2\pi)^d}\int_{-\infty}^{\tau_2} ds_2\, G_{k_2}(\tau_2-s_2)\int_{-\infty}^{\tau_1} ds_1\, G_{k_1}(\tau_1-s_1)\, D_k(s_1,s_2)\, D_{k-k_1}(s_1,s_2) \qquad (D.4)$$

where we have set

$$D_k(s_1,s_2) = 2\int_{-\infty}^{\infty} ds\; G_k(s_1-s)\,G_k(s_2-s) \tag{D.5}$$

$$= \frac{e^{-|s_1-s_2|M_k}}{M_k}$$

To each graph in the standard Feynman expansion of a Green function there corresponds a sum over Langevin diagrams of the same topology. These Langevin diagrams involve integrations over the fictitious times at the vertices. Each line carries a factor G_k or D_k and thus all the integrals are of the form

$$\int_{-\infty}^{\infty} d\tau_1 \cdots d\tau_n \prod_{i,j} e^{-|\tau_i-\tau_j|M_{k_{i,j}}} \tag{D.6}$$

with possible theta functions, e.g., $\theta\,(\tau_i-\tau_j)$. This leads to terms of the form

$$\prod \frac{1}{(M_{k_1}\pm M_{k_2}\pm \cdots)} \tag{D.7}$$

whose sum leads to the standard Feynman result.

We now show that each of these diagrams is obtained with a relative accuracy of $\delta\tau E^2_{max}$ when a discretisation with stepsize $\delta\tau$ is used. E^2 is an eigenvalue of the matrix M for free fields and in the case of Eq. (D.1) is

$$E_k^2 = 4\sum_{\mu} \sin^2(\tfrac{1}{2}k_\mu a) + m^2a^2 \tag{D.8}$$

The discrete version of Eq. (D.2) is given by

$$\phi(n) = \sum_{s=-\infty}^{n-1} (1-\delta\tau M)^{n-1-s}\,[\sqrt{2\delta\tau}\,r(s) - \delta\tau g\,\phi^2(s)] \tag{D.9}$$

which leads to diagrammatic rules similar to the $\delta\tau = 0$ case. Time is labeled by integers, and the weights are slightly changed

$$G_k \rightarrow (1-\delta\tau M_k)^{s_1-s_2-1}\,\theta\,(s_1-s_2-1) \tag{D.10a}$$

$$D_k \rightarrow \frac{(1-\delta\tau M_k)^{|s_1-s_2|}}{M_k(1-\frac{1}{2}\delta\tau M_k)} \tag{D.10b}$$

$$g \rightarrow G\,\delta\tau \qquad \text{at each vertex} \tag{D.10c}$$

The $\delta\tau$ at each vertex provides for the summation over the locations of the vertex.

Consider now a graph with fixed momenta on each line. The sum over Langevin time for the vertex of Fig. 36 is of the form

$$-g\,\delta\tau \sum_{\tau=s_2+1}^{s_3-1} (1-\delta\tau M_{k_1})^{\tau-s_1-1}\,(1-\delta\tau M_{k_2})^{\tau-s_2-1}\,(1-\delta\tau M_{k_3})^{s_3-\tau-1} \tag{D.11}$$

where we have included only those factors which are explicitly τ dependent and the range of the sum is from s_2+1 to s_3-1 (Without loss of generality, we are taking $s_1 \leq s_2 \leq s_3-2$). Summing the expression leads to

$$-g\,\delta\tau x_1^{-s_1-1} x_2^{-s_2-1} x_3^{-s_3-1}\;\frac{(x_1x_2x_3^{-1})^{s_2+1} - (x_1x_2x_3^{-1})^{s_3}}{1 - x_1x_2x_3^{-1}} \tag{D.12}$$

with

$$x_1 \equiv 1 - \delta\tau M_{k_1} \qquad x_2 \equiv 1 - \delta\tau M_{k_2} \qquad x_3 \equiv 1 - \delta\tau M_{k_3} \tag{D.13}$$

After having integrated over all locations in time of the vertices, the final expression for a correlation function, before the momentum integrations are done, is a sum of products of terms of the form

$$\frac{(1 - \delta\tau M_{k_l})^{n_l}}{1 - \prod_i (1 - \delta\tau M_{k_i})^{m_i}} \tag{D.14}$$

times powers of $\delta\tau$ (from the vertices) and factors of

$$\frac{1}{M_k(1 - \frac{1}{2}\delta\tau M_k)} \tag{D.15}$$

coming from the D_k lines. The constants n_l, m_i are integers, independent of $\delta\tau$. This shows that only $\delta\tau M_k$ terms appear in the relative error as $\delta\tau \to 0$.

In conclusion, then, the error due to the $\delta\tau$ discretisation in any particular Langevin graph is of order $\delta\tau E_{max}^2$. The last remaining question is what happens when the Langevin graphs are combined to give Green functions. For theories with symmetries, for example gauge symmetries, there will in general be much cancellation between the divergences of the Feynman graphs. A possible problem now presents itself: If the discrete time Langevin dynamics doesn't exactly respect these symmetries, then error terms, which are down by $\delta\tau$, can be multiplied by divergences which don't quite cancel. This would lead to large errors in the Langevin evolution, and our estimates would not apply. Fortunately, it is not hard to ensure that the discrete time Langevin dynamics are exactly gauge invariant and also respect all other appropriate symmetries.

REFERENCES

[1] T.Kinoshita, *Proceedings of the 19th International Conference on High Energy Physics*, Tokyo (1978)

[2] S.L.Glashow, *Nucl. Phys.* **22**, 579 (1961)

A.Salam, J.C.Ward, *Phys. Lett.* **13**, 168 (1964)

S.Weinberg, *Phys. Rev. Lett.* **19**, 1264 (1967)

S.Weinberg, *Rev. Mod. Phys.* **64**, 255 (1974)

[3] G.Arnison *et al.* (UA1 Collaboration), *Phys. Lett.* **122B**, 103 (1983)

G.Banner *et al.* (UA2 Collaboration), *Phys. Lett.* **122B**,476 (1983)

G.Arnison *et al.* (UA1 Collaboration), *Phys. Lett.* **126B**, 398 (1983)

[4] H.D.Politzer, *Phys. Rev. Lett.* **30**, 1346 (1973)

D.J.Gross, F.Wilczek, *Phys. Rev. Lett.* **30**, 1343 (1973)

H.D.Politzer, *Phys. Reports* **14C**, 130 (1974)

[5] G.t'Hooft, *Nucl. Phys.* **B72**, 461 (1974)

E.Witten, *Nucl. Phys.* **B160**, 57 (1979)

O. Martin, *Phys. Lett.* **130B**, 411 (1983)

[6] L.P.Kadanoff, *Rev. Mod. Phys.* **39**, 395 (1967)

[7] S.Coleman, "Uses of Instantons", *International School of Subnuclear Physics*, Erice (1977) and references therein.

[8] K.G.Wilson, *Phys. Rev.* **D10**, 2445 (1974)

[9] C.N.Yang, R.Mills, *Phys. Rev.* **96**, 191 (1954)

[10] J.B.Kogut, *Rev. Mod .Phys.* **55**, 802 (1983)

[11] M.Creutz, L.Jacobs, C.Rebbi, *Phys. Reports* **95**, 201 (1983)

M.Creutz, "Quarks, Gluons and Lattices", *Cambridge University Press*, (1983)

[12] R.P.Feynman, A.R.Hibbs, "Quantum Mechanics and Path Integrals", McGraw-Hill (1965)

[13] W.E.Caswell, *Phys. Rev. Lett.* **33**, 244 (1974)

D.R.T.Jones, *Nucl. Phys.* **B75**, 531 (1974)

[14] A.Hasenfratz, P.Hasenfratz, *Phys. Lett.* **93B**, 165 (1980)

R.Dashen, D.J.Gross, *Phys. Rev.* **D23**, 2340 (1981)

[15] K.Symanzik, *Nucl. Phys.* **B226**, 187 (1983)

K.Symanzik, *Nucl. Phys.* **B226**, 205 (1983)

K.Symanzik, *Proceedings of Trieste Workshop on Field Theory and QCD*, 61 (1982)

[16] K.G.Wilson, "Recent Developments in Gauge Theories, Cargese 1979", Ed. G.t'Hooft *et al.* (1980)

L.P.Kadanoff, *Rev. Mod. Phys.* **49**, 267 (1977)

R.H.Swendsen, *Phys. Rev. Lett.* **42**, 859 (1979)

S.K.Ma, *Phys. Rev. Lett.* **87**, 461 (1976)

K.C.Bowler *et al., Nucl. Phys.* **B257**, 155 (1985)

R.Gupta, G.Guralnik, A.Patel, T.Warnock, C.Zermach, *Phys. Rev. Lett.* **53**, 1721 (1984)

P.Stolorz, *Phys. Lett.* **172B**, 77 (1986)

[17] J-M.Drouffe, J-B.Zuber, *Phys. Reports* **102** Nos. 1 & 2, (1983)

[18] B.Adeva *et al., Phys. Lett.* **180B**, 181 (1986)

G.Altarelli, R.K.Ellis, G.Martinelli, *Nucl. Phys.* **B157**, 461 (1979)

M.Dine, J.Sapirsten, *Phys. Rev. Lett.* **43**, 668 (1979)

G.P.LePage, S.J.Brodsky, *Phys. Rev. Lett.* **43**, 545 (1979)

[19] W.Buchmuller, *Phys. Lett.* **112B**, 479 (1982)

[20] G.C.Fox, S.W.Otto, *Physics Today* **50**, (May 1984)

E.Brooks III *et al., Phys. Rev. Lett.* **52**, 2324 (1984)

G.C.Fox, S.W.Otto, "Caltech Concurrent Computation Program: A Status Report", to appear in a supercomputer theme issue of *Computers in Mechanical Engineering* published by Springer-Verlag, (March 1986)

[21] E.Brooks III *et al., Nucl. Phys.* **B220**, 383 (1983)

[22] E. Cunlar, "Introduction to Stochastic Processes", Prentice-Hall (1975)

[23] N.Metropolis, A.W.Rosenbluth, M.N.Rosenbluth, A.M.Teller, E.Teller, *J. Chem. Phys.* **21**, 1087 (1953)

[24] A.Einstein, *Ann. Phys.* **17**, 549 (1905)

M.Von Smoluchowski, *Ann. Phys.* **21**, 756 (1906)

[25] P. Langevin, *Comptes Rendus* **146**, 530 (1908)

[26] M.Sargent III, M.O.Scully, W.E.Lamb, "Laser Physics", Addison-Wesley (1974)

[27] D.Callaway, A.Rahman, *Phys. Rev. Lett.* **49**, 613 (1982)

J.Polonyi, H.W.Wyld, *Phys. Rev. Lett* **51**, 2257 (1983)

J.B.Kogut, *J. Stat. Phys.* **43**, 771 (1986)

[28] G.Bhanot, M.Creutz, H.Neuberger, *Nucl. Phys.* **B235**, 417 (1984)

M.Creutz, "Gauge Theories on a Lattice, 1984", Argonne (1984)

[29] M.Creutz, *Phys. Rev. Lett.* **50**, 41 (1983)

[30] S.Duane, *Nucl. Phys.* **B257**, 652 (1985)

[31] K.Binder, "Phase Transitions and Critical Phenomena", Ed. C.Domb, M.S.Green, Academic Press (1976)

[32] S.L.Adler, *Phys. Rev.* **177**, 2426 (1969)

J.S.Bell, R.Jackiw, *Nuovo. Cim.* **60A**, 427 (1969)

[33] For an up to date review and detailed references see

"Review of Particle Properties", *Phys. Lett.* **170B**,1 (1986)

[34] J.J.Aubert *et al., Phys. Rev. Lett.* **33**, 1404 (1974)

J.E.Augistin *et al., Phys. Rev. Lett.* **33**, 1406 (1974)

[35] S.W.Herb *et al., Phys. Rev. Lett.* **39**, 252 (1977)

W.R.Innes *et al., Phys. Rev. Lett.* **39**, 1240 (1977)

W.R.Innes *et al., Phys. Rev. Lett.* **39**, 1640 (1977)

[36] M.E.Peskin, "Proceedings of the SLAC Summer Institute", 151 (1983)

[37] S.Mandelstam, *Phys. Reports* **13C**, 259 (1974)

[38] A.Hasenfratz, P.Hasenfratz, U.Heller, F.Karsch, *Z. Phys.* **C25**, 191 (1984)

[39] T.Celik, J.Engels, H.Satz, *Phys. Lett.* **129B**, 323 (1983)

[40] F.Karsch, R.Petronzio, *Phys. Lett.* **139B**, 403 (1984)

A.D.Kennedy, J.Kuti, S.Meyer, B.J.Pendleton, *Phys. Rev. Lett.* **54**, 87 (1985)

S.A.Gottlieb *et al.*, *Phys. Rev. Lett.* **55**, 1958 (1985)

A.D.Kennedy, J.Kuti, S.Meyer, B.J.Pendleton, *Phys. Lett.* **155B**, 414 (1985)

N.Christ, A.Terrano, *Phys. Rev. Lett.* **56**, 111 (1986)

[41] D.Toussaint *et al.*, UC San Diego preprint, UCSD-10P10-269 (1986)

[42] N.Cabibbo, E.Marinari, *Phys. Lett.* **119B**, 387 (1982)

[43] G.Parisi, R.Petronzio, F.Rapuano, *Phys. Lett.* **128B**, 418 (1983)

[44] A.Duncan, H.Vaidya, *Phys. Rev.* **D20**, 903 (1979)

N.Kimiwa, *Prog. Theor. Phys.* **64**, 310 (1980)

[45] D.Barkai, K.J.M.Moriarty, C.Rebbi, *Phys. Rev.* **D30**, 1293 (1984)

D.Barkai, K.J.M.Moriarty, C.Rebbi, *Phys. Rev.* **D30**, 2201 (1984)

S.W.Otto, J.D.Stack, *Phys. Rev. Lett.* **52**, 2320 (1984)

P.de Forcrand, G.Schierholz, H.Scheider, M.Teper, *Phys. Lett.* **160B**, 137 (1985)

K.C.Bowler *et al.*, *Phys. Lett.* **163B**, 367 (1985)

[46] J.W.Flower, S.W.Otto, *Phys. Rev.* **D34**, 1649 (1986)

[47] K.C. Bowler, *et al.*, *Phys. Lett.* **179B**, 375 (1986)

D. Petcher, *Nucl. Phys.* **B275**, 241 (1986)

[48] J.D.Stack, *Phys. Rev.* **D27**, 412 (1983)

J.D.Stack, *Phys. Rev.* **D29**, 1213 (1984)

[49] L.Susskind, *Nuovo Cim.* **69A**, 457 (1970)

J.B.Kogut, L.Susskind, *Phys. Rev.* **D9**, 3501 (1974)

[50] M.Luscher, K.Symanzik, P.Weiss, *Nucl. Phys.* **B173**, 305 (1980)

M.Luscher, *Nucl. Phys.* **B180**, 317 (1981)

J.D.Stack, M.Stone, *Phys. Lett.* **100B**,476 (1981)

[51] P.Olesen, *Phys. Lett.* **160B**, 144 (1985)

M.Flensburg, C.Peterson, *Phys. Lett.* **153B**,412 (1985)

[52] R.Sommer, K.Schilling, *Z.Phys.* **C29**, 95 (1985)

[53] J.W.Flower, Caltech preprint CALT-68-1369 (1986)

[54] C.B.Lang, M.Wiltgen, *Phys. Lett.* **131B**, 153 (1983)

R.Sommer, J.Wosiek, *Nucl. Phys.* **B267**, 531 (1986)

J.W.Flower, Caltech preprint CALT-68-1377 (1986)

[55] D.Gromes, *Nucl. Phys.* **B130**, 18 (1977)

D.Gromes, I.O.Stamatescu, *Nucl. Phys.* **B112**, 213 (1976)

I.M.Barbour, D.K.Ponting, *Z. Phys.* **C4**, 119 (1980)

A.de Rujula, H.Georgi, S.L.Glashow, *Phys. Rev.* **D12**, 147 (1975)

[56] J.Carlson, J.B.Kogut, V.R.Pandharipande, *Phys. Rev.* **D27**, 233 (1983)

[57] S.Capstick, N.Isgur, *Phys. Rev.* **D34**, 2809 (1986)

[58] N.Isgur, G.Karl, *Phys. Lett.* **72B**, 109 (1977)

N.Isgur, G.Karl, *Phys. Rev.* **D18**, 4187 (1978)

N.Isgur, G.Karl, *Phys. Lett.* **74B**, 353 (1978)

N.Isgur, G.Karl, *Phys. Rev. Lett.* **41**, 1269 (1978)

N.Isgur, G.Karl, *Phys. Rev.* **D19**, 2653 (1979)

[59] M.S.Plyuschai, G.P.Pronko, A.V.Ramuzov, *Theor. Math. Phys.* **63**, 389 (1985)
S.V.Klimenko, V.N.Kochin, M.S.Plyuschai, G.P.Pronko, A.V.Ramuzov, A.V.Samarin, *Theor. Math. Phys.* **64**, 810 (1986)
M.S.Plyuschai, G.P.Pronko, A.V.Ramuzov, Serphukov preprint IFVE-85-70 (1986)

[60] X.Artru, *Nucl. Phys.* **B85**, 442 (1975)

[61] N.Isgur, J.Paton, *Phys. Rev.* **D31**, 2910 (1985)
N.Isgur, University of Toronto preprint UTPT-85-18 (1985)

[62] G.Rossi, G.Veneziano, *Nucl. Phys.* **B123**, 507 (1977)

[63] T.W.Ruijgrok, *Eur. J. Phys.* **5**, 21 (1984)

[64] H.G.Dosch, V.F.Muller, *Nucl. Phys.* **B116**, 470 (1976)

[65] T.D.Lee in "A Festschrift for Maurice Goldhaber", ed. G.Feinberg, A.W.Sunyar, J.Weneser, New York Academy of Sciences (1980)

[66] Y.S.Wu, A.Zee, *Z. Phys.* **C20**, 181 (1983)

[67] M.Rosina, A.Schuh, H.J.Pirner, *Nucl. Phys.* **A448**, 557 (1986)
R.T.Cahill, C.D.Roberts, *Phys. Rev.* **D32**, 2419 (1985)
R.Friedberg, T.D.Lee, *Phys. Rev.* **D18**, 2623 (1978)
For a general review of bags see
P.Hasenfratz, J.Kuti, *Phys. Reports* **40**, 75 (1978)

[68] S.Adler, *Phys. Lett.* **110B**, 302 (1982)

[69] G.Parisi, *Phys. Rev.* **D11**, 970 (1975)

[70] H.B.Nielsen, P.Olesen, *Nucl. Phys.* **B61**, 45 (1973)

[71] S.Adler, T.Piran, *Phys. Lett.* **113B**, 405 (1982)

S.Adler, T.Piran, *Phys. Lett.* **117B**, 91 (1982)

S.Adler, T.Piran, *Rev. Mod. Phys.* **56**, 1 (1984)

G.t'Hooft, *Nucl. Phys.* **B153**, 141 (1979)

V.P.Nair, C.Rosenzweig, *Phys. Lett.* **B135**, 450 (1984)

[72] M.Fukugita, T.Niuya, *Phys. Lett.* **132B**, 374 (1983)

J.Kiskis, K.Sparks, *Phys. Rev.* **D30**, 1326 (1984)

[73] J.W.Flower, S.W.Otto, *Phys. Lett.* **160B**, 128 (1985)

[74] R.Sommer, Wuppertal University Thesis WU B 86-13 (1986)

[75] J.B.Kogut, D.Sinclair, R.Pearson, J.Richardson, *Phys. Rev.* **D23**, 2945 (1981)

A.Hasenfratz, E.Hasenfratz, P.Hasenfratz, *Nucl. Phys.* **B180**, 353 (1981)

[76] J.W.Flower, Caltech preprint CALT-68-1372 (1986)

[77] E.Eichten, F.L.Feinberg, *Phys. Rev. Lett.* **43**, 1205 (1979)

E.Eichten, F.L.Feinberg, *Phys. Rev.* **D23**,2724 (1981)

[78] D.Gromes, *Z. Phys.* **C26**, 401 (1984)

[79] P.de Forcrand, J.D.Stack, *Phys. Rev. Lett.* **55**, 1254 (1985)

M.Campostrini, K.J.M.Moriarty, C.Rebbi, *Phys. Rev. Lett.* **57**, 44 (1986)

[80] H.Lipps, G.Martinelli, R.Petronzio, F.Rapuano, *Phys. Lett.* **126B**, 250 (1983)

K.C.Bowler, D.L.Chalmers, A.Kenway, K.D.Kenway, G.S.Pawley, D.J.Wallace, *Nucl. Phys.* **B240**, 213 (1983)

A.Billoire, E.Marinari, R.Petronzio, *Nucl. Phys.* **B251**, 141 (1985)

[81] J.L.Rosner, Enrico Fermi Institute preprint EFI-85-63 (1986)

[82] E.Eichten, K.Gottfried, T.Kinoshita, K.D.Lane, T.M.Yan, *Phys. Rev.* **D17**, 3090 (1978)

E.Eichten, K.Gottfried, T.Kinoshita, K.D.Lane, T.M.Yan, *Phys. Rev.* **D21**, 203 (1980) and references therein

[83] R.Barbieri, R.Kogerler, Z.Kunst, R.Gatto, *Nucl. Phys.* **B105**, 125 (1976)

A.B.Henriques, B.H.Kellet, R.G.Moorhouse, *Phys. Lett.* **64B**, 85 (1976)

S.N.Gupta, S.F.Radford, *Phys. Rev.* **D26**, 3305 (1982)

[84] C.Quigg, J.L.Rosner, *Phys. Lett.* **71B**, 153 (1977)

D.Pignon, C.A.Piketty, *Phys. Lett.* **74B**, 108 (1978)

[85] A.Martin, *Phys. Lett.* **93B**, 338 (1980)

A.Martin, *Phys. Lett.* **100B**, 511 (1981)

[86] R.Van Royen, V.F.Weisskopf, *Nuovo Cim.* **50**, 617 (1967)

[87] R.Barbieri, R.Gatto, R.Kogerler, Z.Kunst, *Phys. Lett.* **57B**, 455 (1975)

[88] S.Jacobs, M.G.Olsson, P.Kaus, S.Meshkov, University of Madison report MAD/Ph/255 (1985)

[89] M.G.Olsson, C.J.Sachyta III, *Phys. Rev. Lett.* **57**, 37 (1986)

Models incorporating these corrections can be found in

N.Barik, S.N.Jena, *Phys. Rev.* **D21**, 2647 (1980)

M.Campostrini, *Phys. Lett.* **147B**, 348 (1984)

[90] P.Moxhay, J.L.Rosner, *Phys. Rev.* **D31**, 1762 (1985)

[91] C.E.Carlson, F.Gross, *Phys. Lett.* **74B**, 404 (1978)

[92] H.Albrecht *et al., Phys. Lett.* **160B**, 331 (1985)

[93] T.Skwarnicki *et al.*, DESY preprint DESY-85-042 (1985)
W.Walk *et al.*, SLAC report SLAC-PUB-4045 (1986)

[94] S.Godfrey, N.Isgur, *Phys. Rev.* **D32**, 189 (1985)

[95] H.Risken, "The Fokker-Planck Equation", Springer-Verlag (1984)

[96] J.R.Klauder, W.Peterson, *J. Stat. Phys.***39**, 53 (1985)

[97] J.R.Klauder, *Acta. Phys. Austriaca* **XXV**, 251 (1983)
G.Parisi, *Phys. Lett.* **131B**, 393 (1983)
E.Gozzi, *Phys. Lett.* **150B**, 119 (1985)
J.Ambjorn, M.Flensburg, C.Peterson, *Phys. Lett.* **159B**, 335 (1985)
H.Gausterer, J.R.Klauder, *Phys. Rev.* **D33**, 3678 (1986)

[98] T.Kato, "Perturbation Theory for Linear Operators", Springer-Verlag (1966)

[99] J.W.Flower, S.W.Otto, S.M.Callahan, *Phys. Rev.* **D35**, 598 (1986)

[100] T.Sterling, J.Greensite, *Nucl. Phys.* **B220**, 327 (1983)

[101] J.Ambjorn, S-K.Yang, *Phys. Lett.* **165B**, 140 (1985)

[102] H.W.Hamber, G.Parisi, *Phys. Lett.* **159B**, 330 (1985)

[103] R.Morison, S.W.Otto, Caltech Concurrent Computation Project preprint C^3P-286 (1986)

[104] J.Ambjorn, M.Flensburg, C.Peterson, *Phys. Lett.* **159B**, 335 (1985)

[105] G.Bhanot, M.Creutz, *Phys. Rev.***D21**, 2892 (1980)

[106] J.Ambjorn, A.J.G.Hey, S.W.Otto, *Nucl.Phys.* **B210**, 347 (1982)

[107] I.T.Drummond, S.Duane, R.Horgan, *Nucl. Phys.* **B220**, 199 (1983)

[108] M.Nagasawa, *J. Math. Biol.* **9**, 213 (1980)

[109] J.Ambjorn, S-K.Yang, *Nucl. Phys.* **275**, 18 (1986)

[110] F.Karsch, H.W.Wyld, *Phys. Rev. Lett.* **55**, 2242 (1985)

[111] J.R.Klauder, private communication.

[112] H.Hamber, G.Parisi, *Phys. Rev. Lett.* **47**, 1792 (1981)

A.Hasenfratz, Z.Kunst, P.Hasenfratz, C.B.Lang, **Phys. Lett. 110b**, 289 (1982)

F.Fucito *et al.*, *Nucl. Phys.* **B210**, 407 (1982)

D.Weingarten, *Nucl. Phys.* **B215**, 1 (1983)

J.P.Gilchrist, G.Schierholz, H.Scheider, M.Teper, *Nucl. Phys.* **B248**, 29 (1984)

D.Barkai, K.J.M.Moriarty, C.Rebbi, *Phys. Lett.* **156B**, 385 (1985)

A.Konig, K.H.Mutter, K.Schilling, *Nucl. Phys.* **B259**,33 (1985)

K.C.Bowler, C.B.Chalmers, R.D.Kenway, G.S.Pawley, D.Raseth, D.J.Wallace, University of Edinburgh preprint 86/369

P.de Forcrand, A.Konig, K.H.Mutter, R.Sommer, Wuppertal University preprint WU B 86-3

[113] L.McLerran, B.Svetitsky, *Phys. Rev.* **D24**, 450 (1981)

L.G.Yaffe, B.Svetitsky, *Phys. Rev.* **D26**, 963 (1982)

B.Svetitsky, L.G.Yaffe, *Nucl. Phys.* **B210**, 423 (1982)

[114] Ya.B.Zeldovich, *JEPT* **37**, 659 (1959)

A.M.Polyakov, *Phys. Lett.* **72B**, 477 (1978)

L.Susskind, *Phys. Rev.* **D20**, 2610 (1979)

L.McLerran, *Rev. Mod. Phys.* **58**, 1021 (1986)

[115] K.G.Wilson, "New Phenomena in Subnuclear Physics", Ed. A.Zichichi, Erice 1975 (Plenum, NY 1977)

[116] J.B.Kogut, L.Sussskind, *Phys. Rev.* **D11**, 395 (1975)
L.Susskind, *Phys. Rev.* **D16**, 3031 (1977)

[117] H.B.Nielsen, M.Ninomiya, *Phys. Lett.* **105B**, 219 (1981)

[118] S.D.Drell, M.Weinstein, S.Yankielowicz, *Phys. Rev.* **D14**, 1627 (1976)
M.Weinstein, S.D.Drell, H.R.Quinn, B.Svetitsky, *Phys. Rev.* **D22**, 1190 (1980)

[119] H.R.Quinn, M.Weinstein, *Phys. Rev. Lett.* **57**, 2617 (!986)

[120] P.T.Matthews, A.Salam, *Nuovo Cim.* **12**, 563 (1954)
P.T.Matthews, A.Salam, *Nuovo Cim.* **2**, 120 (1955)

[121] H.Kluberg-Stern, A.Morel, O.Napoly, B.Petersson, *Nucl. Phys.* **220**, 447 (1983)

[122] O.Martin, S.W.Otto, *Phys. Rev.* **D31**, 435 (1985)

[123] D.Scalapino, R.L.Sugar, *Phys. Rev. Lett.* **46**, 519 (1981)

[124] A.Duncan, M.Furman, *Nucl. Phys.* **B190**, 767 (1981)
D.Weingarten, D.Petcher, *Phys. Lett.* **99B**, 333 (1981)
A.Duncan, R.Roskies, *Phys. Lett.* **114B**, 439 (1981)
S.Gottlieb, W.Liu, D.Toussaint, R.L.Sugar, UC San Diego preprint UCSD-10P10-267

[125] D.Zwanziger, *Phys. Rev. Lett.* **50**, 1886 (1983)

[126] S.W.Otto, M.Randeria, *Nucl. Phys.* **B220**, 479 (1983)
S.W.Otto, *Phys. Lett.* **135B**, 129 (1984)

[127] D.Weingarten, *Nucl. Phys.* **B257**, 629 (1985)

[128] F.Fucito, E.Marinari, G.Parisi, C.Rebbi, *Nucl. Phys.* **B180**, 369 (1981)
E.Marinari, G.Parisi, C.Rebbi, *Nucl. Phys.* **B190**, 266 (1981)

[129] F.Fucito, C.Rebbi, S.Solomon, *Nucl. Phys.* **B248**, 615 (1984)
F.Fucito, S.Solomon, *Phys. Rev. Lett.* **55**, 2641 (1985)
F.Fucito, R.Kinney, S.Solomon, *Nucl. Phys.* **B253**, 727 (1985)
F.Fucito, S.Solomon, C.Rebbi, *Phys. Rev.* **D31**, 1460 (1985)
R.Gavai, *Nucl. Phys.* **B269**, 530 (1986)

[130] F.Fucito, K.J.M.Moriarty, S.Solomon, *Phys. Lett.* **172B**, 235 (1986)

[131] G.Batrouni, G.R.Katz, A.S.Kronfeld, G.P.LePage, B.Svetitsky, K.G.Wilson, *Phys. Rev.* **D32**, 2736 (1985)

[132] A.S.Kronfeld, DESY preprint DESY-86-021 (1986)

[133] O.C.Martin, S.W.Otto, J.W.Flower, *Nucl. Phys.* **B264**, 89 (1986)

[134] C.de Dominicis, *Lett. Nuovo Cim.* **12**, 567 (1975)

[135] T.Banks, A.Ukawa, *Nucl. Phys.* **B225**, 145 (1983)
P.Hasenfratz, F.Karsch, I.O.Stamatescu, *Phys. Lett.* **133B**, 221 (1983)
T.Celik, J.Engels, H.Satz, *Phys. Lett.* **133B**, 427 (1983)
R.Gavai, M.Lev, B.Peterson, *Phys. Lett.* **140B**, 397 (1984)
J.Polonyi, H.W.Wyld, J.B.Kogut, J.Shigemitsu, D.K.Sinclair, *Phys. Rev. Lett.* **53**, 644 (1984)
J.B.Kogut, D.K.Sinclair, University of Illinois preprint ILL-TH-86-46 (1986)

[136] A.Ukawa, M.Fukugita, *Phys. Rev. Lett.* **55**, 1854 (1985)
M.Fukugita, A.Ukawa, *Phys. Rev. Lett.* **57**, 503 (1986)

[137] E.Helfand, *Bell System Technical Journal* **58**, 2283 (1979)
H.Greensite, E.Helfand, *Bell System Technical Journal* **60**, 1927 (1981)

[138] P.Meakin, H.Metiu, R.Petschek, D.Scalapino, *J. Chem. Phys.* **79(4)**, 1948 (1983)

[139] L.A.Hageman, D.M.Young, "Applied Iterative Methods", Academic Press (1981)

[140] G.H.Golub, C.F.Van Loan, "Matrix Computations", John Hopkins University Press (1983)

[141] M. Creutz, *Phys. Rev.* **D21**, 2308 (1980)

[142] H-Q.Ding, Columbia University preprint CU-TP-312 (1986)

[143] A.D.Kennedy, B.J.Pendleton, *Phys. Lett.* **156B**, 393 (1985)

[144] H.A.Kramers, *Physica* **7**, 284 (1940)
J.E.Moyal, *J. Roy. Stat. Soc.* **B11**, 150 (1944)

[145] G.Parisi, Y.Wu, *Scienta Sinica* **24**, 483 (1981)

Table Captions

1. Dimensionless lattice potentials in the mesonic sector at $\beta = 6.1, 6.3, 6.5, 6.7$.

2. χ^2 values for pairwise fits of the mesonic lattice potentials at separate β values to the linear + Coulomb form, Eq. (3.15), assuming asymptotic scaling.

3. Dimensionless lattice potentials from off-axis Wilson loops in the mesonic sector at $\beta = 6.1, 6.3$

4. Parameters of the mesonic potential as extracted from the off-axis loops. Calculated both with and without contribution from strong coupling.

5. Dimensionless lattice potentials in the baryonic sector at $\beta = 6.1, 6.3$.

6. Parameters of the linear + Coulomb fit to the potentials

   a) Mesonic sector.

   b) Baryonic sector, assuming 'Δ' configuration for the confining strings.

   c) Baryonic sector, assuming 'Y' configuration for the confining strings.

7. Monte Carlo and fitted data values for the baryonic potential.

8. Peak and mid-point values of the squared chromoelectric field in the $q\bar{q}$ system.

9. Heat bath acceptance probability p_{acc} and inverse coupling β.

Figure Captions

1. Showing the notation for lattice links and a sample plaquette.

2. The topology of the hypercube in $doc = 2,3,4$ dimensions.

3. Calculating 2×3 Wilson loops on a sequential uniprocessor.

4. Calculating 1×3 Wilson loops in parallel. Each 5×5 block represents a two dimensional sublattice contained within a single processor.

5. Single and multiple gluon exchanges between quarks possibly responsible for the Coulombic and confining terms in the potential respectively.

6. The lattice world lines of a $q\bar{q}$ pair showing the δ-function contractions necessary to ensure that the meson is a colour singlet.

7. Mesonic lattice potentials, $\tilde{V}$, plotted against the dimensionless length variable, x, before self-energy subtractions.

8. Mesonic lattice potentials, $\tilde{V}$, plotted against the dimensionless length variable, x, after self-energy subtractions.

9. Mesonic lattice potentials for the four β values fitted single to the Coulomb plus linear form.

10. The off-axis Wilson loop observable $W(3,2;4)$.

11. The baryonic potential observable $Q(3,2,4;3)$.

12. Alternative string configurations inside a baryon

    a) The 'Δ' configuration.

    b) The 'Y' configuration.

13. Screening of charges in media with dielectric constants

    a) $\kappa > 1$.

    b) $\kappa < 1$.

14. Energy density and Higgs field in the Nielsen-Olesen string model.

15. Relative orientations of Wilson loop, W, and plaquette, P, used to measure the squared chromoelectric energy densities.

16. Squared energy densities in the $q\bar{q}$ system

    a) $\langle E_{\parallel}^2 \rangle$.

    b) $\langle E_{\perp}^2 \rangle$.

    c) $\langle -B_{\perp}^2 \rangle$.

17. Showing the relation between $\langle E_{\perp}^2 \rangle$ and $\langle -B_{\perp}^2 \rangle$ due to the discrete rotational symmetry of the lattice.

18. Showing the progressive delocalisation of the strong coupling string due to the formation of 'kinks'.

19. The operator used to measure the baryonic energy density. P_{xy} measures the magnetic and P_{xt} the electric fields.

20. Energy densities inside the baryon with quark locations indicated by $*$.

    a) Squared electric field.

    b) Squared magnetic field perpendicular to the plane containing the charges.

21. Showing the correspondence between finite velocity second order corrections and the insertion of 'electric field' operators.

22. Spin-dependent loop operators corresponding to the off-diagonal spin-spin force, Eq. (3.46), at $R = 1,2,3$.

23. Showing the loop-plaquette correlation corresponding to the measurement of the squared parallel electric field in two dimensions.

24. Contour used in proof of Eq. (4.33)

25. Squared parallel electric field in two dimensions. Solid curves show theoretical results.

    a) Test probe inside 5×5 loop, Eq. (4.44)

    b) Test probe outside 5×5 loop, Eq. (4.45)

26. Squared parallel electric field in three dimensions at $\beta = 2.0$.

    a) 5×5 loop.

    b) 7×7 loop.

27. Results of simulations in SU(2) by complex Langevin. Dashed curve is theoretical value of integral $L(\beta)$, Eq. (4.46), and data shown are from simulations of Eq. (4.55).

28. Trajectories in the complex plane of the deterministic parts of the Langevin equation of motion for the model case $P(x) \propto \cos x$, Eq. (4.60).

29. Estimates of $K(\beta)$, Eq. (4.57), according to numerical Langevin simulation, Eq. (4.60), analytic result (Dashed, Eq. (4.57)) and segregation theorem prediction (Solid, Eq. (4.61)) for the model case $P(x) \propto \cos x$.

30. $\langle \bar{\phi}\phi \rangle$ in simulations on a 4^4 lattice.

    a) Fixed Metropolis hitsize

    b) Fixed number of conjugate gradient iterations.

31. The thermal Wilson line as order parameter for the finite temperature deconfinement transition on an $8^3 \times 4$ lattice.

32. Dimensionless lattice potentials derived at $\beta = 6.1$ both in the quenched approximation (Upper curve) and also with four flavours of dynamical fermions (Lower curve).

33. The load imbalance, Eq. (A.4), in the Creutz heat bath as a function of hypercube dimension.

34. Diagrammatic rules for stochastic quantisation. Scalar fields with cubic interaction, Eq. (D.1).

35. Diagrams contributing to the two point function, $\langle \phi_i \phi_j \rangle$.

36. Three particle interaction vertex.

R	$\beta = 6.1$		$\beta = 6.3$		$\beta = 6.5$		$\beta = 6.7$	
2	0.5661	(0.0009)	0.5144	(0.0006)	0.4748	(0.0003)	0.4436	(0.0003)
3	0.6532	(0.0018)	0.5845	(0.0011)	0.5360	(0.0007)	0.4970	(0.0006)
4	0.7108	(0.0028)	0.6285	(0.0026)	0.5708	(0.0012)	0.5284	(0.0011)
5	0.7537	(0.0058)	0.6659	(0.0049)	0.5954	(0.0019)	0.5490	(0.0016)
6	0.784	(0.011)	0.6956	(0.0062)	0.6130	(0.0036)	0.5605	(0.0023)
7	0.798	(0.066)	0.726	(0.024)	0.6411	(0.0052)	0.5779	(0.0030)
8	0.757	(0.071)	0.758	(0.035)	0.656	(0.011)	0.5847	(0.0055)

Table 1

	6.1	6.3	6.5	6.7
6.1	0.26	2.92	7.31	8.83
6.3		0.12	4.73	7.06
6.5			0.05	14.04
6.7				1.71

Table 2

(R_1,R_2)	$\tilde{V}(x)$, $\beta = 6.1$	$\tilde{V}(x)$, $\beta = 6.3$
(0,2)	2.971 (0.003)	3.385 (0.003)
(0,3)	3.426 (0.007)	3.846 (0.006)
(0,4)	3.724 (0.013)	4.135 (0.013)
(0,5)	3.934 (0.024)	4.380 (0.026)
(0,6)	3.896 (0.056)	4.572 (0.037)
(1,1)	2.642 (0.001)	3.035 (0.001)
(1,2)	3.131 (0.006)	3.551 (0.007)
(1,3)	3.504 (0.008)	3.927 (0.009)
(1,4)	3.787 (0.011)	4.179 (0.011)
(1,5)	3.989 (0.020)	4.416 (0.017)
(2,2)	3.407 (0.003)	3.831 (0.004)
(2,3)	3.632 (0.009)	4.042 (0.010)
(2,4)	3.855 (0.015)	4.253 (0.015)
(2,5)	4.071 (0.035)	4.445 (0.024)
(3,3)	3.791 (0.014)	4.194 (0.012)
(3,4)	3.972 (0.023)	4.313 (0.018)

Table 3

Parameters	$\beta = 6.1$		$\beta = 6.3$	
	Conventional Eq. (3.15)	Conventional + Strong Coupling Eq. (3.24)	Conventional Eq. (3.15)	Conventional + Strong Coupling Eq. (3.24)
α	- .292 ± 0.010	-.285 ± 0.009	-.246 ± 0.008	-.246 ± 0.006
V_0	3.47 ± 0.12	3.44 ± 0.12	3.95 ± 0.06	3.95 ± 0.05
K	0.837 ± 0.015	0.724 ± 0.028	0.977 ± 0.010	0.986 ± 0.014
K'	--	0.12 ± 0.02	--	0.011 ± 0.007
Reduced χ^2	3.5	1.9	2.1	2.1

Table 4

$(R1,R2,R3)$	$\tilde{V}$, $\beta = 6.1$		$\tilde{V}$, $\beta = 6.3$	
(1,0,1)	3.4205	(0.0012)	3.9574	(0.0017)
(1,1,1)	4.1396	(0.0029)	4.7390	(0.0038)
(2,0,1)	4.1120	(0.0036)	4.6949	(0.0049)
(2,0,2)	4.7027	(0.0058)	5.3361	(0.0073)
(2,1,1)	4.6386	(0.0036)	5.2589	(0.0049)
(2,2,1)	5.0755	(0.0058)	5.6786	(0.0057)
(2,2,2)	5.3184	(0.0147)	5.9059	(0.0091)
(3,2,2)	5.5056	(0.0522)	6.0999	(0.0300)
(3,3,2)	5.734	(0.126)	6.4350	(0.0609)
(3,3,3)	5.838	(0.245)	6.647	(0.112)

Table 5

a)

$q\bar{q}$	$\beta = 6.1$	$\beta = 6.3$
$\alpha^{q\bar{q}}$	- 0.366 (.029)	- 0.287 (.019)
V_0	3.66 (.11)	4.03 (.10)
$K^{q\bar{q}}$	0.71 (.10)	0.95 (.10)

b)

qqq_Δ	$\beta = 6.1$	$\beta = 6.3$
α^{qqq}	- 0.147 (.008)	- 0.127 (.006)
V_0	5.20 (.16)	5.94 (.04)
K_Δ^{qqq}	0.90 (.15)	1.07 (.08)

c)

qqq_Y	$\beta = 6.1$	$\beta = 6.3$
α^{qqq}	- 0.153 (.008)	- 0.129 (.007)
V_0	5.30 (.16)	5.97 (.05)
K_Y^{qqq}	0.74 (.14)	0.94 (.04)

Table 6

($R1$,$R2$,$R3$)	Monte Carlo	'Δ' fit	'Y' fit
(1,0,1)	3.9574	3.9567	3.9561
(1,1,1)	4.7390	4.7314	4.7406
(2,0,1)	4.6949	4.7366	4.7380
(2,0,2)	5.3361	5.3600	5.3771
(2,1,1)	5.2589	5.2338	5.2305
(2,2,1)	5.6786	5.6671	5.6408
(2,2,2)	5.9059	5.9190	5.9420
(3,2,2)	6.0999	6.1676	6.1755
(3,3,2)	6.4350	6.4023	6.3898
(3,3,3)	6.6470	6.5750	6.6040

Table 7

Loop size	$\langle \mathrm{tr} E^2_{\parallel,peak} \rangle$	$\langle \mathrm{tr} E^2_{\parallel,mid} \rangle$	$\langle \mathrm{tr} E^2_{\parallel,peak} \rangle / \langle \mathrm{tr} E^2_{\parallel,mid} \rangle$
3×3	605 ± 18	345 ± 20	1.75 ± 0.11
3×4	534 ± 18	286 ± 21	1.85 ± 0.18
3×5	440 ± 38	252 ± 40	1.75 ± 0.32
3×6	353 ± 37	228 ± 68	1.55 ± 0.49

Table 8

β	k_{av}	p_{acc}
5.6	14.7	.32
6.0	15.9	.31
6.4	18.0	.29
6.8	19.5	.27
8.0	24.7	.25
10.0	32.9	.21

Table 9

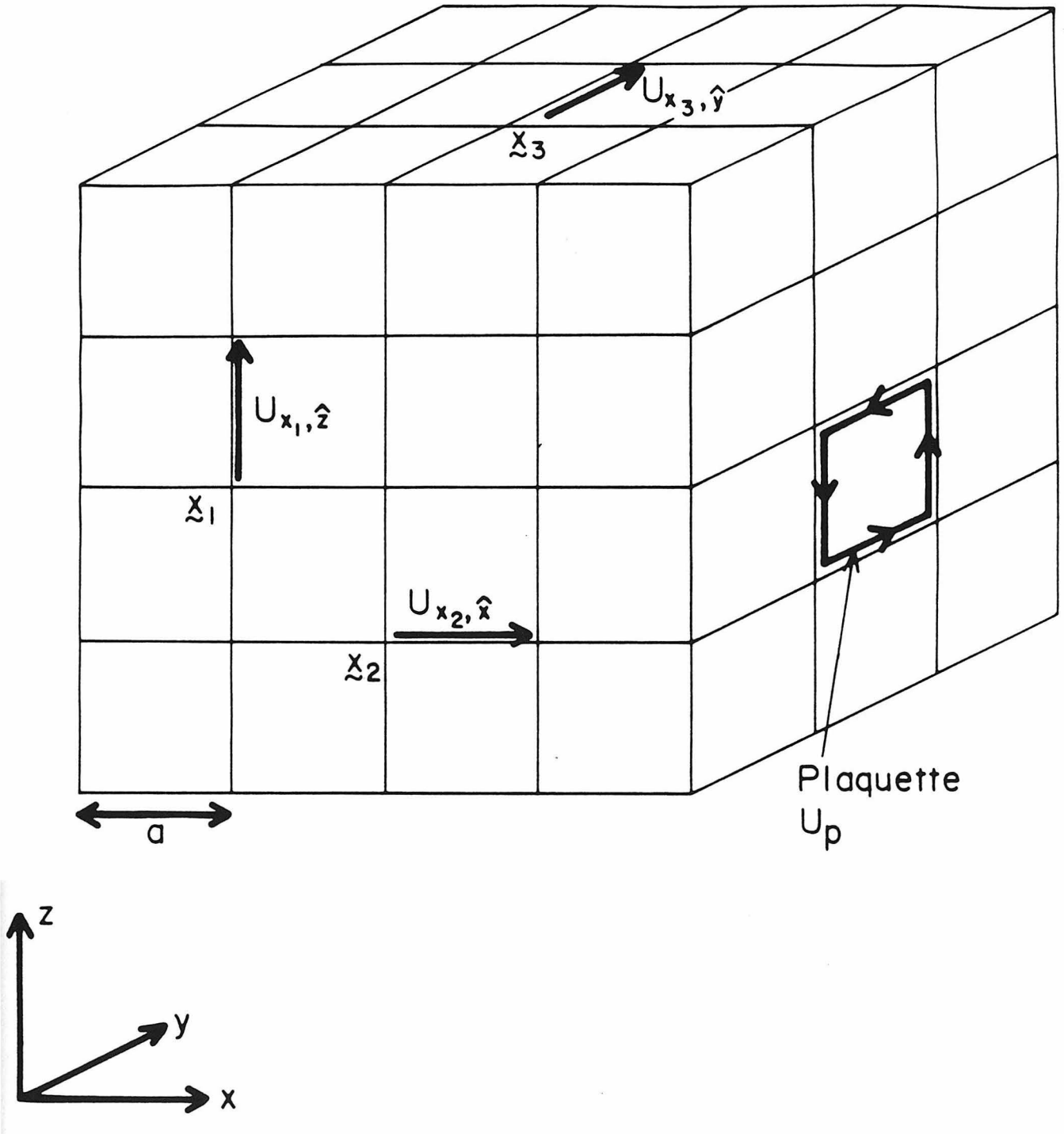
$U_{x_3,\hat{y}}$
$\underset{\sim}{x}_3$
$U_{x_1,\hat{z}}$
$\underset{\sim}{x}_1$
$U_{x_2,\hat{x}}$
$\underset{\sim}{x}_2$
Plaquette
U_p
a
z
y
x

Figure 1

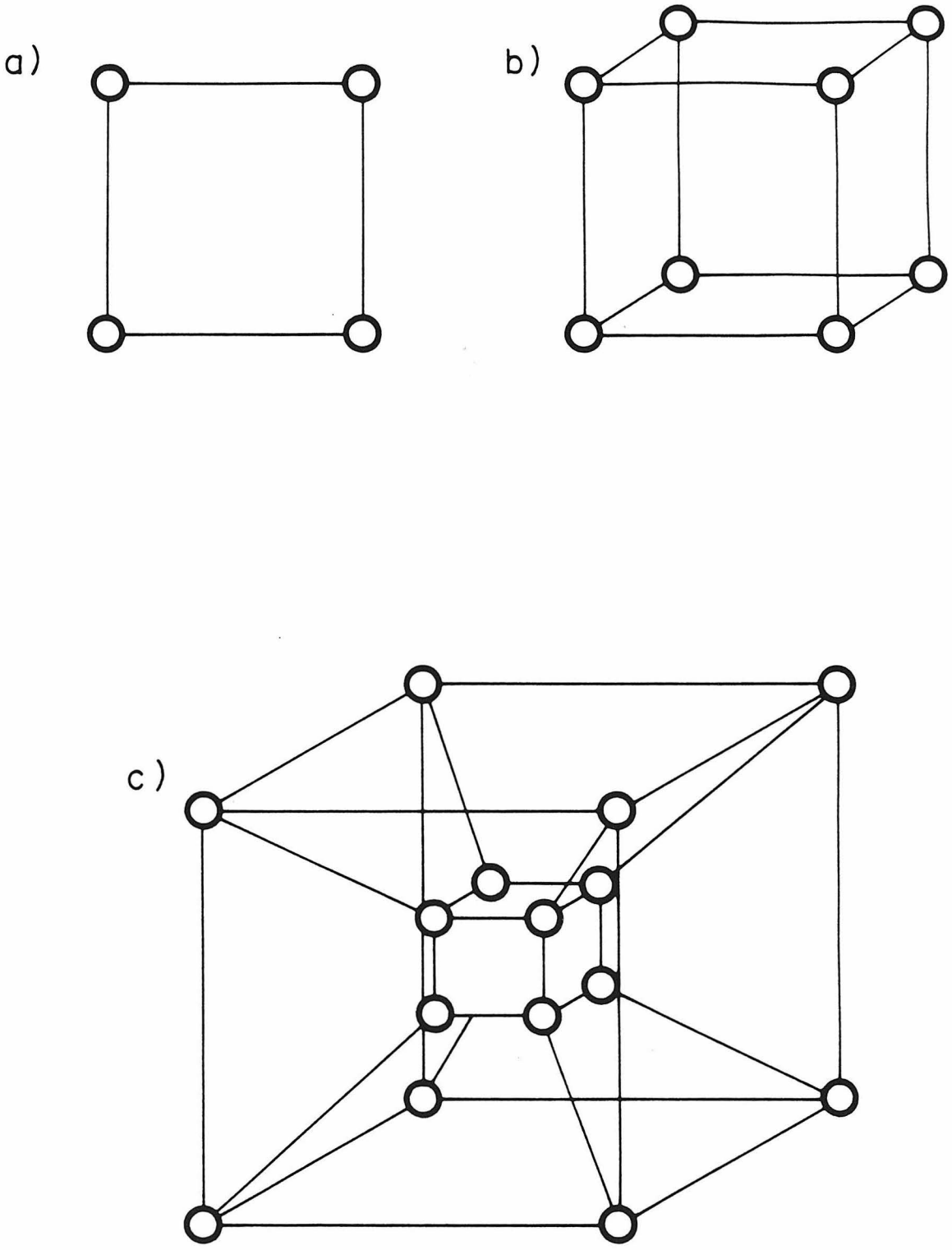

Figure 2

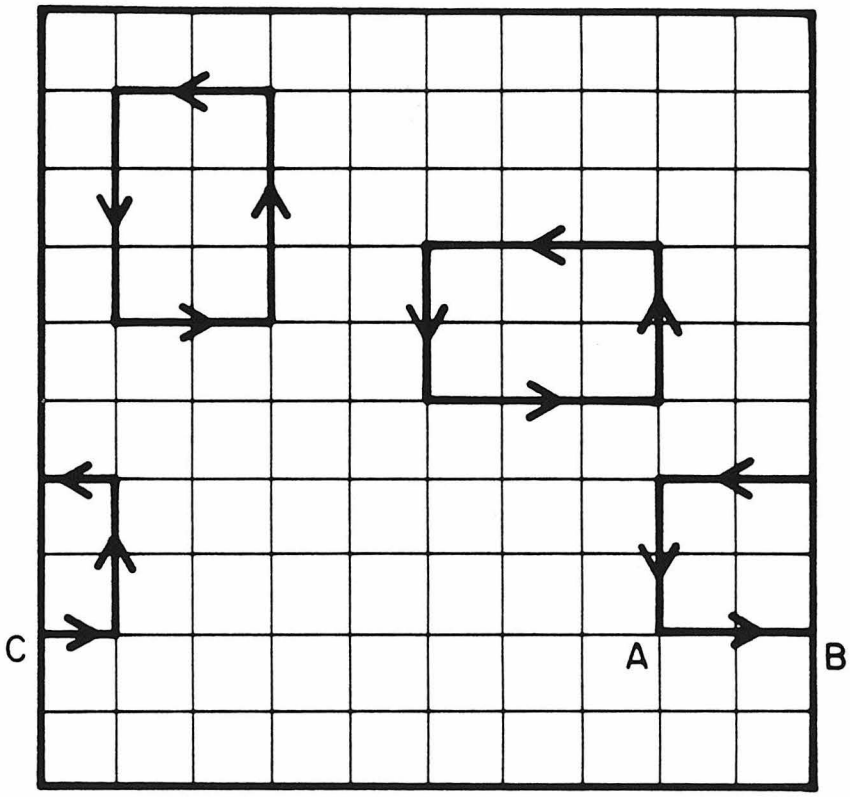

Figure 3

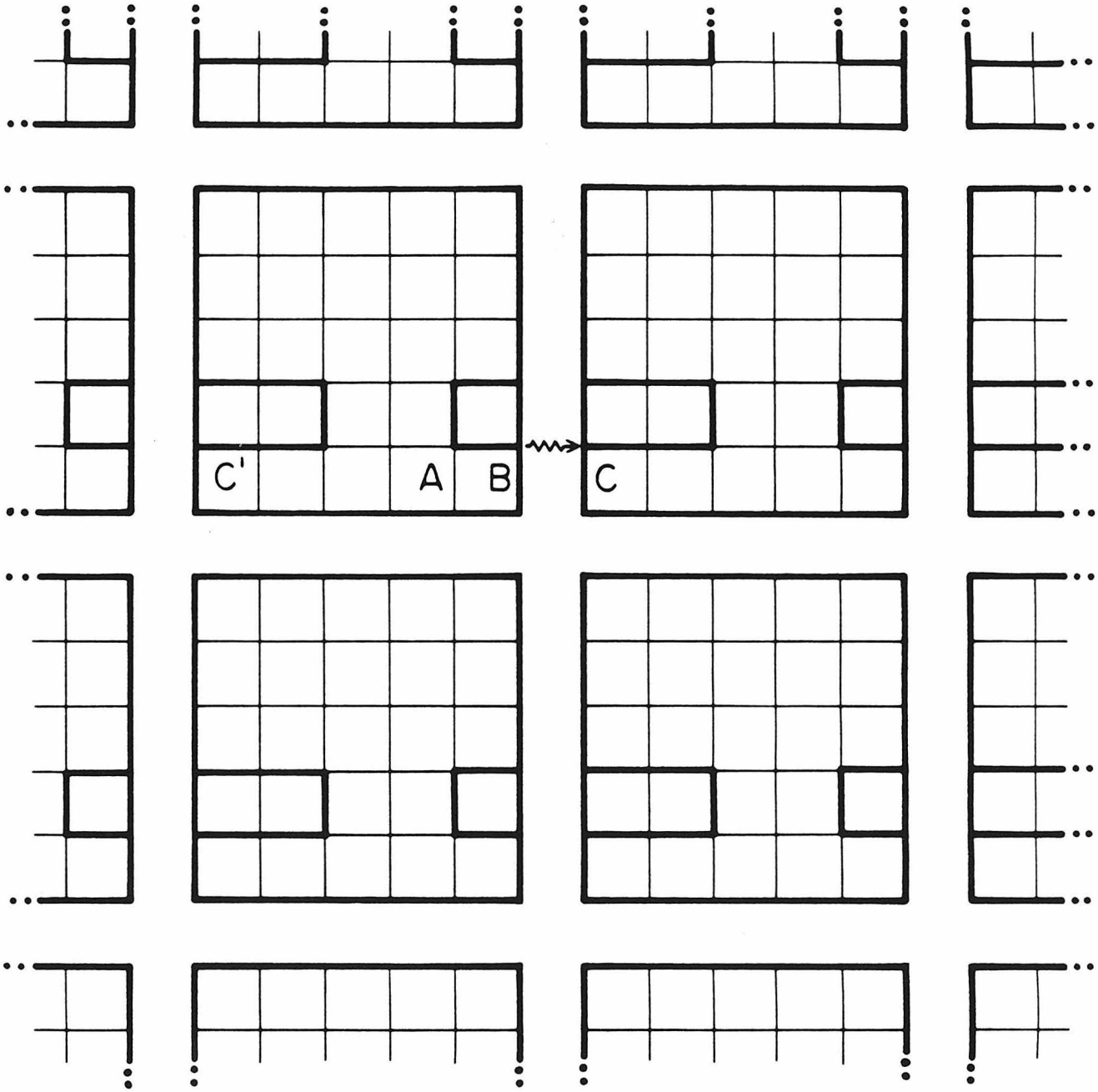

Figure 4

a)

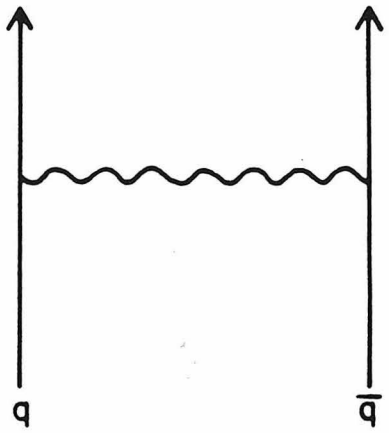

b)

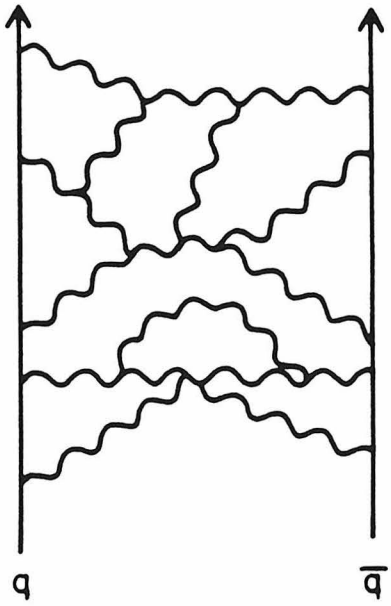

Figure 5

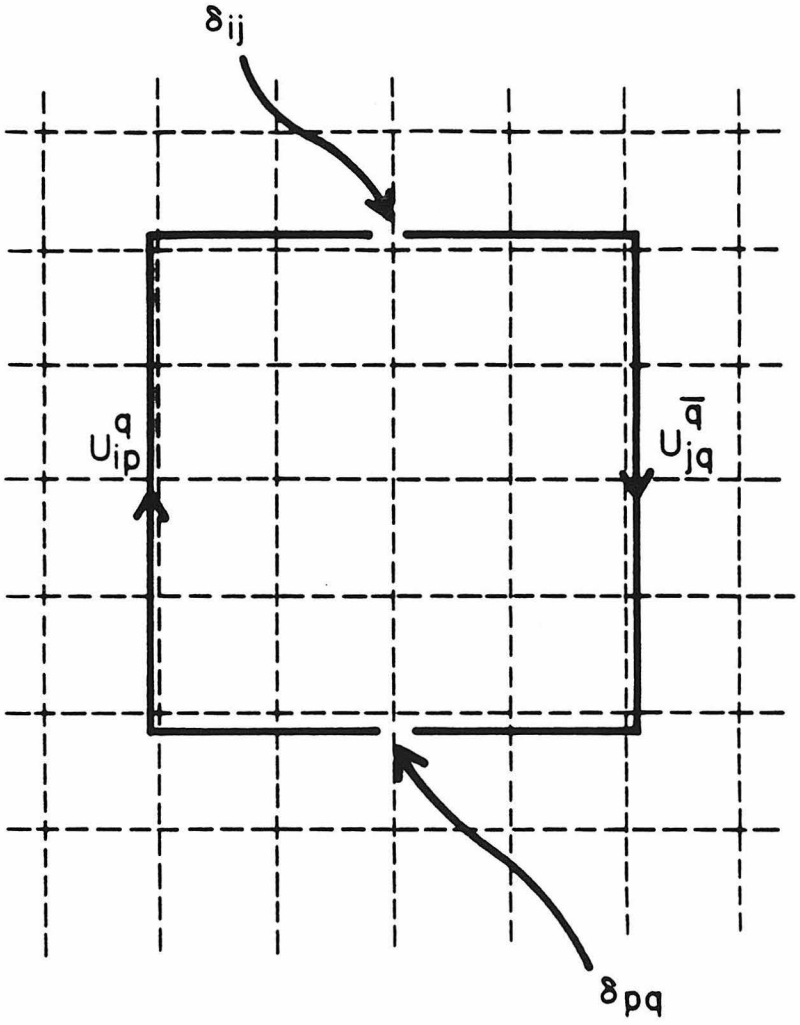

Figure 6

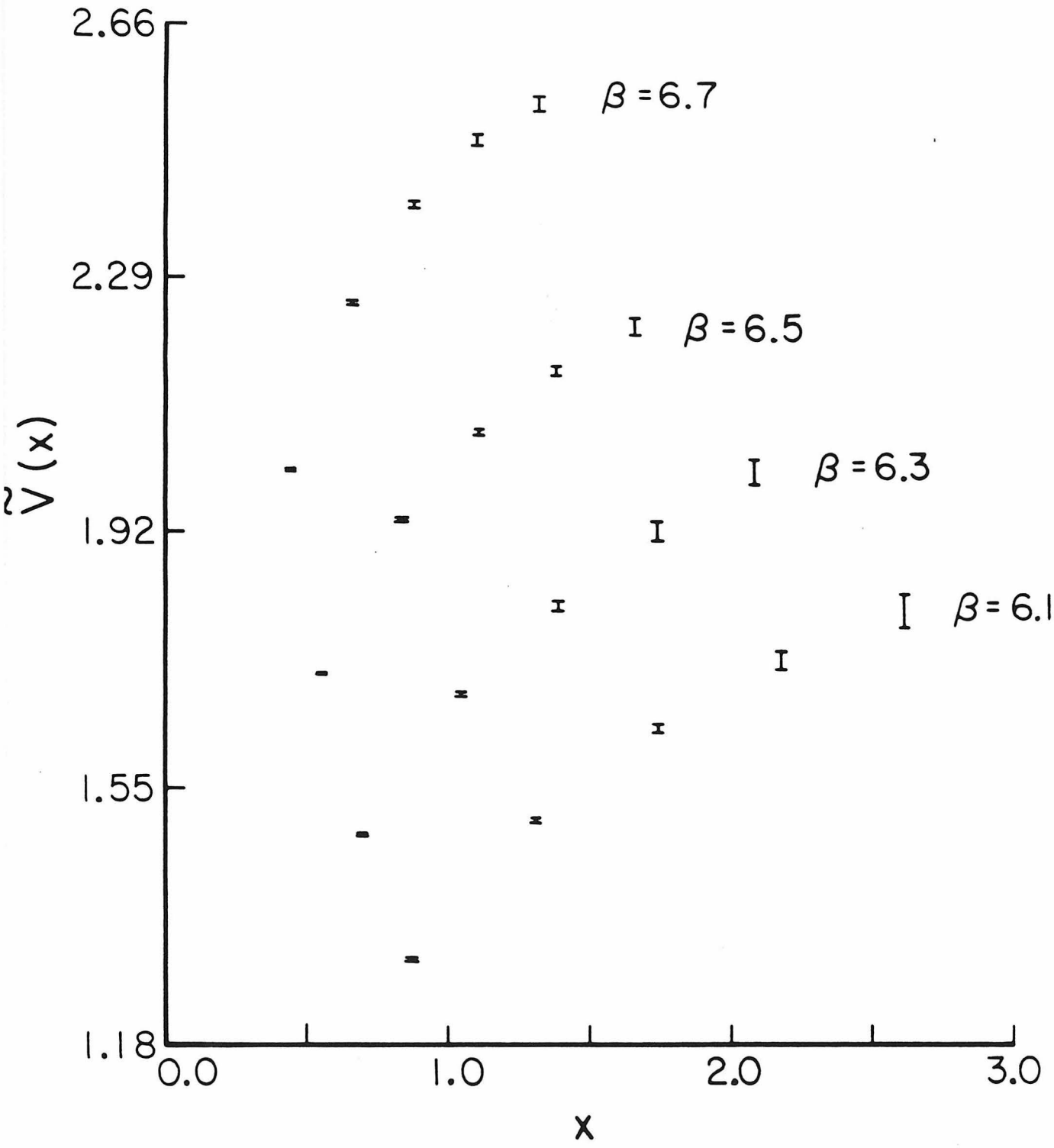

Figure 7

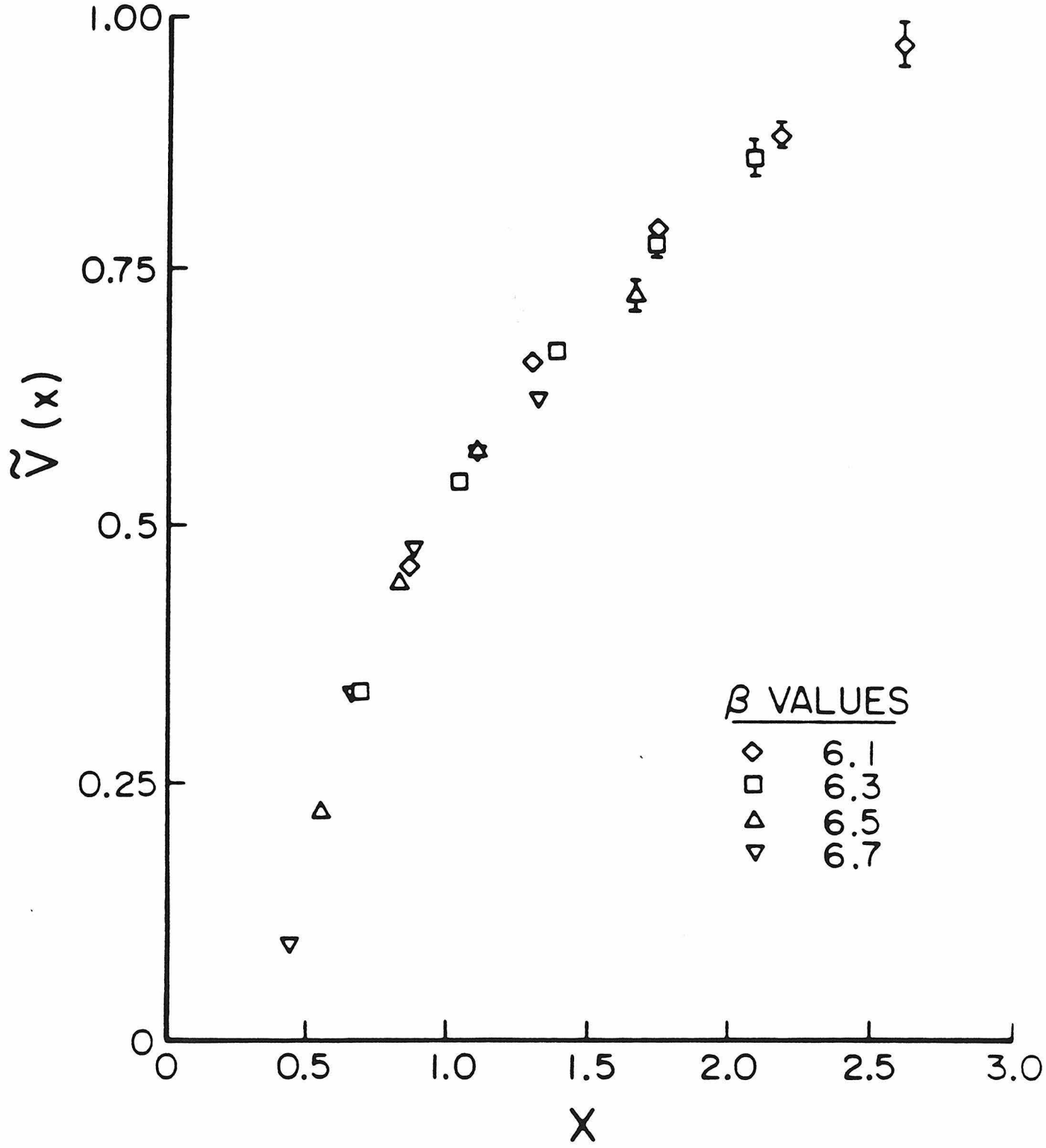

Figure 8

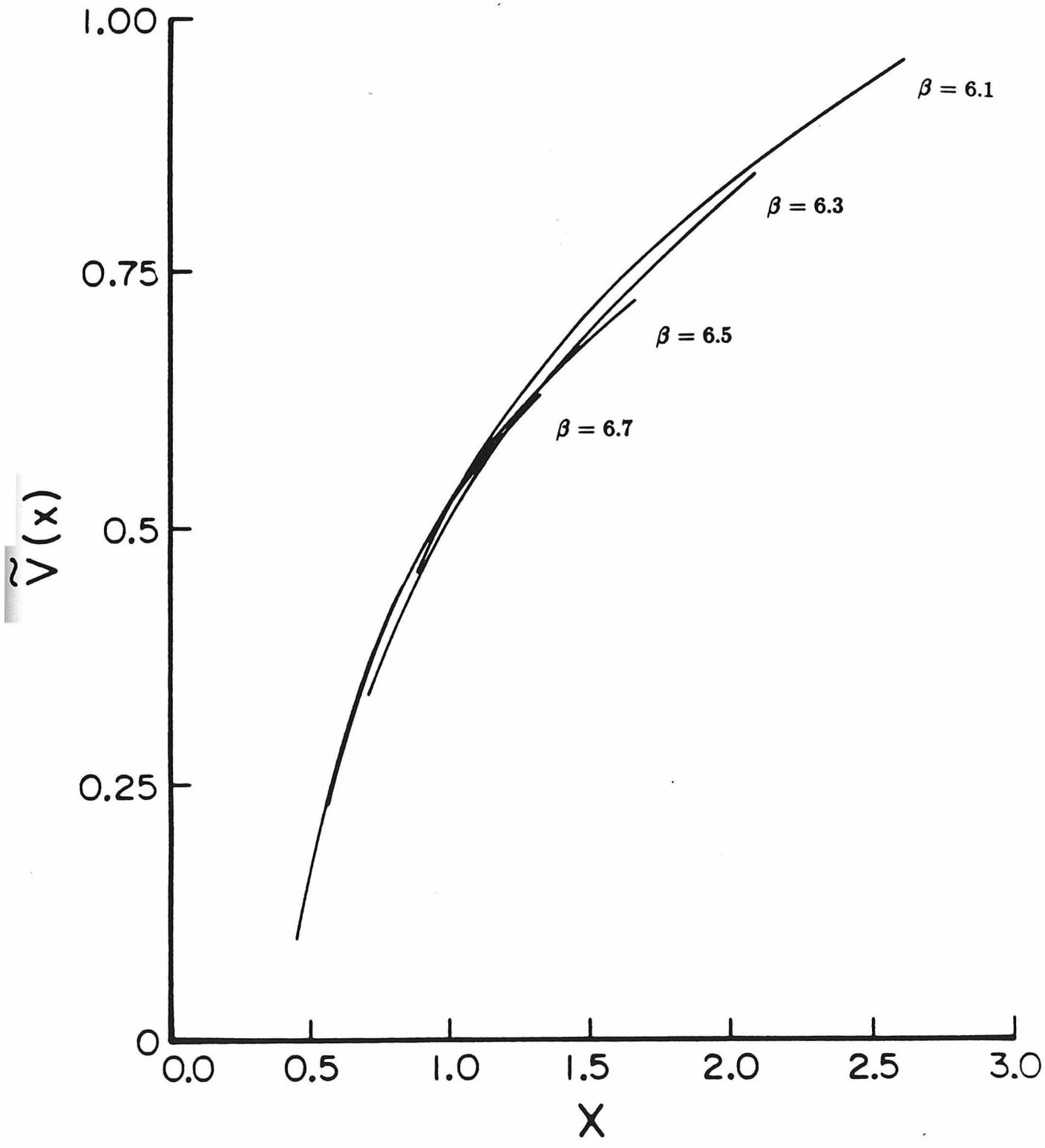

Figure 9

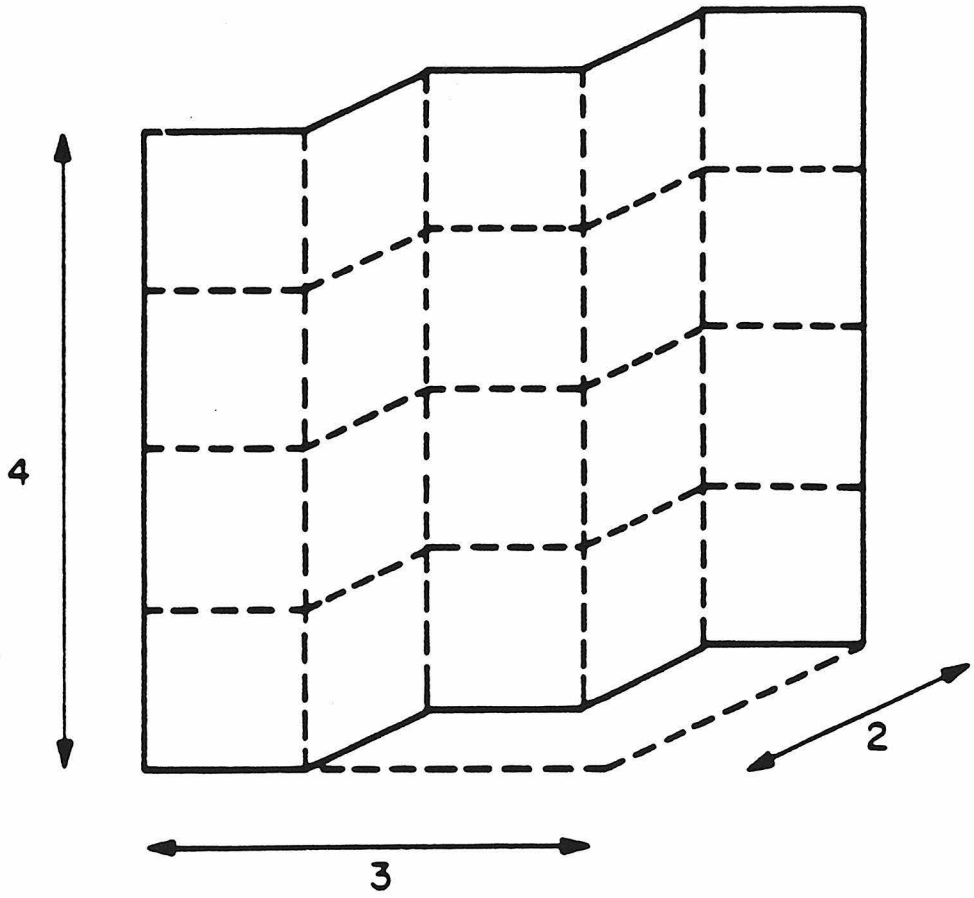

Figure 10

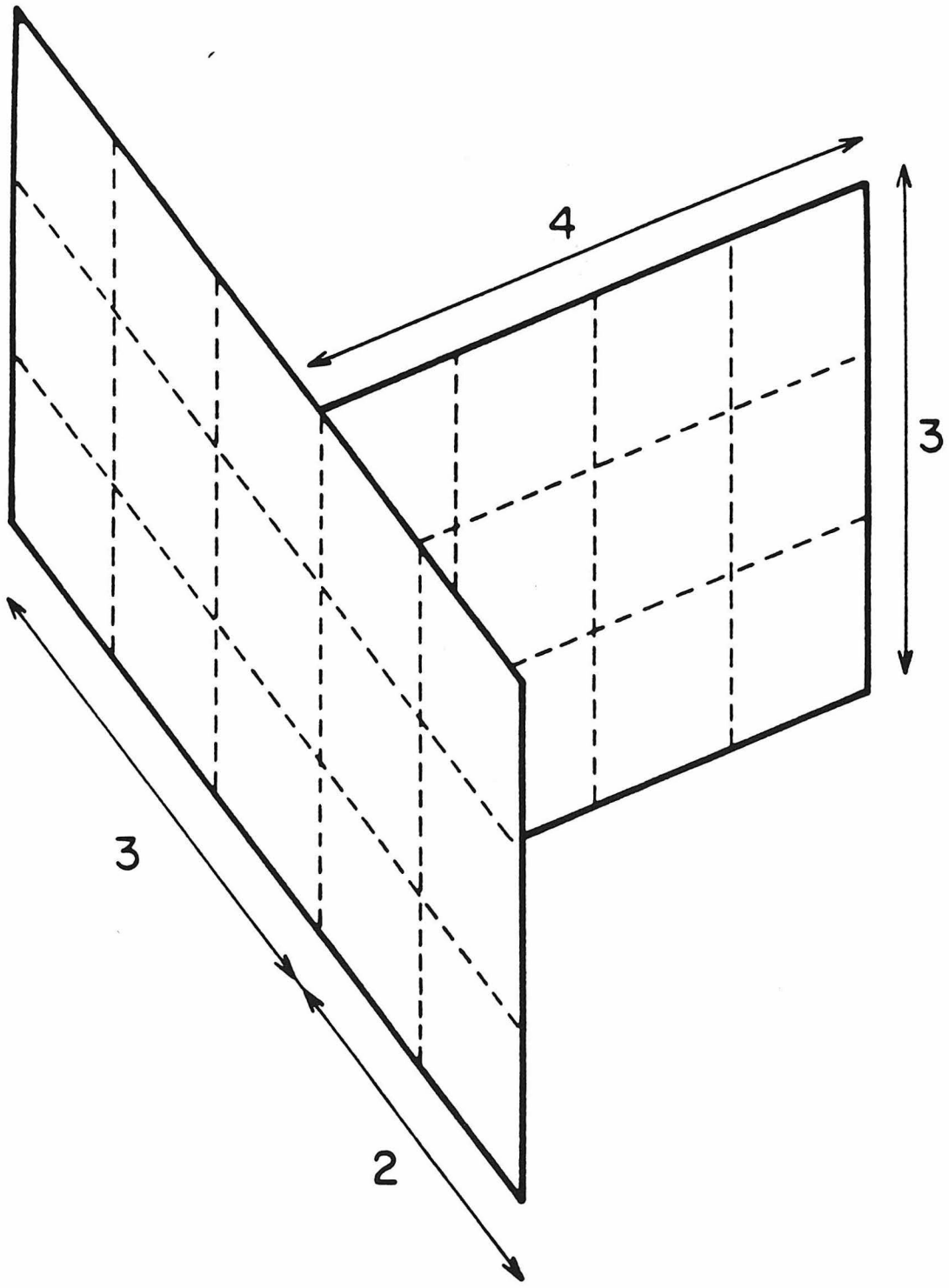

Figure 11

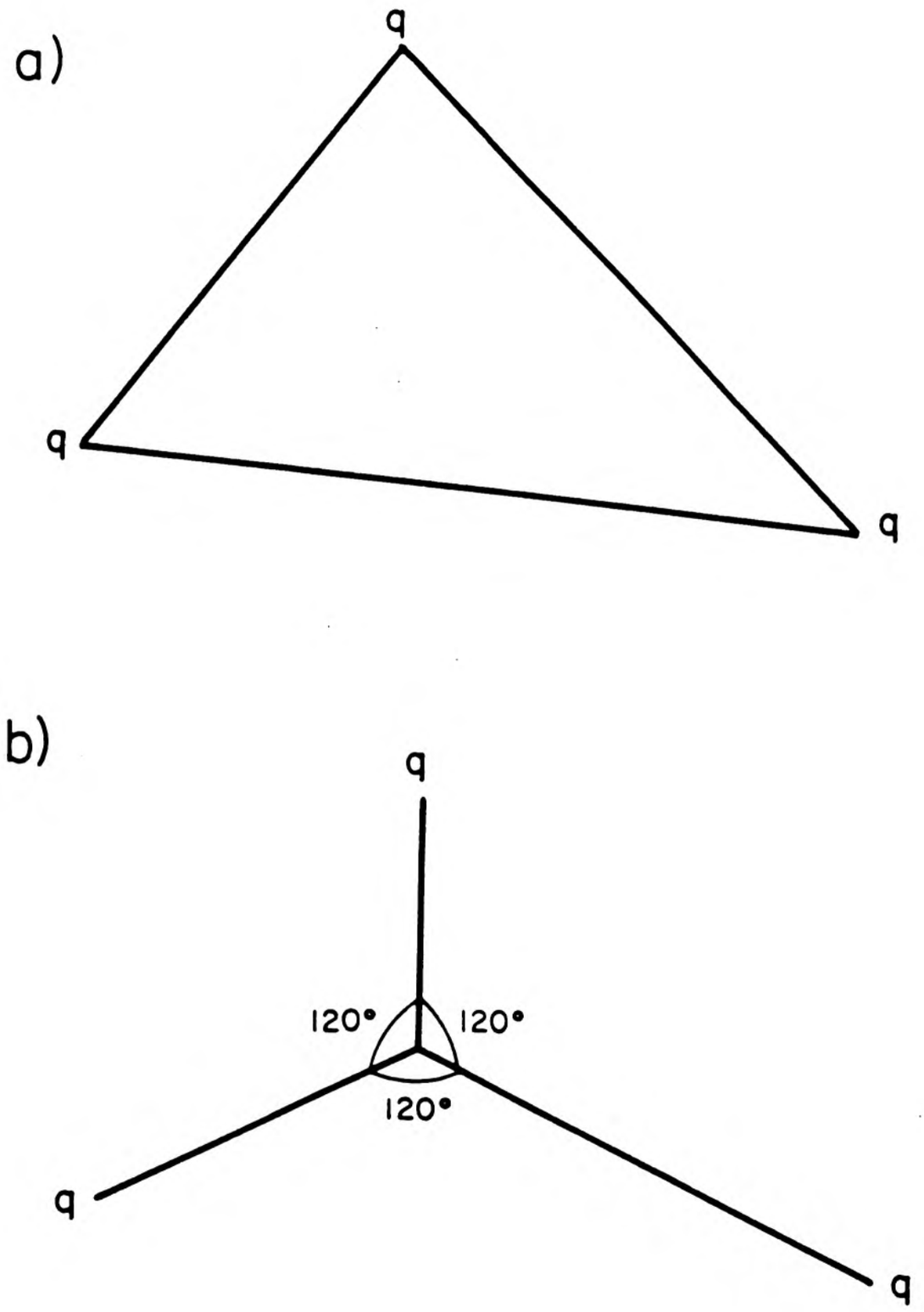

Figure 12

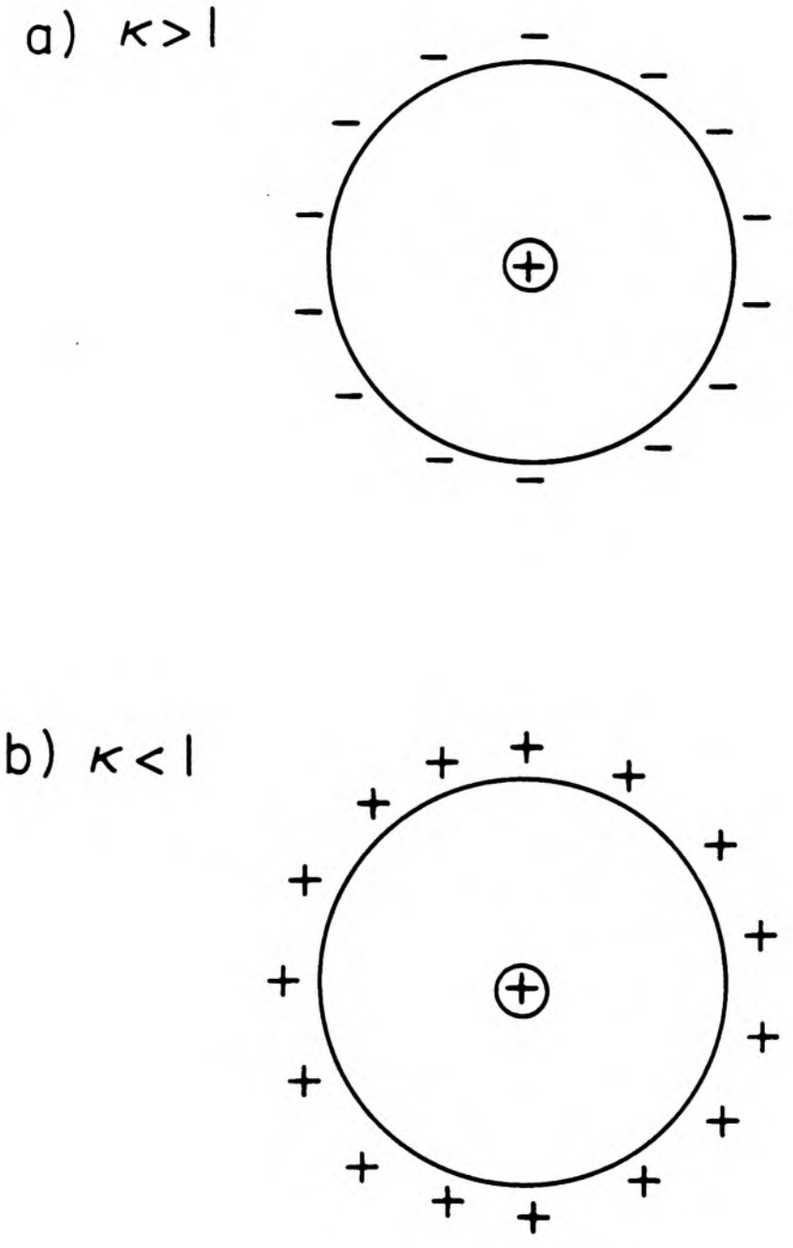

Figure 13

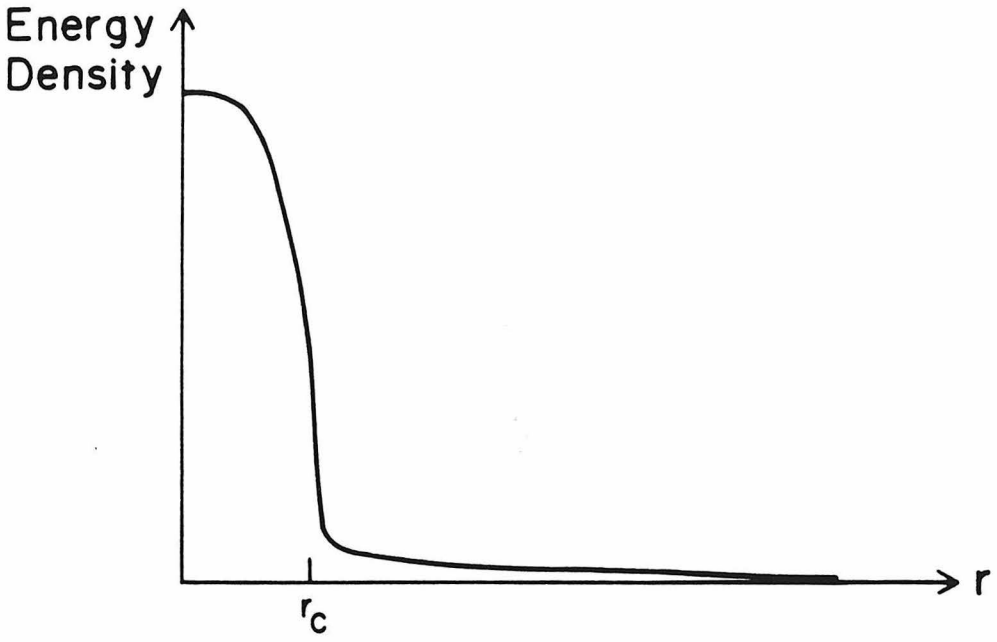

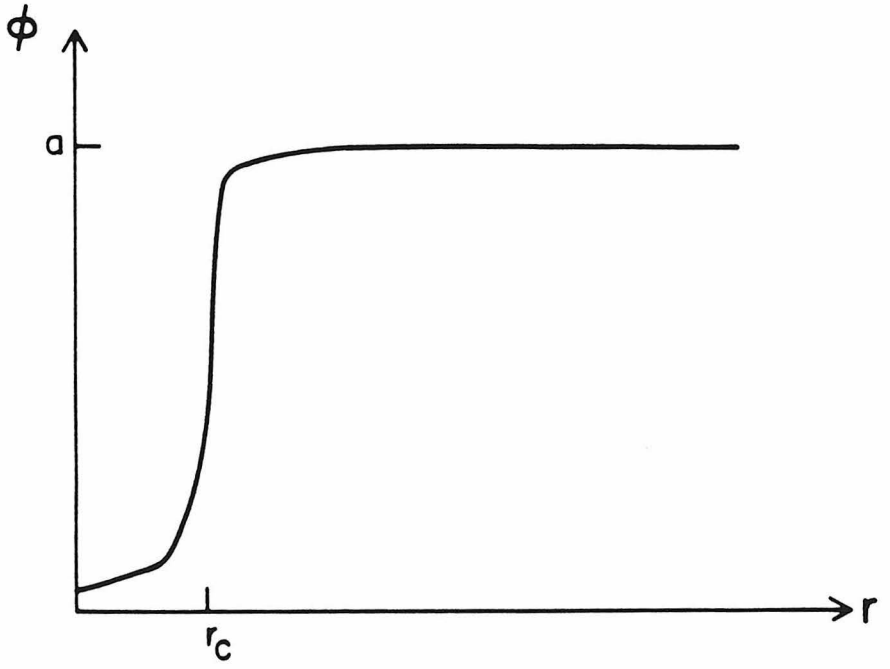

Figure 14

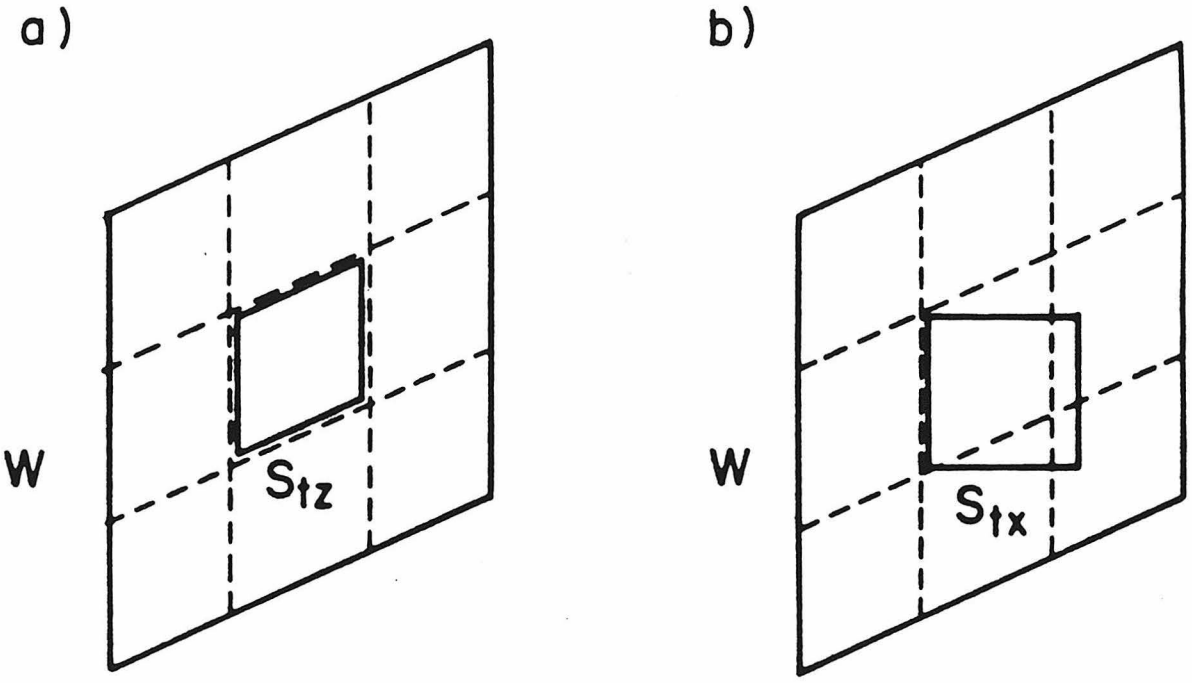

a) $P_{tz} \sim \langle \mathrm{tr}\ E_{\parallel}^2 \rangle$

b) $P_{tx} \sim \langle \mathrm{tr}\ E_{\perp}^2 \rangle$

Figure 15

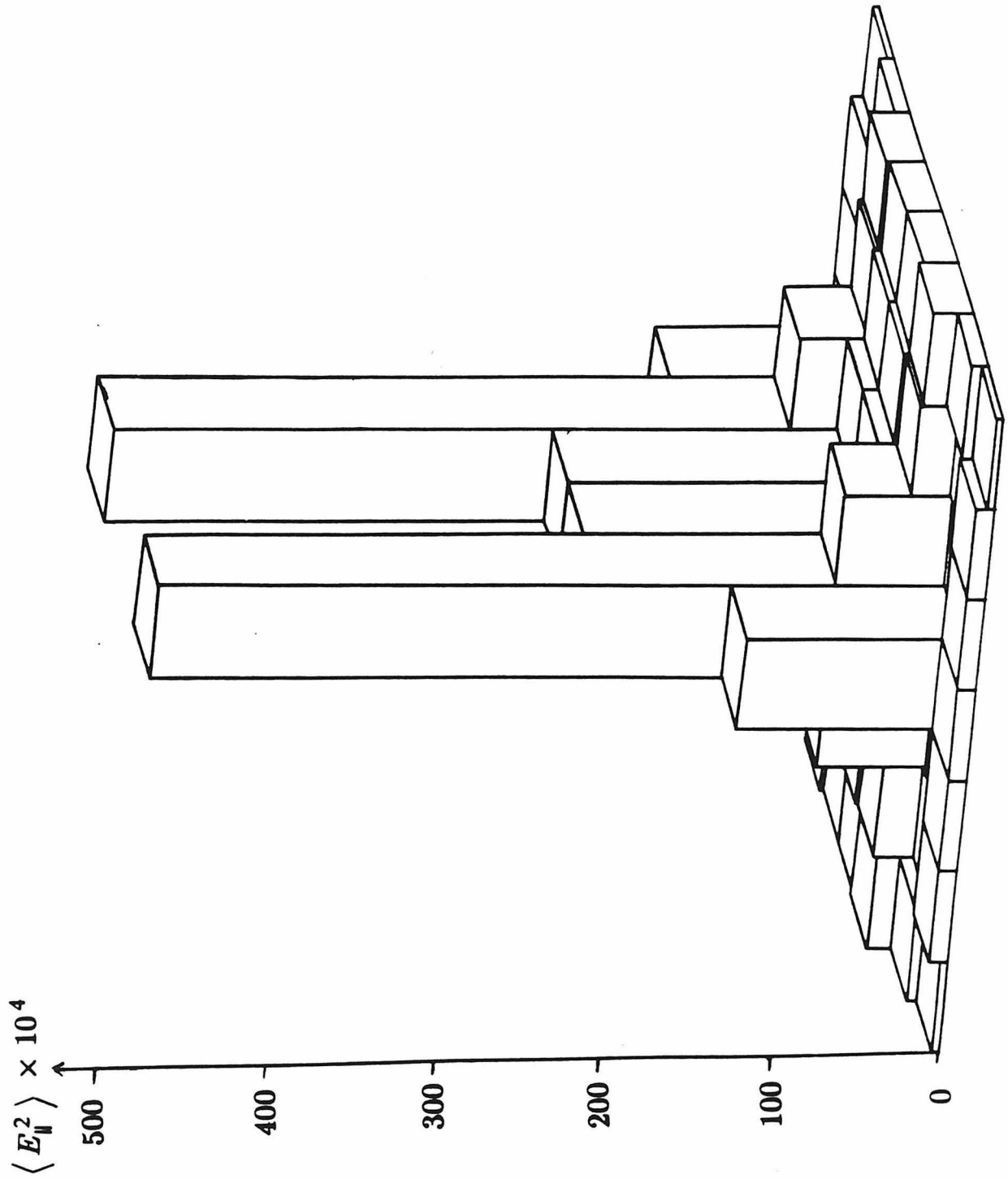

Figure 16a)

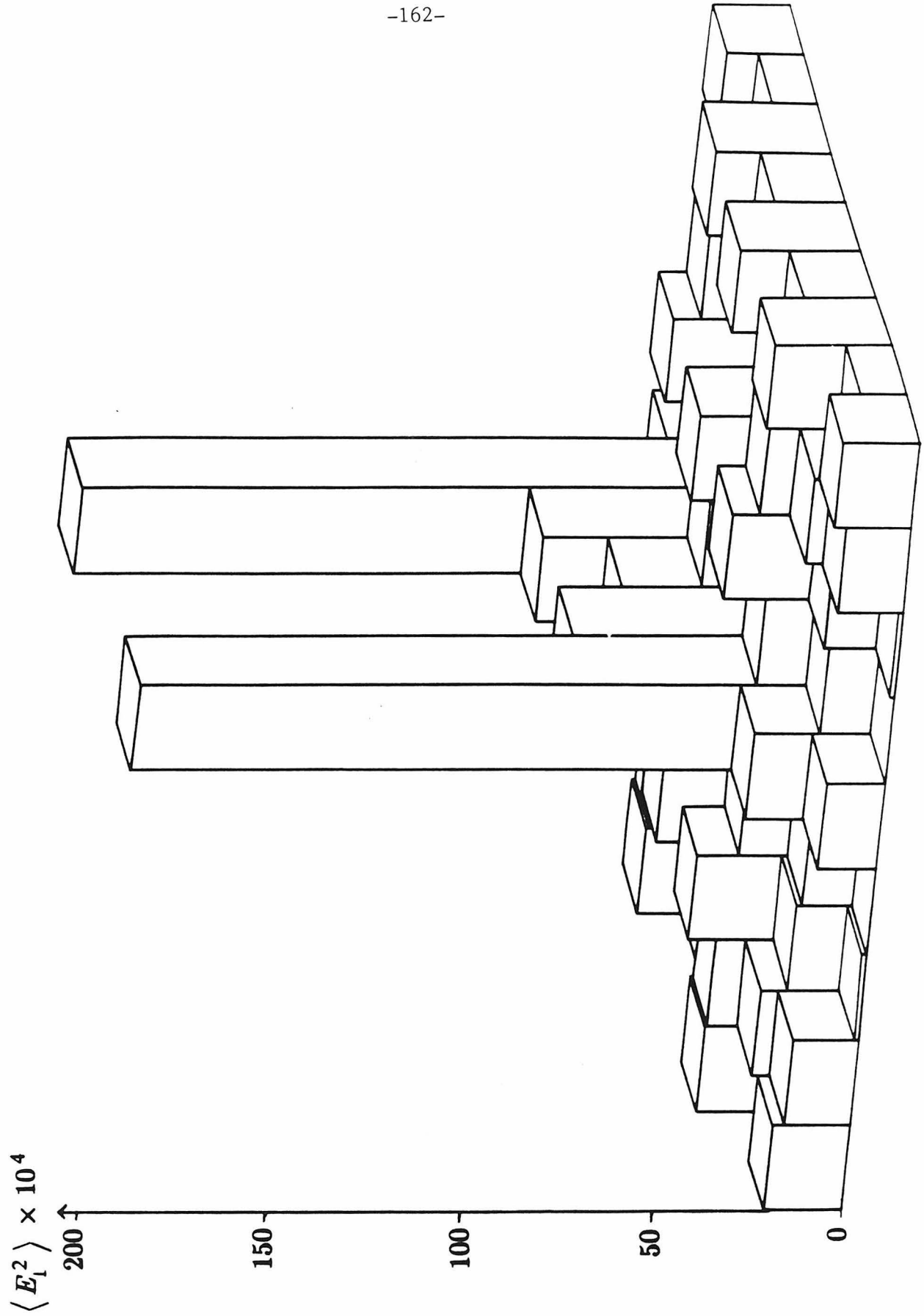

Figure 16b)

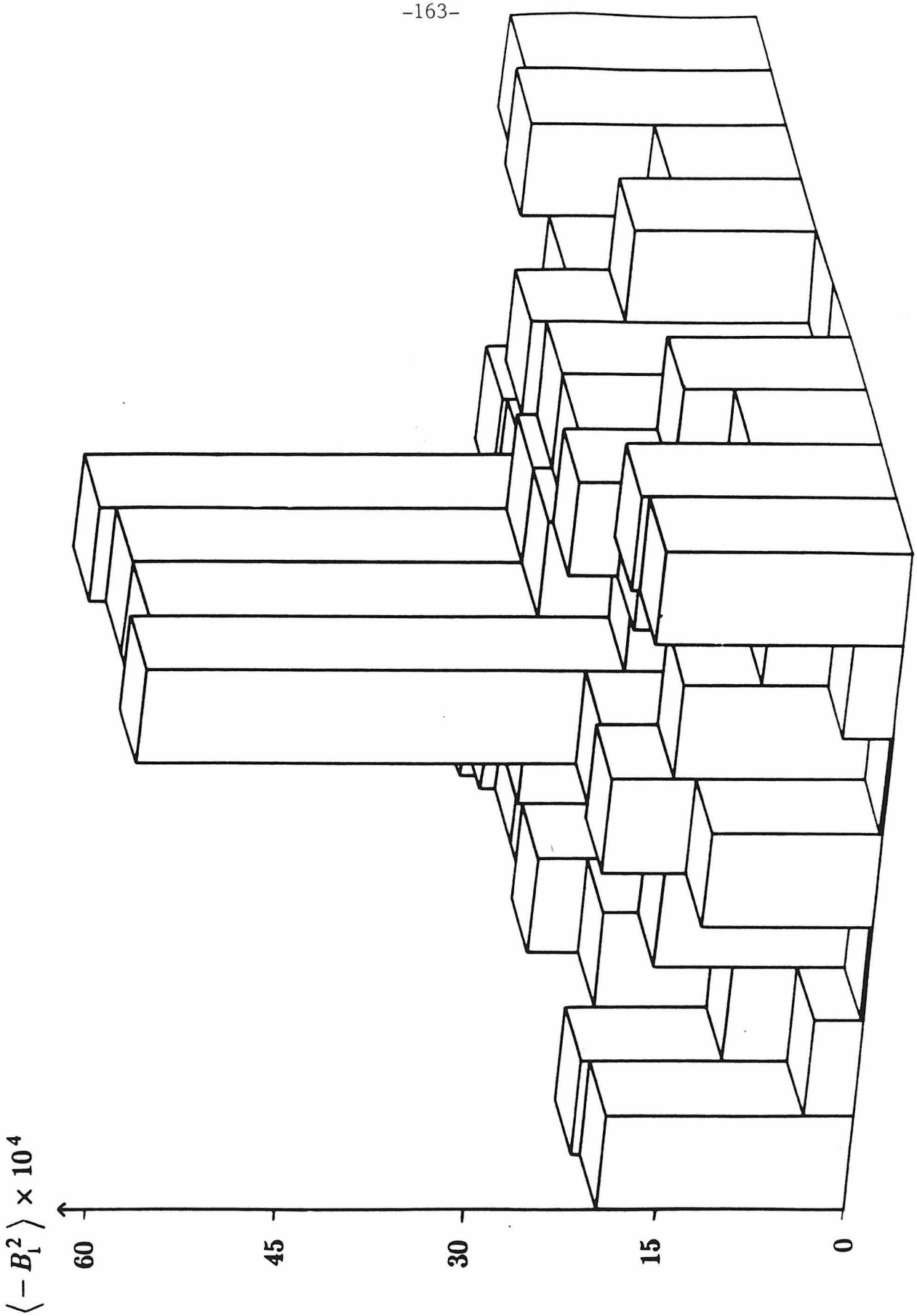

Figure 16c)

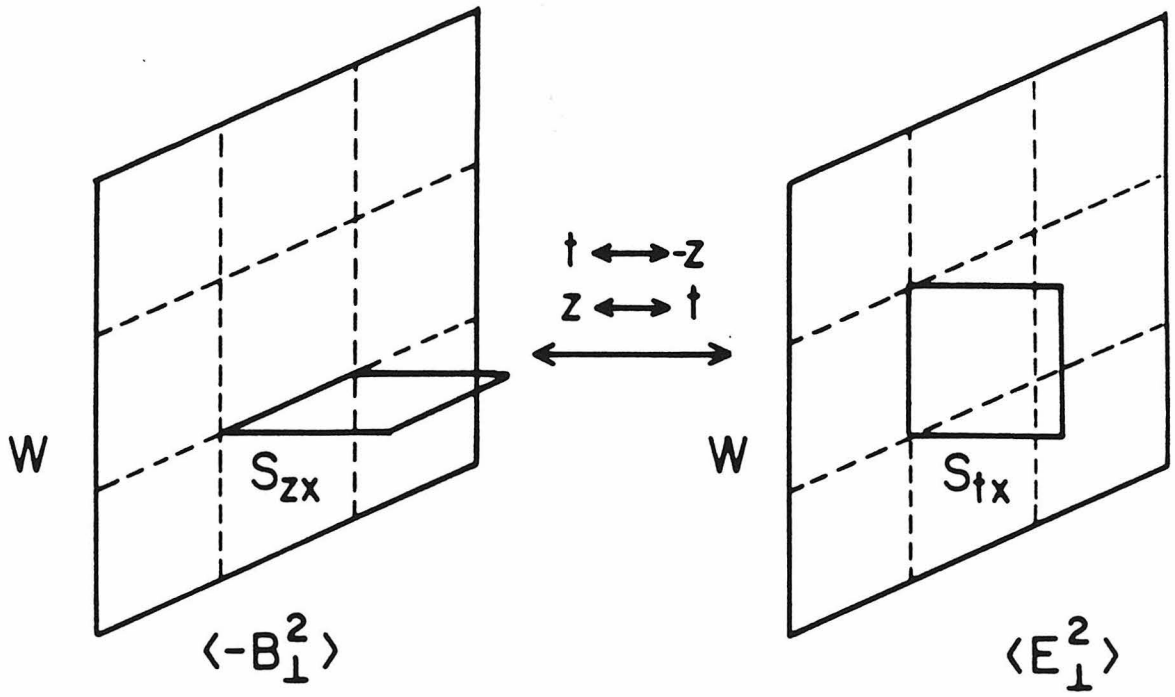

Figure 17

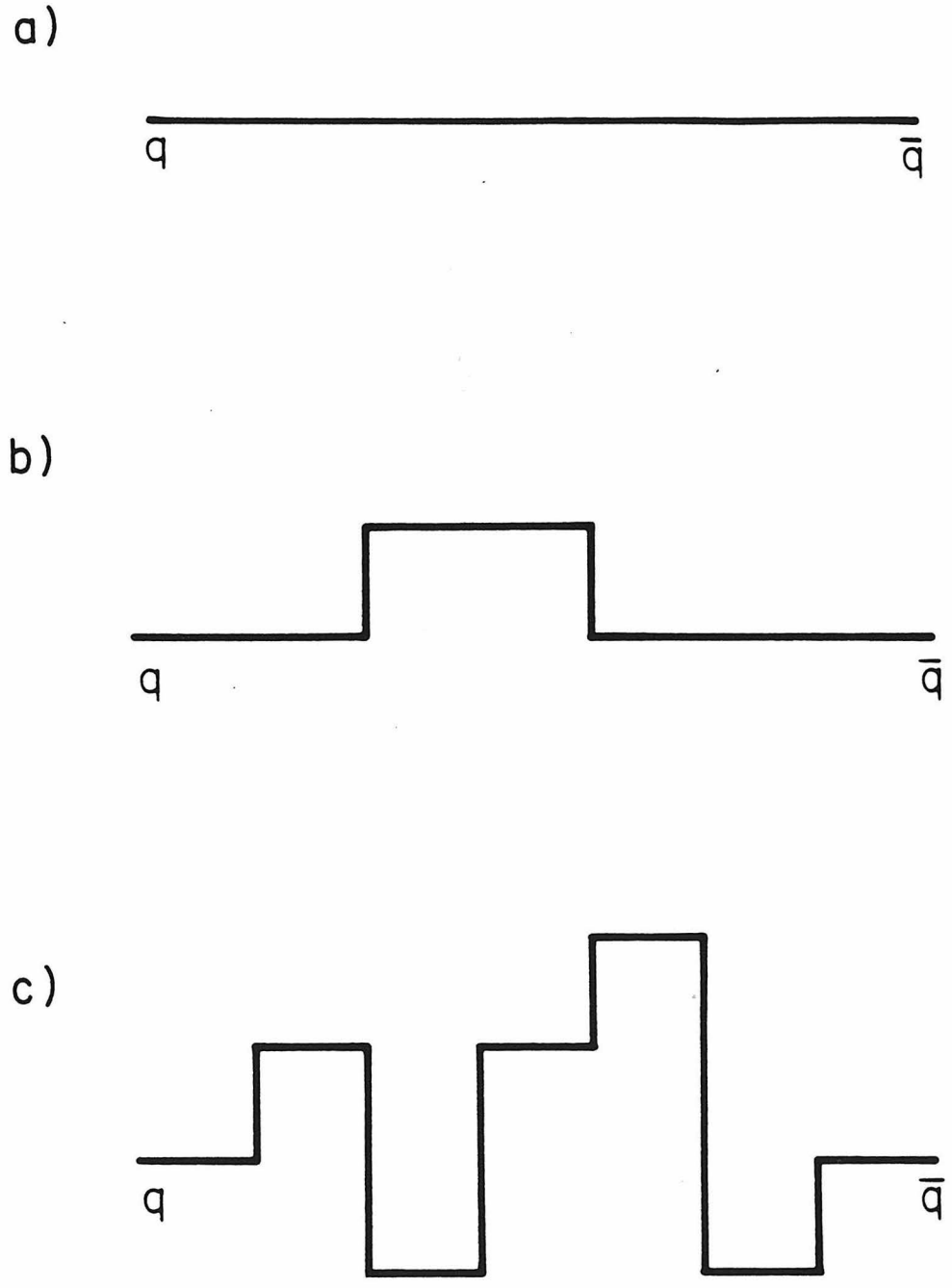

Figure 18

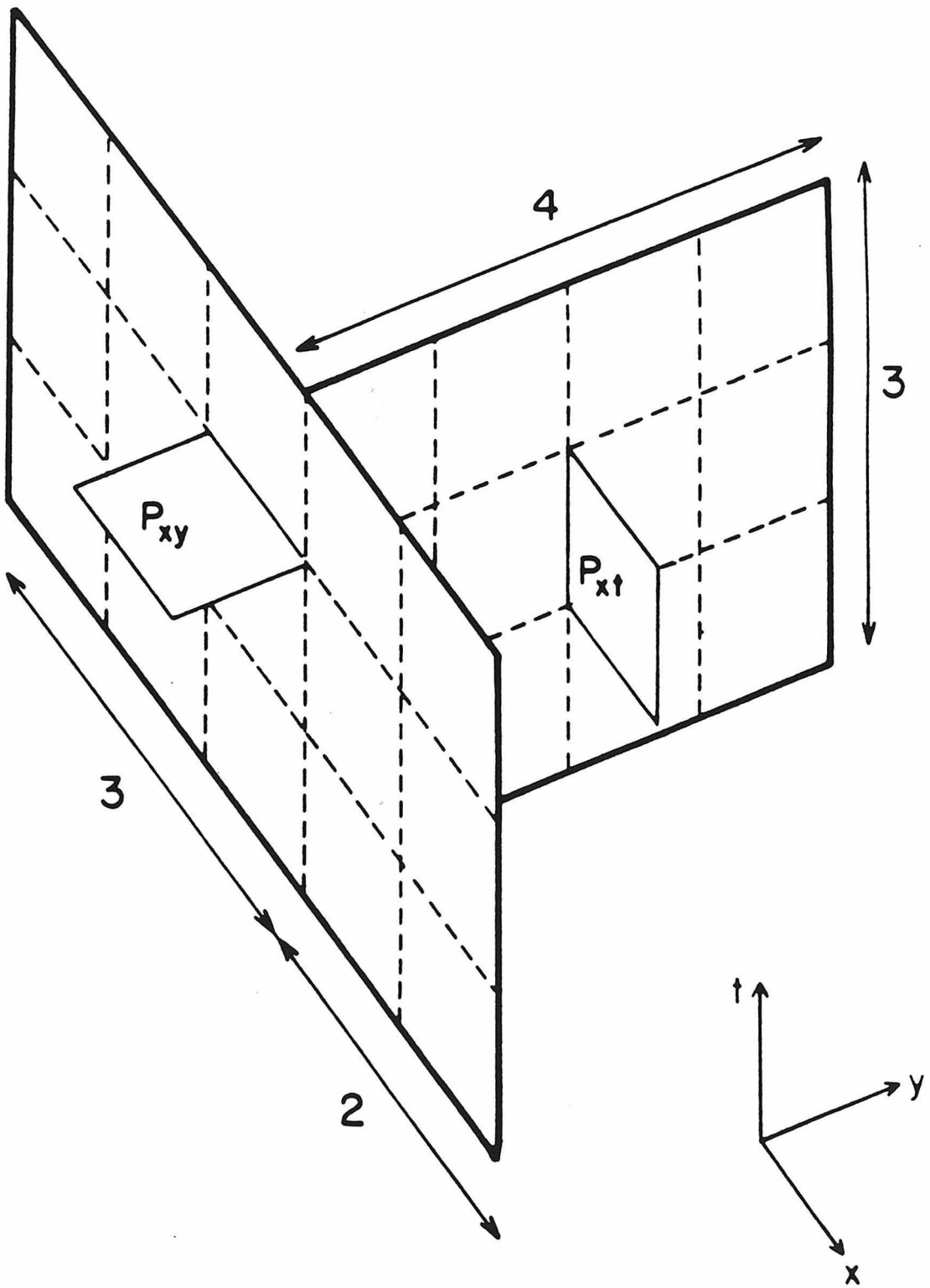

Figure 19

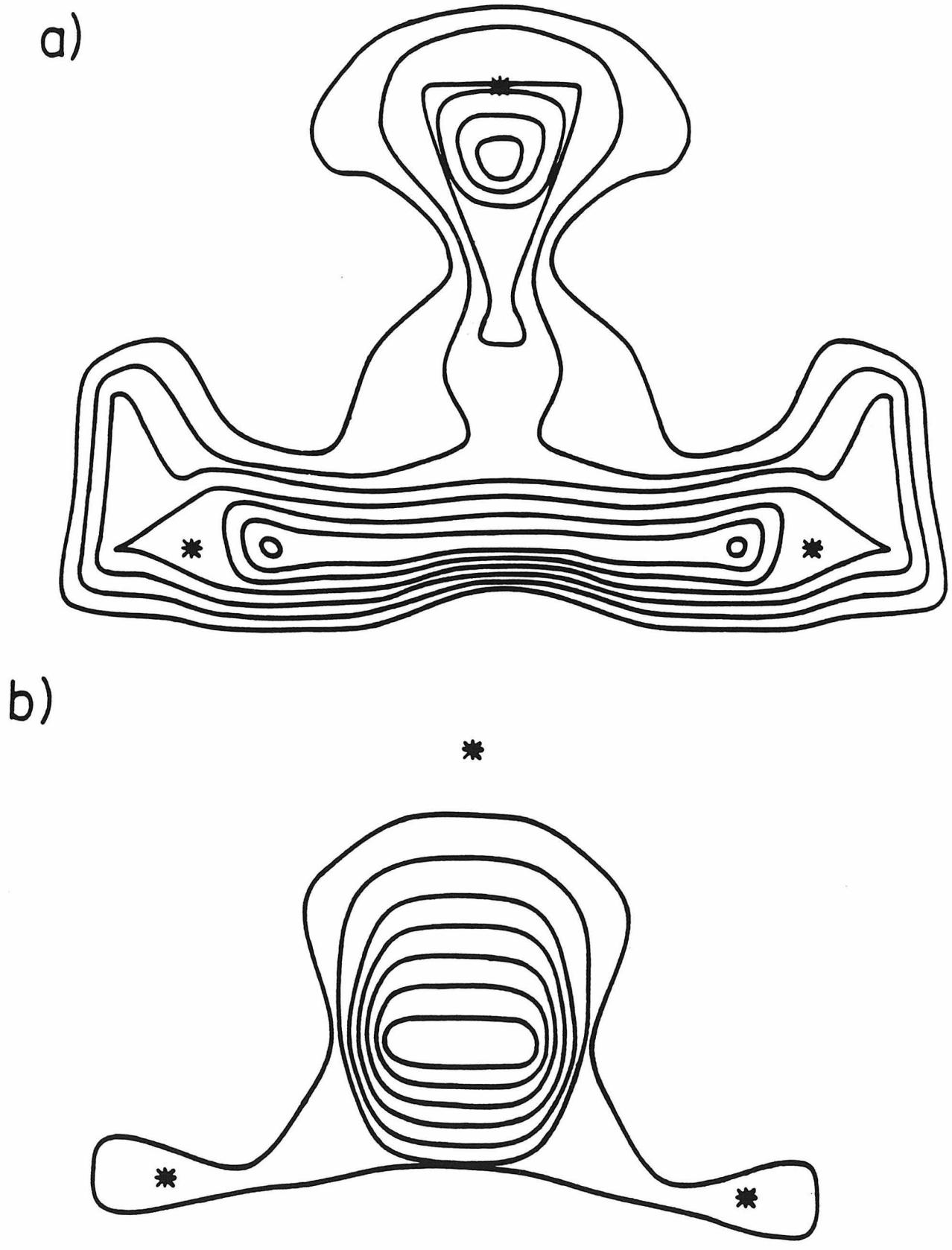

Figure 20

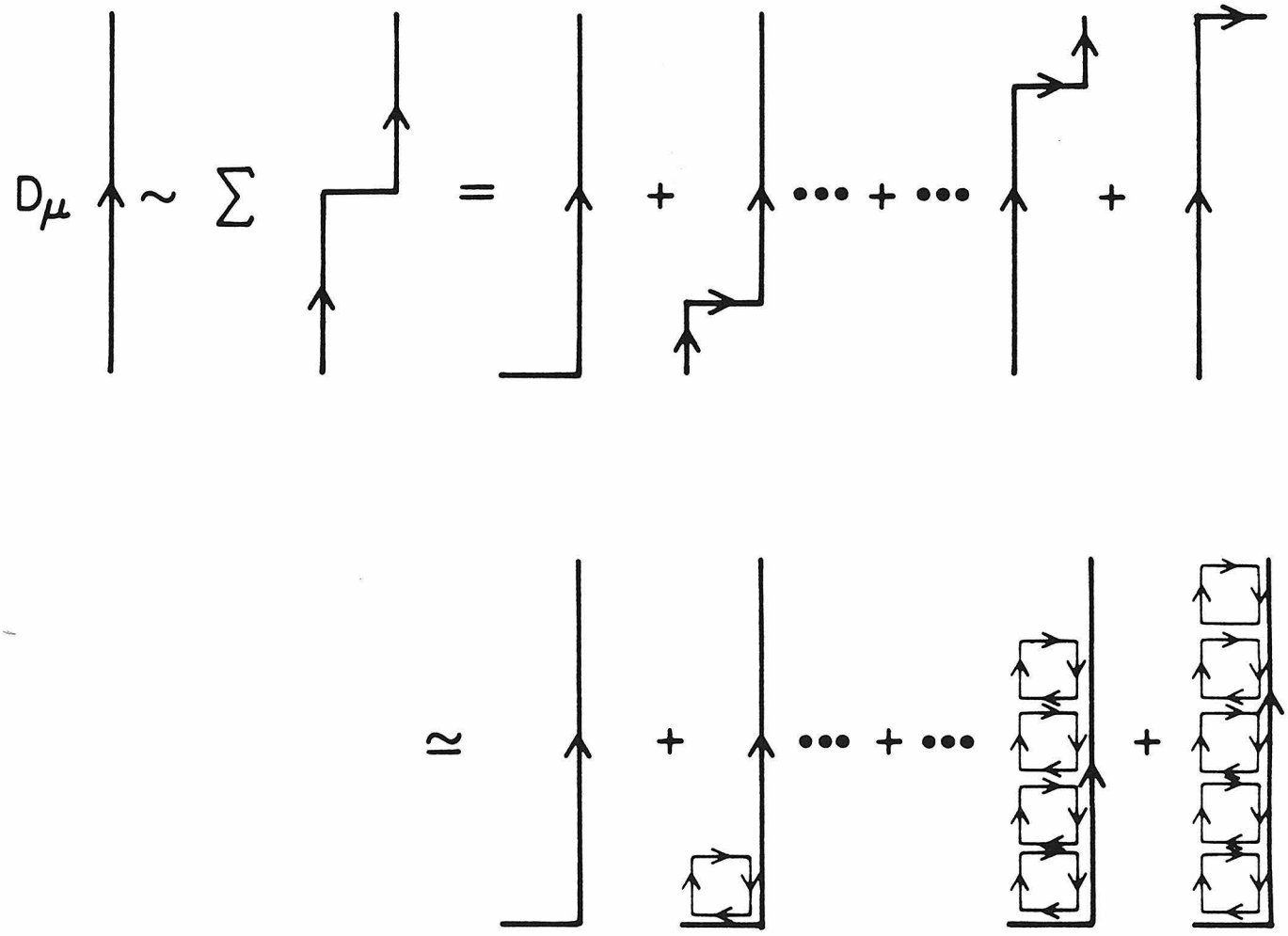

Figure 21

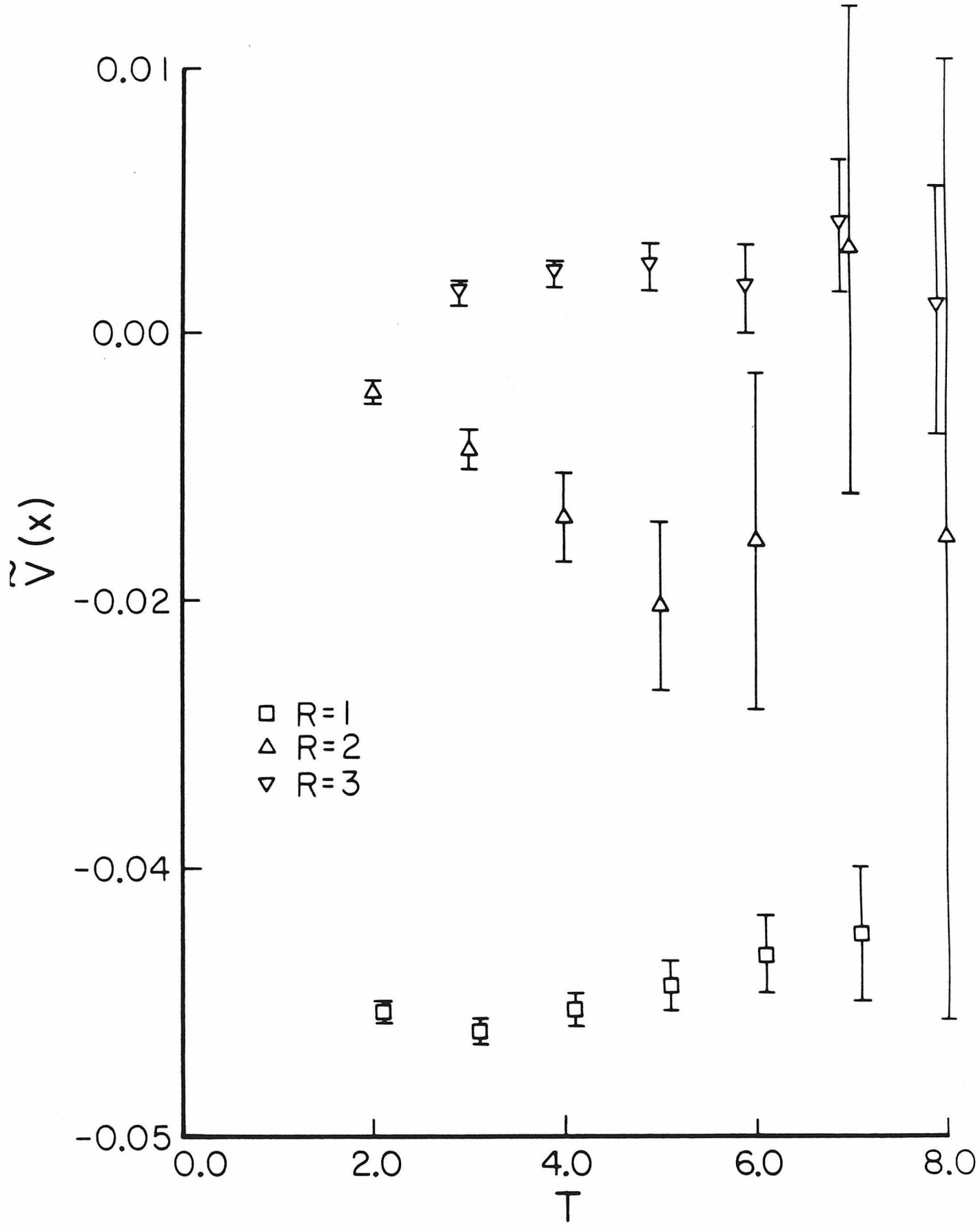

Figure 22

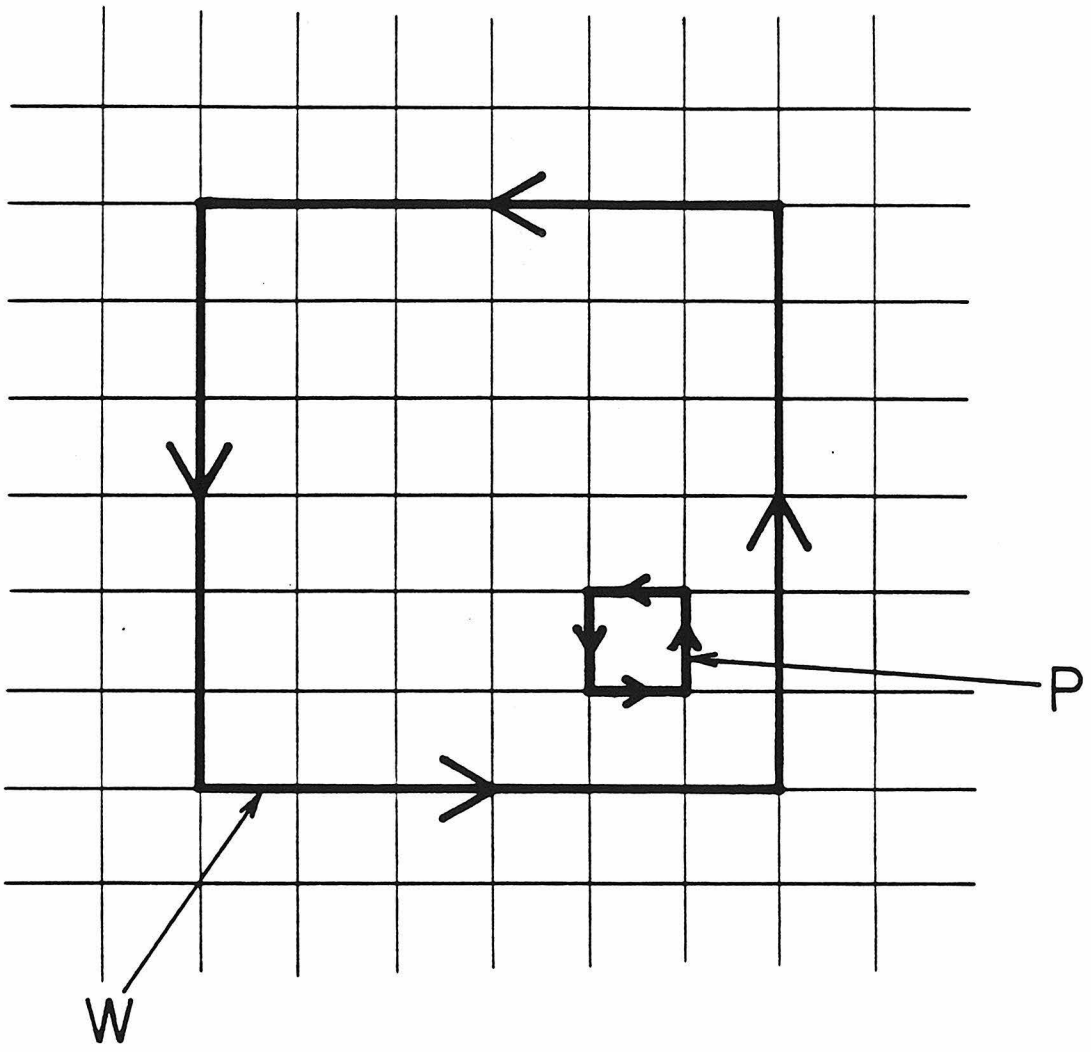

Figure 23

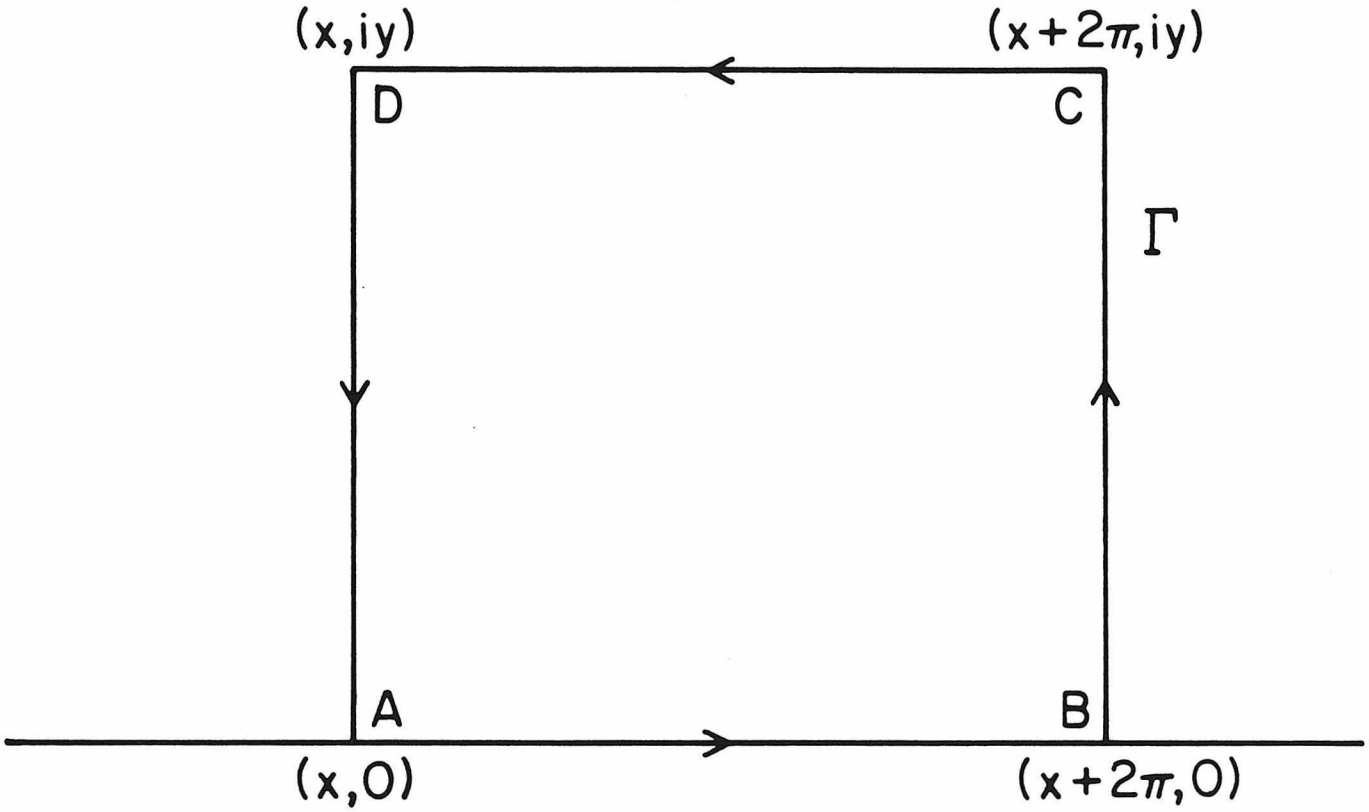

Figure 24

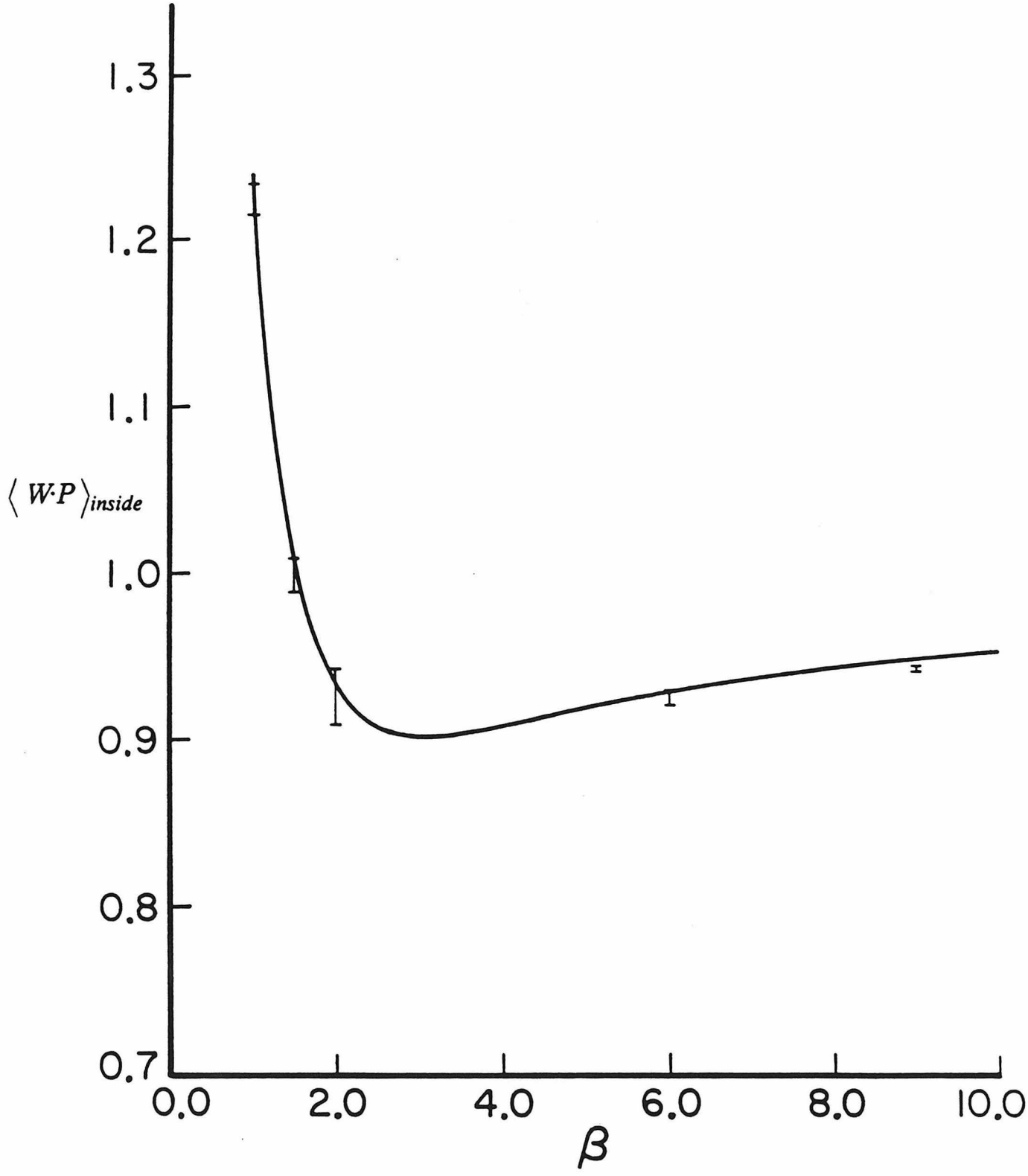

Figure 25a)

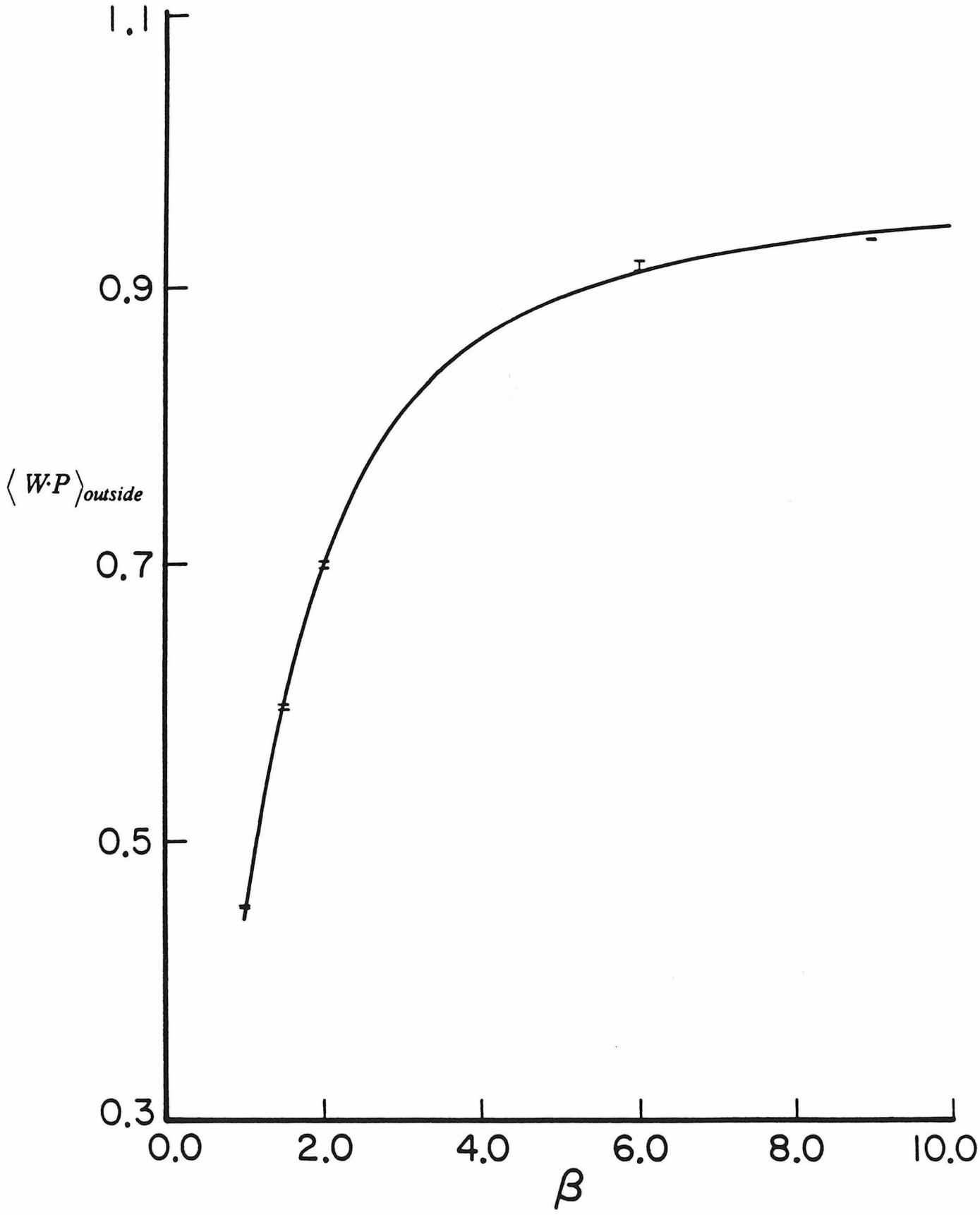

Figure 25b)

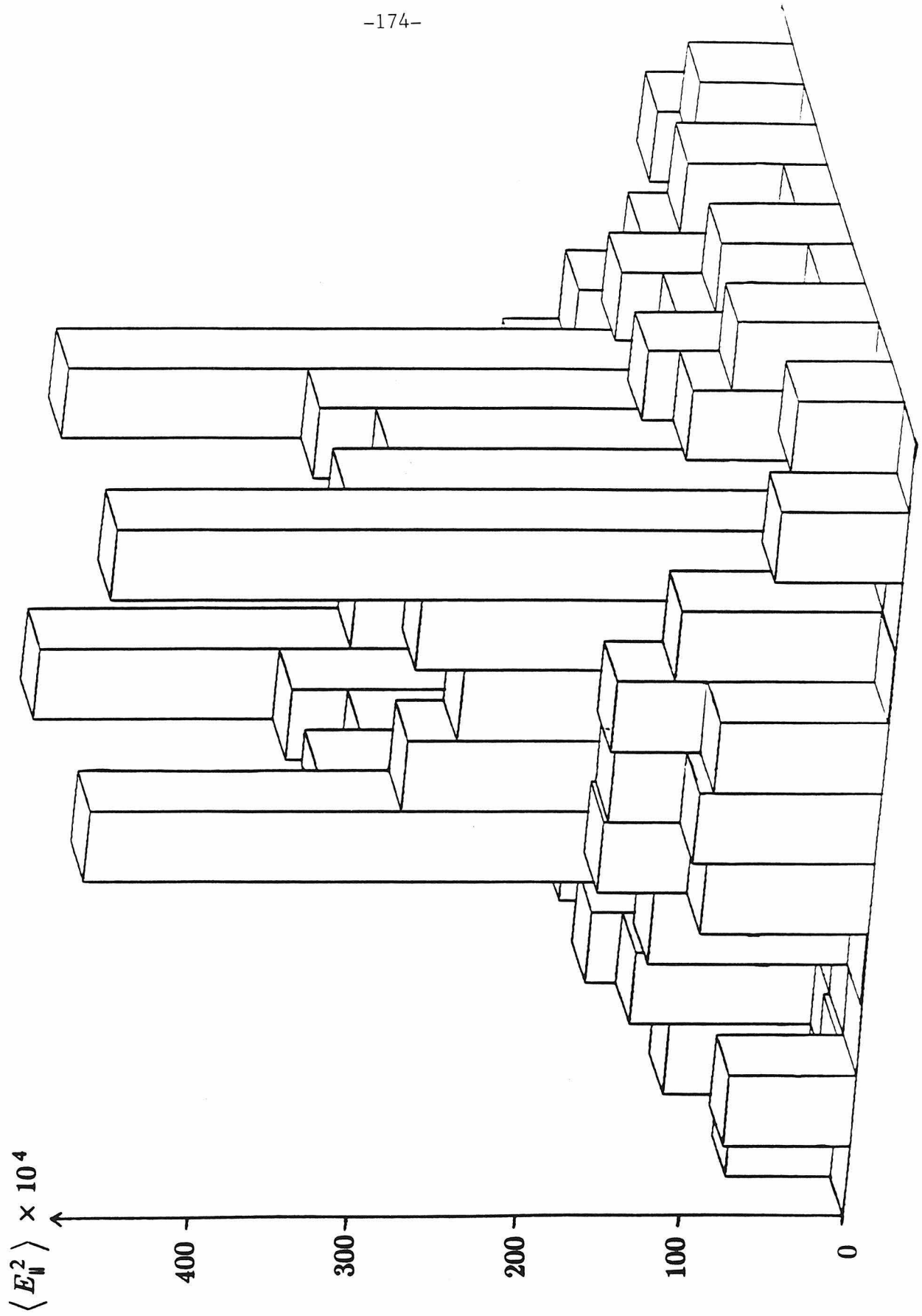

Figure 26a)

Figure 26b)

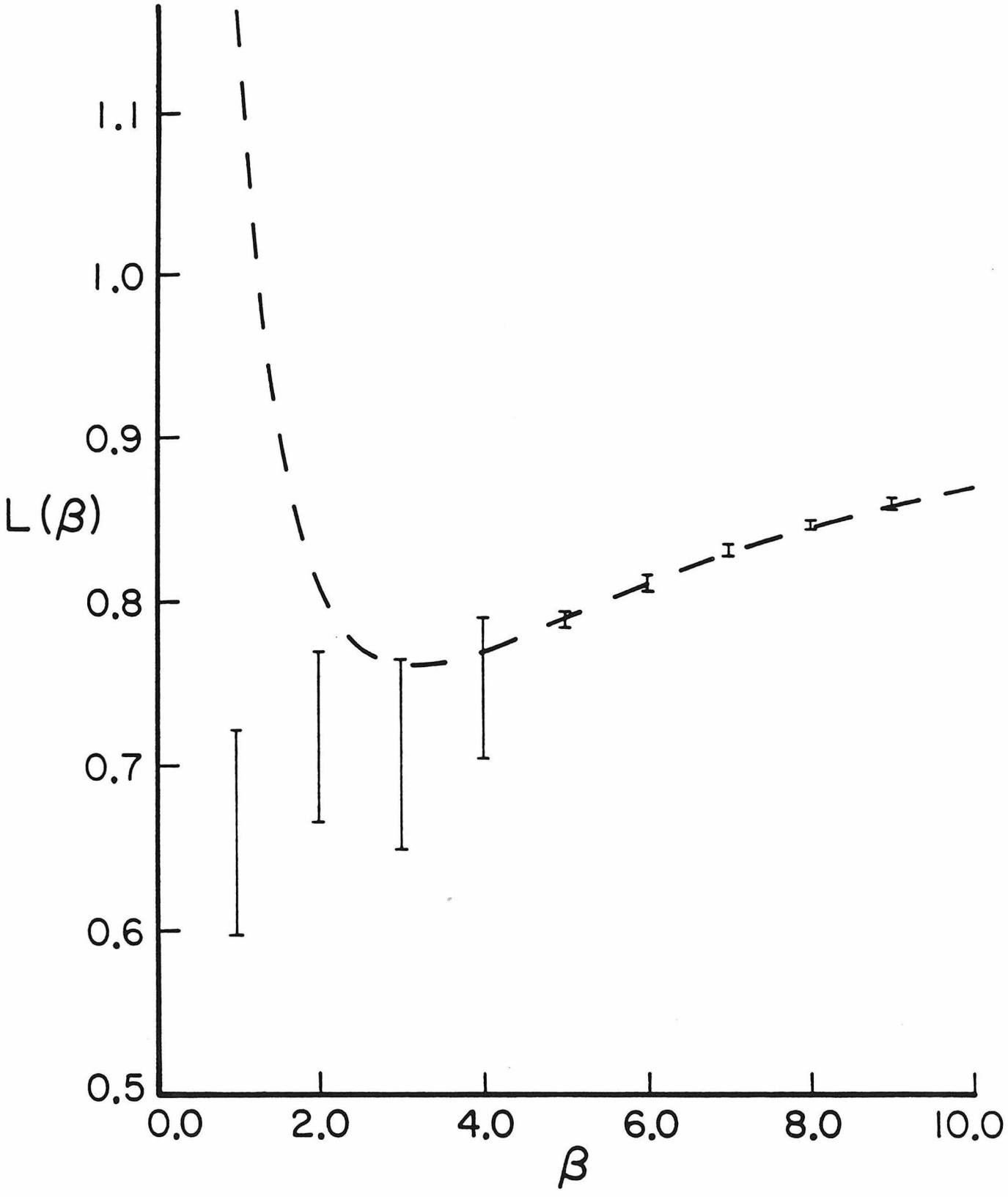

Figure 27

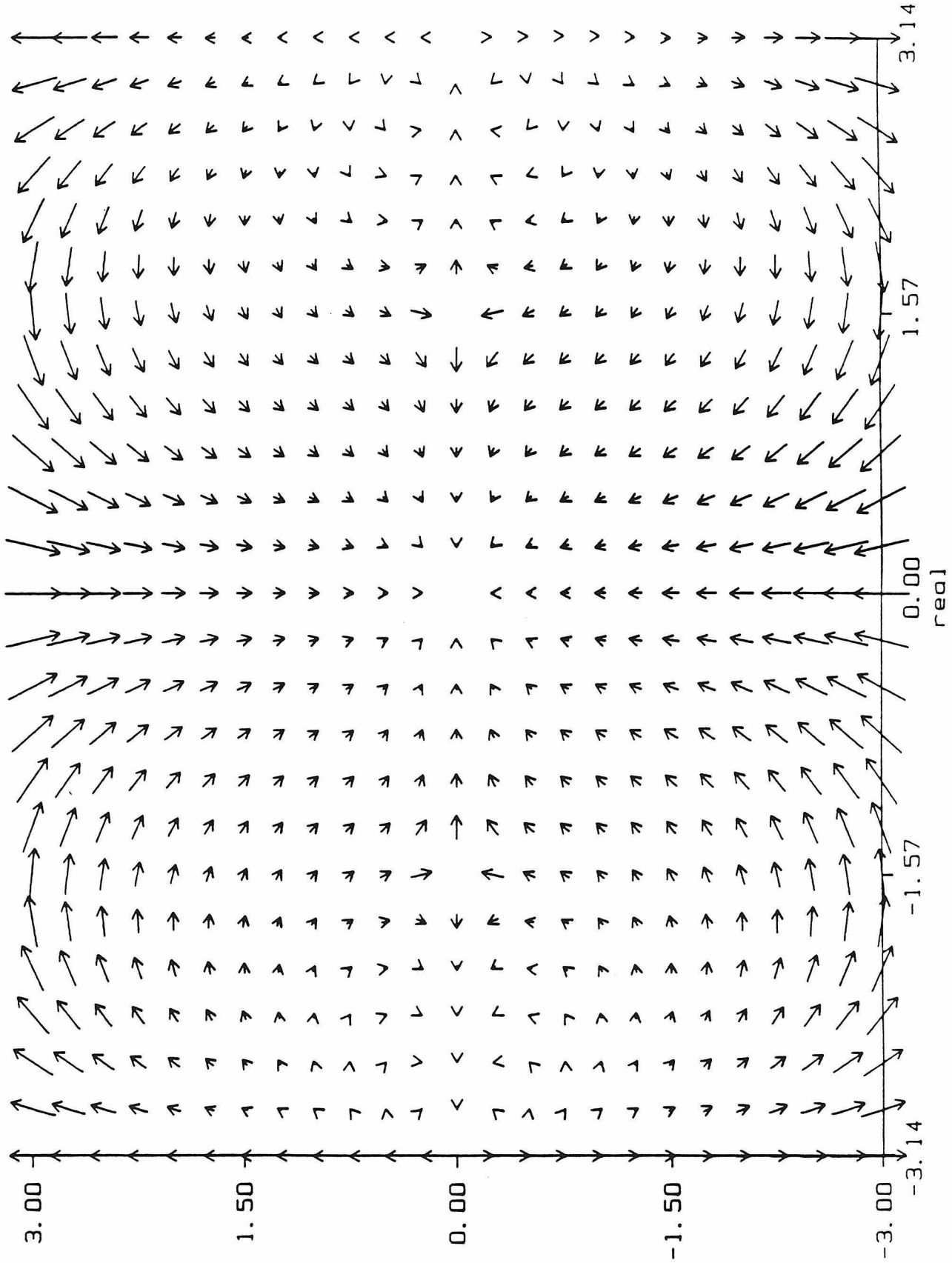

Figure 28

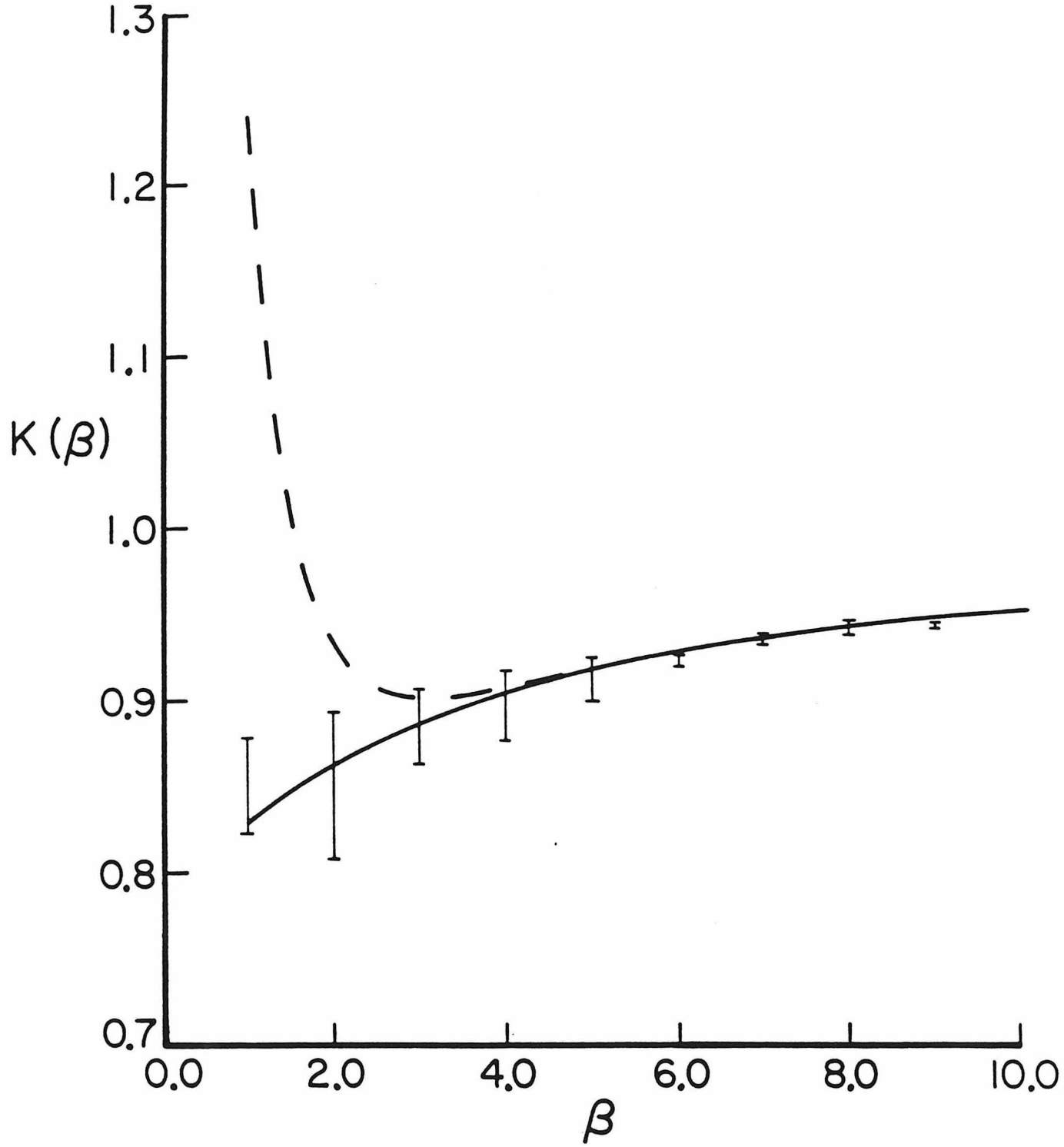

Figure 29

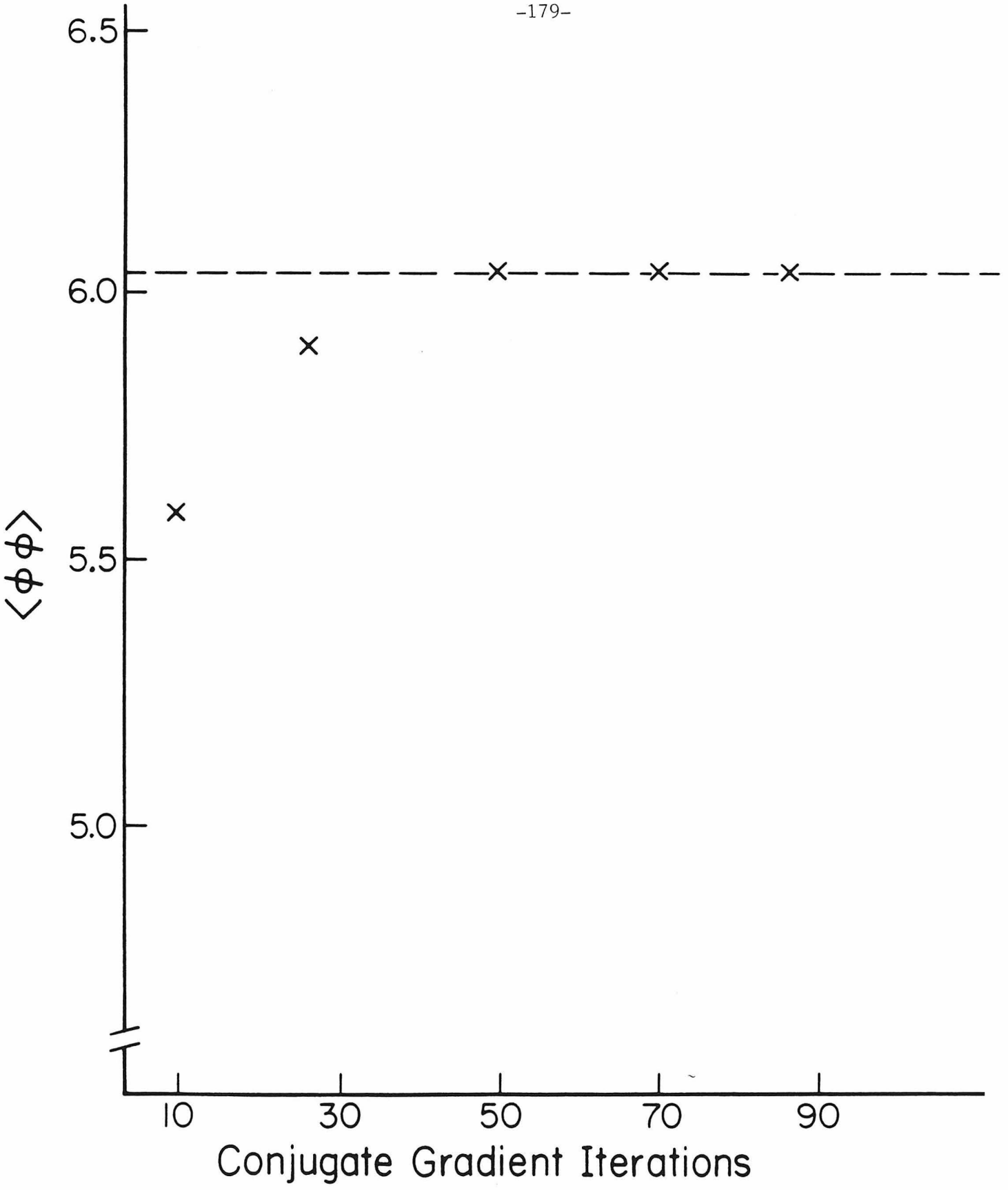
6.5
6.0
5.5
5.0
$\langle \phi\phi \rangle$
10
30
50
70
90
Conjugate Gradient Iterations

Figure 30a)

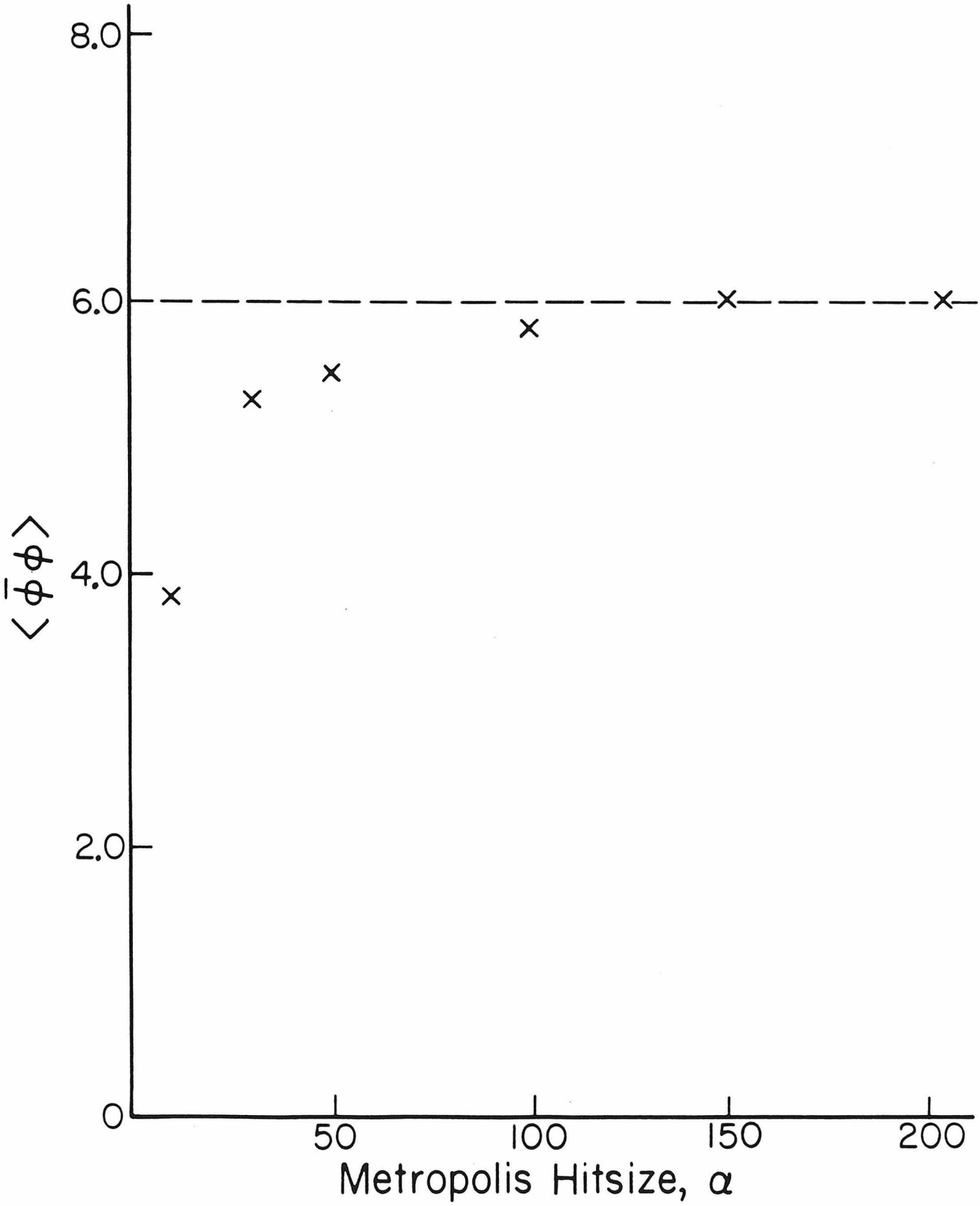
8.0
6.0
4.0
2.0
0
$\langle \bar{\phi}\phi \rangle$
50
100
150
200
Metropolis Hitsize, α

Figure 30b)

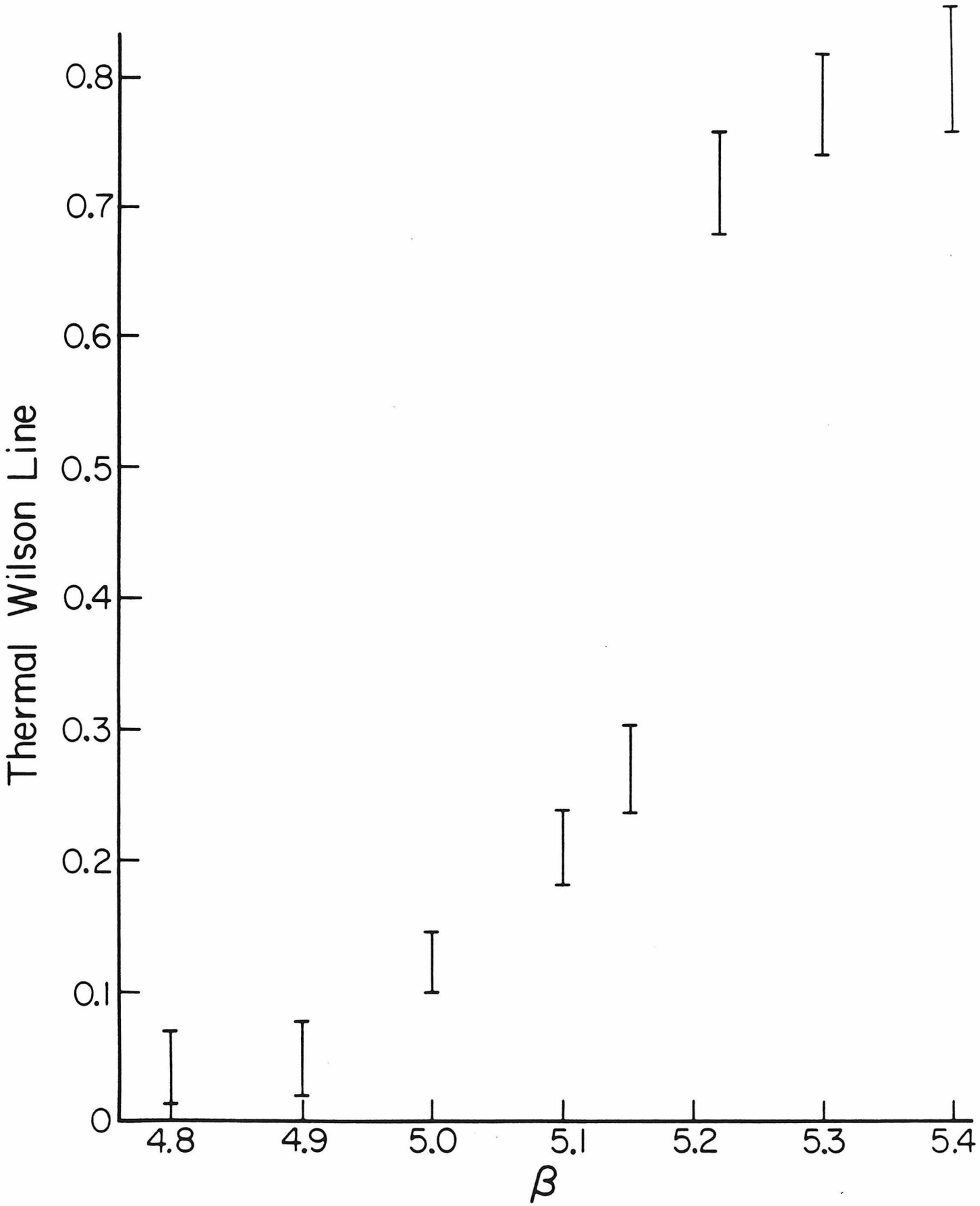

Figure 31

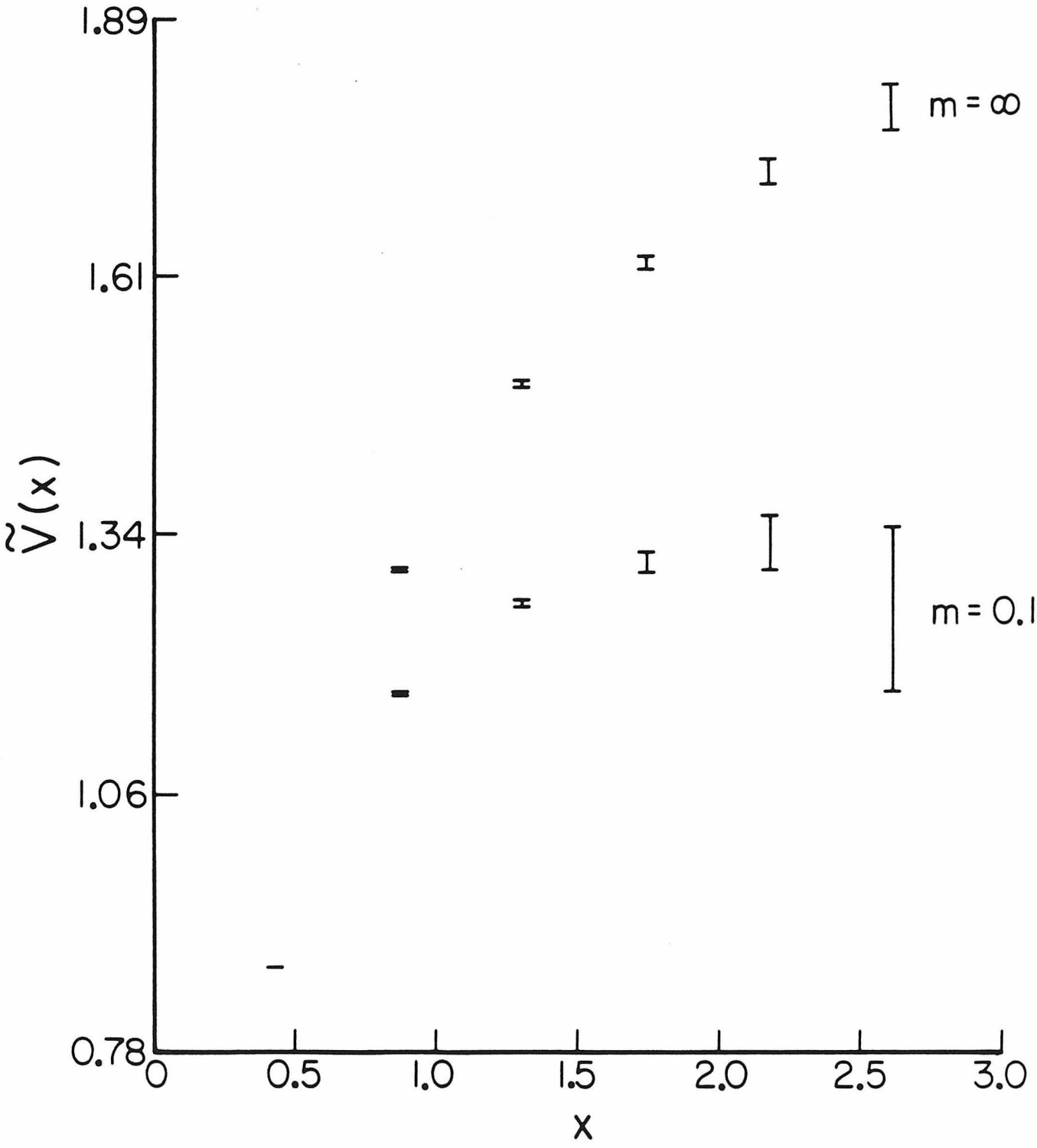

Figure 32

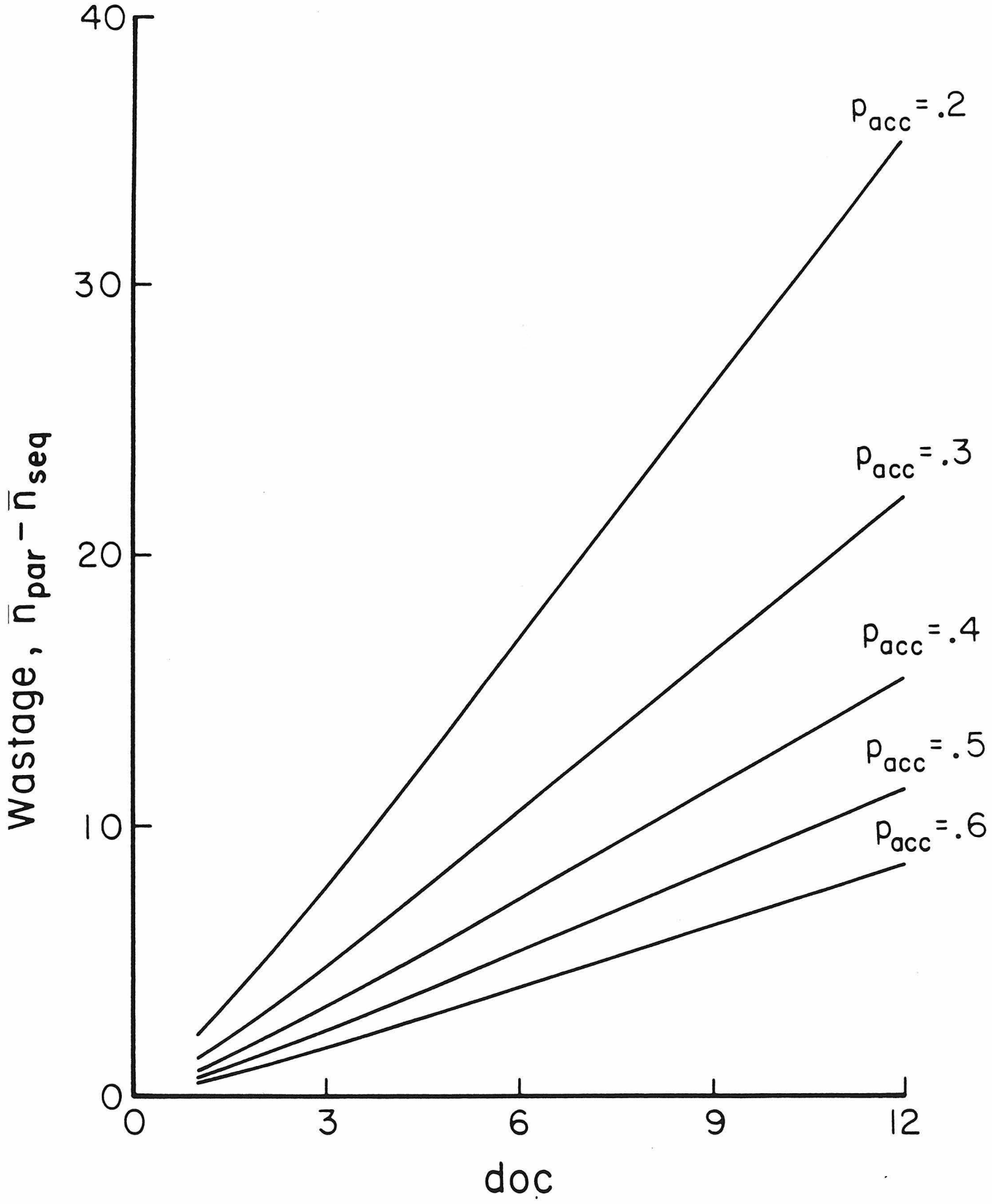
40
30
20
10
0
0
3
6
9
12
doc
Wastage, $\bar{n}_{par} - \bar{n}_{seq}$
$p_{acc} = .2$
$p_{acc} = .3$
$p_{acc} = .4$
$p_{acc} = .5$
$p_{acc} = .6$

Figure 33

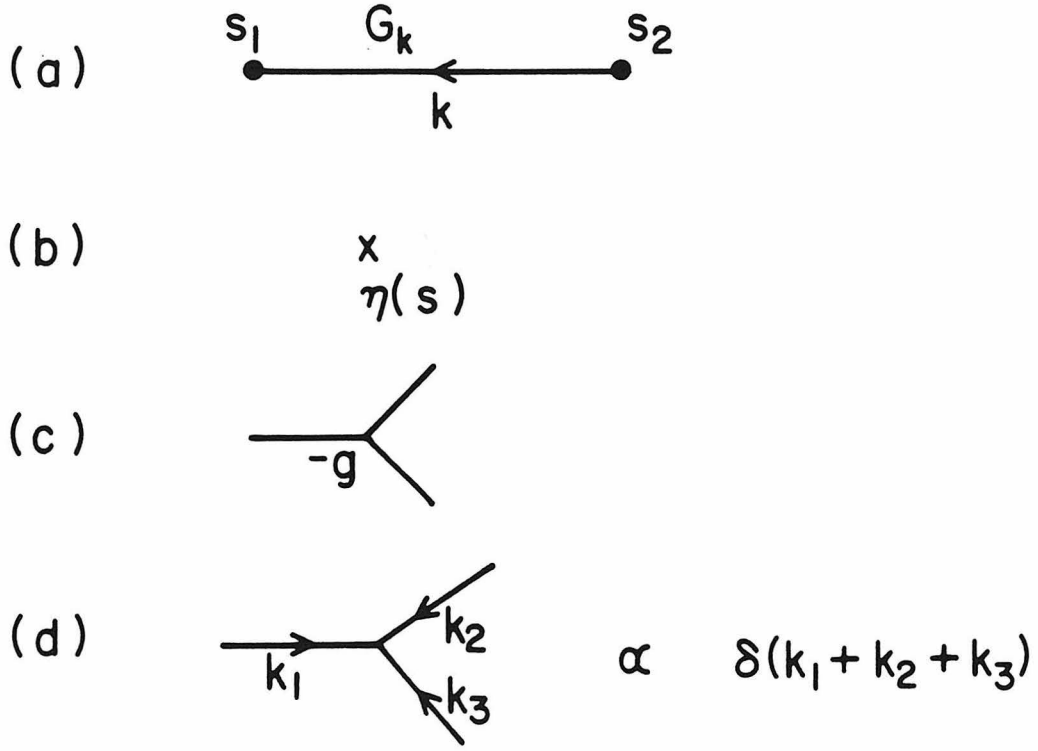

Figure 34

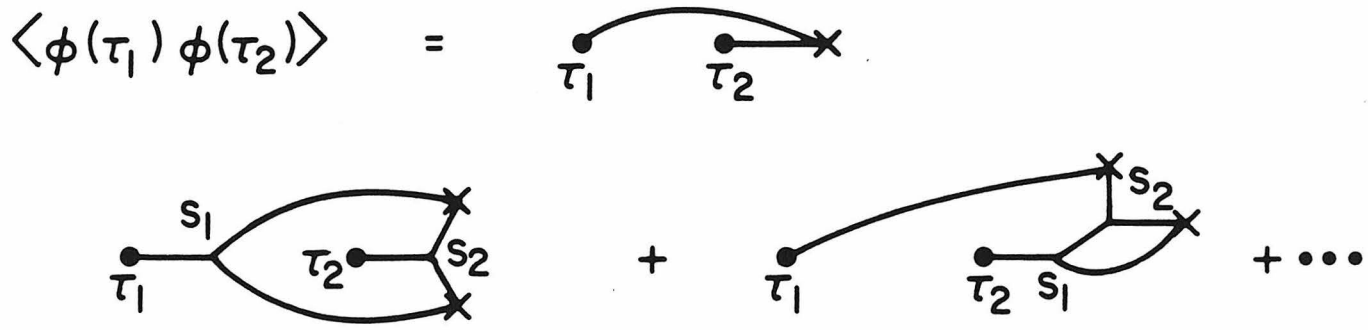

Figure 35

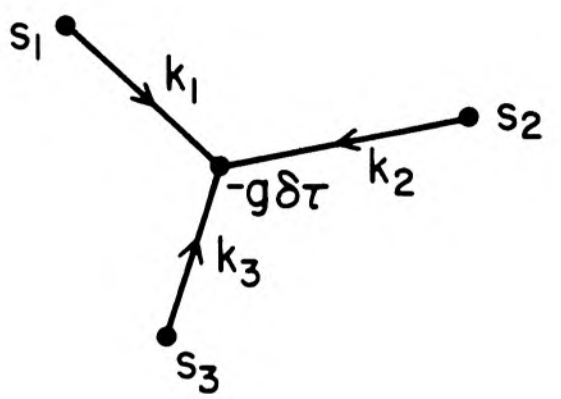

Figure 36